Valorisation of renewable feedstocks by metabolically engineered *Actinomycetes*

Dissertation

zur Erlangung des Grades

der Doktorin der Ingenieurwissenschaften

der Naturwissenschaftlich-Technischen Fakultät

der Universität des Saarlandes

von

Kyoyoung Seo

Saarbrücken

2024

Tag des Kolloquiums :	10. 12. 2024
Dekan :	Prof. Dr.-Ing. Dirk Bähre
Berichterstatter :	Prof. Dr. Christoph Wittmann
	Prof. Dr. Andriy Luzhetskyy
Akad. Mitarbeiter :	Dr. Markus Neuber
Vorsitz :	Priv.-Doz. Dr. Frank Breinig

Publications

Portions of this work have been published with prior authorization from the Institute of Systems Biotechnology (Universität des Saarlandes), as represented by Prof. Dr. Christoph Wittmann.

Peer-reviewed article

Seo, K., Shu, W., Rückert-Reed, C., Gerlinger, P., Erb, T.J., Kalinowski, J., Wittmann, C. (2023). From waste to health-supporting molecules: biosynthesis of natural products from lignin-, plastic- and seaweed-based monomers using metabolically engineered *Streptomyces lividans*. *Microb Cell Fact* 22, 262.

Conference contribution

Seo, K., Rückert-Reed, C, Kalinowski, J., Luzhetskyy, A., Wittmann, C. Advanced production of bottromycin and pamamycin from lignin-based aromatics. Gordon Research Conference on Lignin, 2022, Massachusetts, United States.

Acknowledgment

Above all, I would like to express my deepest gratitude to my supervisor, Prof. Dr. Christoph Wittmann, for giving me the wonderful opportunity to work with him, and for his unwavering scientific support and insightful discussions. Whenever I was critical of my achievements, he served as a solid anchor, keeping me grounded. His support extended beyond the scientific realm, helping me remain a more relaxed, calm, and creative person.

I would also like to thank Prof. Dr. Andriy Luzhetskyy, my second supervisor, for reviewing this study and providing valuable scientific insights. My thanks extend to the other members of the examination committee for chairing the examination and serving as academic observers.

I am deeply appreciative of my scientific collaborators: special thanks to Dr. Patrick D. Gerlinger for providing novel CoA thioesters and sharing his expertise on CoA thioester production, and to Dr. Christian Rückert-Reed for his assistance with the complex transcriptomic analysis of Streptomyces. My thanks also go to my iSBio colleagues, including Fabia Weiland, who not only provided her expertise on *C. glutamicum* and the necessary strains, but also engaged in intensive discussions and shared her motivation and support. I am grateful to Wei Shu, my Streptomyces colleague, for sharing seaweed hydrolysates, insights on Streptomyces, and for fostering a positive working environment.

I am grateful to all iSBio members for sharing both professional and personal experiences with me and for creating a motivating work atmosphere. Special thanks to Michel Fritz for our intensive discussions about analytics and devices, and for allowing me to explore challenging method developments. I learned a great deal about analytics from our everyday conversation. Susanne, thank you for your administrative support and friendly talks. Dr. Fabian Ries, thank you for broadening my scientific perspective, fuelling my motivation, and encouraging me to persevere. Agatha Giniaux, thank you for being my first student and for always staying motivated in the lab.

Peng Cao and Hanling, thank you for the delicious food, teas, and, most importantly, for all the relaxing moments that helped me more relieved.

I want to extend special thanks to my true friends Muzi Tangyu, Izabook Gutiérrez, and Anna Weimer, who supported me both inside and outside the lab. Thank you for engaging in scientific discussions, unconditional supports, playing games, sharing silly and beautiful moments, and for all the trips and memories we created together.

저의 긴 학위 시간을 처음부터 지켜보고, 많은 시간동안 이야기 들어주고, 공감해준 내 친구 아롱이, 채현이에게도 감사드립니다.

가장 마지막으로, 저의 모든 시간과 결정을 지켜보고, 들어주고, 그리고 지지해준 세상에서 가장 큰 저의 지지자이자 사랑하는 우리 가족에게 가장 감사드립니다.

I remember and thank everyone who has supported me through this long journey, even if I cannot mention them in this brief acknowledgment. I am deeply grateful to each and every one of you.

Table of Contents

Summary

Considering the heterogeneity of renewable feedstocks, biotechnological valorisation of advanced renewable feedstocks heavily relies on substrate utilization capacities of microorganisms. In this study, industrially important strains, *C. glutamicum* and *S. lividans*, were employed to valorise renewable feedstocks by deciphering catabolic pathways of lignin-derived aromatics and seaweed-derived mannitol.

Through development of targeted analysis of aromatic CoA thioesters, β-oxidative degradation of phenylpropanoids in *C. glutamicum* was demonstrated. Metabolomic analysis revealed that metabolically engineered *C. glutamicum* strain processed the β-oxidative pathway more efficiently than the wild type. Additionally, cross-pathway interactions between ferulate and caffeate during degradation, as well as a decrease in acetyl-CoA pool in presence of aromatics, were observed.

Based on systematic approaches, substrate utilization systems in *S. lividans* were identified. Moreover, production of two distinct classes of natural products, pamamycin and bottromycin, from renewable feedstock-derived monomers was demonstrated. Strikingly, utilization of aromatics activated ethylmalonyl-CoA pathway, resulting in a diversification of the pamamycin spectrum. As an advanced approach, minimally treated seaweed hydrolysate was utilized, showcasing the production of pamamycin.

Zusammenfassung

In Anbetracht der Heterogenität erneuerbarer Rohstoffe hängt die biotechnologische Verwertung fortschrittlicher erneuerbarer Rohstoffe stark von den Substratnutzungsfähigkeiten der Mikroorganismen ab. In dieser Studie wurden die industriell wichtigen Stämme, *C. glutamicum* und *S. lividans* eingesetzt, um erneuerbare Rohstoffe, durch die Entschlüsselung der Abbauwege von aus Lignin gewonnenen Aromaten und aus Algen gewonnenen Mannitol, zu verwerten.

Durch die Entwicklung einer gezielten Analyse von aromatischen CoA-Thioestern wurde der β-oxidative Abbau von Phenylpropanoiden in *C. glutamicum* nachgewiesen. Die Metabolomanalyse ergab, dass ein metabolisch veränderte *C. glutamicum*-Stamm den β-Oxidationsweg effizienter nutzte als der Wildtyp. Darüber hinaus wurden stoffwechselwegübegreifende Interaktionen zwischen Ferulat und Kaffeesäure während des Abbaus, sowie eine Abnahme des Acetyl-CoA-Pools in Gegenwart von Aromaten beobachtet.

Auf der Grundlage systematischer Ansätze wurden Substratverwertungssysteme in *S. lividans* identifiziert. Darüber hinaus wurde die Produktion von zwei verschiedenen Klassen von Naturstoffen, Pamamycin und Bottromycin aus Monomeren von erneuerbaren Rohstoffen nachgewiesen. Bemerkenswerterweise aktivierte die Nutzung von Aromaten den Ethylmalonyl-CoA-Stoffwechselweg,was zu einer Diversifizierung des Pamamycin-Spektrums führte. Als fortschrittlicher Ansatz wurde minimal behandeltes Seetanghydrolysat verwendet, um die Produktion von Pamamycin zu demonstrieren.

1 Introduction

1.1 General introduction

With increasing environmental concerns, the concept of sustainability in biotechnology has become a prominent focus leading to extensive research on the production of biofuels, bioenergy, and bio-based chemicals from renewable feedstocks. In the first major report on biotechnology on sustainable development in 1994 by OECD (OECD, 1994), highlighted four critical characteristics: production based on renewable feedstocks, mild production process, environmentally compatible products and generation of recyclable wastes. Subsequently, follow-up reports have been continuously published from OECD, promoting the utilization of renewable feedstock in industrial biotechnology.

Biotechnology is considered as a promising solution for sustainable development, by shifting traditional petrochemical-based to biomass-based economy. However, despite immense global concerns about sustainability and intensive research on bioeconomic strategies (Popp et al., 2021), questions still remain regarding the substitution of traditional feedstock in biotechnology, largely due to economic conflicts. The comparison between the value of industrial economics and the value of the global ecosystem in 1997 revealed that industrial economics significantly outweighed natural resources (Costanza et al., 1998), indicating the market bias towards to traditional fossil-based economics. Currently, the global economy and current circumstances are largely adjusted to petrochemical industry. Therefore, a bio-based economic necessitate cost-efficient scaled-up processes and high performance to compete pre-existing systems in the market (Calvo-Flores & Martin-Martinez, 2022). Specifically, producing 'high-value complex molecules' from waste materials under mild conditions emerges as a key solution to address these economic conflicts (H. P. Meyer, 2011).

Traditionally, biomass, which constitutes the majority of renewable feedstock, has been consumed as foods, animal feeding, heating, construction materials, and other purposes. In biorefinery, biomass encompasses a wide range of materials, from plant biomass such as crops and wood, to microbes and algae (Kumar & Verma, 2021). Several critical challenges exist in utilizing biomass in biorefinery including feedstock availability, infrastructure, logistics, pretreatment, and land-use (Katakojwala & Mohan, 2021). In order to achieve a sustainable biorefinery environment, the value of product should be increased by obtaining multiple products from the renewable feedstock, ultimately, producing high-value low-volume (HVLV) chemicals and low-value high-volume (LVHV) in the process (Melero et al., 2012).

To expand the bio-based economics, the adoption of microbial cell factories is regarded as a promising approach. Microbes efficiently utilize renewable feedstocks under mild conditions, requiring lower pressure and temperature compared to conventional chemical reactions, indicating lower energy inputs in a technoeconomic perspective (Erickson et al., 2012). Furthermore, microbes have the ability to selectively produce a wide range of products, thereby simplifying downstream processing.

Despite the environmentally friendly procedures, a major concern with employing microbes for renewable feedstock is the diversity of substrates and the limited capacities of microorganisms for substrate utilization. The compositions of raw materials are largely various depending on type, seasons, and regions. Commonly used microorganisms in biotechnology, including *E. coli* and *C. glutamicum*, naturally possess the capability to catabolize only a limited spectrum of advanced renewable feedstocks. Hence, the development of finely tuned engineered cells is essential to expand the substrate spectrum or improve tolerance levels (Buschke et al., 2013). This feasibility of metabolic engineering in microbial cell factories further enhances the attractiveness of utilizing microorganisms (Straathof et al., 2019).

1.2 Objectives

This study aims to improve the utilization of renewable resources for natural product production through microbial cell factories by investigating catabolic pathways involved in the utilization of renewable feedstock-derived monomers in Actinomycetes, including *S. lividans* and *C. glutamicum*.

For *C. glutamicum*, the objective includes conducting a metabolomic analysis using LC-MS/MS to understand the catabolic pathways of aromatic compounds, ultimately advancing strategies for lignin valorization. After establishing the enzymatic synthesis of aromatic CoA thioesters, the study should focus on optimizing LC-MS/MS methods to explore intracellular aromatic CoA thioesters and analyze their influence on central metabolism.

For *S. lividans*, systematic transcriptomic and metabolomic analyses should be conducted to identify mannitol- and aromatic-catabolic systems. After identifying genes involved in catabolism, the study will also explore how these substrates affect central metabolism and natural product formation.

Overall, the study should demonstrate the production of high-value low-volume (HVLV) and low-value high-volume (LVHV) materials from renewable sources. By utilizing lignin-based aromatics and seaweed-based mannitol in *S. lividans* and *C. glutamicum*, their potential to create valuable pharmaceuticals from renewable feedstocks should be showcased.

2 Theoretical background

2.1 Advanced renewable feedstocks for microbial cell factories

Depends on characteristics and origin of feedstocks, pretreatment and microbial production process are largely influenced. Sugar-rich renewable feedstock (first generation) contains high carbohydrates contents, such as starch and sugar, and can be easily fermented into biofuels and value-added products (Lee & Lavoie, 2013). Typically, the agricultural crops are pretreated via hydrolysis, dissolution, and saccharification before being utilized as substrates for fermentation (Singh et al., 2023). The utilization of food-based renewable feedstock is highly commercialized, with approximately 1,000 biorefinery companies producing ethanol (Straathof et al., 2019). However, this competition of land-use contributes to increased food prices and global starvation (Singh et al., 2023), as well as environmental pollution by using pesticides and fertilizer (Mishra et al., 2020).

On the contrary, advanced renewable feedstocks, including non-food terrestrial waste (second generation) and algae (third generation) (Lee & Lavoie, 2013; Singh et al., 2023; Straathof et al., 2019), are promising resources for sustainable biotechnology as they are readily available and do not compete with food production. Non-food terrestrial wastes, such as lignocellulose, are widely available worldwide, inexpensive, require less fertilizer, and are also produced as industrial wastes (Abraham et al., 2020). However, due to their rigid chemical structures, lignocellulosic materials require harsh pretreatment processes, including depolymerization. Globally, fewer than 10 companies produce bioethanol from lignocellulosic biomass, primarily focusing on cellulose utilization (Straathof et al., 2019).

Compared to lignocellulosic biomass, algae-based renewable feedstocks contain high levels of carbohydrates and proteins, while lignin contents are low (Poblete-Castro et al., 2020), necessitating relatively milder pre-treatment conditions those required for lignocellulosic biomass.

With its rapid growth, high abundance (Poblete-Castro et al., 2020), and significant potential for CO_2 capture (Sayre, 2010), seaweed shows promise as an advanced renewable feedstock. However, its commercialization is currently limited to food and animal feeds, and energy production and valorisation are confined to demonstration or pilot scale (Straathof et al., 2019).

2.1.1 Lignin as a second-generation renewable feedstock

2.1.1.1 Applied and relevant use of lignin

Lignin, a second-generation renewable feedstock and the second most abundant polymer on earth, is a primary component of plant biomass along with cellulose and hemicellulose (Boudet, 1998). Globally, abundance of native lignin is over 300 billion tonnes, with an increase of 20 billion tonnes per year (Smolarski, 2012). Technical lignin, a side product of pulp and paper industry and biorefineries, is particularly produced over 70 billion tonnes (Luo & Abu-Omar, 2017), with an expected annual growth of 225 million tonnes by 2023 (Bajwa et al., 2019). Unlike cellulose and hemicellulose in plant biomass, which are extensively used in industries for the production of pulp, textiles, or chemicals (Akagawa et al., 1995; Mathews et al., 2015; Reddy & Yang, 2005), lignin has been underutilized due to its structural complexity and recalcitrance. The majority of technical lignin produced by industrial waste is simply burned to generate heat, valued at approximately $0.08 per kg (Luo & Abu-Omar, 2017).

Recent studies have sought to address this underutilization by demonstrating microbial valorisation of lignin-derived aromatics into fine-chemicals. For example, *cis, cis*-muconate, a precursor for biodegradable polymers, has been produced in various microorganisms, including *Sphingobium* sp. strain SYK-6 (Sonoki et al., 2018), *Amycolatopsis* sp. strain ATCC 39116 (Barton et al., 2018), *P. putida* KT2440 (Kohlstedt et al., 2022), and *C. glutamicum* (Weiland et al., 2023). Lipid production has been predominantly performed using *Rhodococcus* strains such as *R. opacus* DSM1069 (Kosa & Ragauskas, 2012), *R. jostii* RHA1 (He et al., 2017), and *R. opacus*

PD630 (Z. H. Liu et al., 2018). Furthermore, vanillin, a food additive, has been produced using *P. putida* KT2440 (Graf & Altenbuchner, 2014) and *Amycolatopsis* sp. strain ATCC 39116 (Fleige et al., 2016). The production of polyhydroxyalkanoate (PHA), a biodegradable plastic, has been successfully demonstrated using *P. putida* KT2440 (Salvachúa et al., 2020).

2.1.1.2 Chemical structure of lignin

Lignin is composed of phenylpropanoids linked via mainly C-C and C-O bonds including β-O-4, α-O-4, β-1, β-β, 4-O-5, β-5, and 5-5 (Ralph et al., 2004), contributing the cell wall rigidity (Schuetz et al., 2014), protection against pests and pathogens (Ithal et al., 2007), and various environmental stresses (Q. Liu et al., 2018; Moura et al., 2010). Lignin building blocks, mainly phenylpropanoids, are classified into *p*-coumaryl alcohol (H unit, one hydroxy group on aromatic ring), caffeoyl alcohol (C unit, harbouring two hydroxy group), coniferyl alcohol (G unit, containing one methoxy group), sinapyl alcohol (S unit, possessing two methoxy groups), and cinnamoyl alcohol (a precursor of building blocks; no hydroxy or methoxy group) (Abdelaziz et al., 2016; Becker & Wittmann, 2019).

The distribution of monolignols exhibits notable variations depending on the plant types (Ponnusamy et al., 2019). Softwoods lignin is composed of majority of 90-95% of coniferyl alcohol (G unit), whereas grasses and hardwoods include 75% and 50%, respectively. Sinapyl alcohol (S unit) is mainly found in hardwoods (50%), observed in low contents in softwoods (5-10%) and grasses (25%). In contrast, *p*-coumaryl alcohol (H unit) found in softwoods (5%) (Brunow, 2005; Ponnusamy et al., 2019).

2.1.1.3 Microbial utilization of lignin-derived monomers

The biotechnological valorisation of lignin requires depolymerization steps, achieved through thermal, chemical, or biological processes (Fig. 1) (Chio et al., 2019; N. N. Zhou et al., 2022). This heterogeneity of lignin types and depolymerization processes leads to diverse variation in the production of aromatic monomers (Abdelaziz et al., 2016; Lancefield et al., 2016; Schutyser et al., 2018) including ferulate, *p*-coumarate, caffeate, catechol, guaiacol, among others (Becker &

Wittmann, 2019; Weiland et al., 2022). In order to overcome selective valorisation of lignin, “biological funnelling” using microorganism has been explored, allowing production of uniform compounds (Linger et al., 2014).

In bacterium, *p*-coumaryl alcohol, caffeoyl alcohol, coniferyl alcohol, and cinnamoyl alcohol are funnelled into either catechol or protocatechuate as main intermediates, and further processed into central metabolism by cleaving aromatic ring structure (Becker & Wittmann, 2019; Mohammad & Bhukya, 2022; R. Zhang et al., 2019) (Fig. 2).

The ring-cleavage pathways of catechol and protocatechuate are highly conserved and well-characterized in diverse bacteria (Harwood & Parales, 1996). Protocatechuate is cleaved at three different sites by distinct enzymes: 2,3-dioxygenase, 3,4-dioxygenase, and 4,5-dioxygenase, respectively. The 2,3-cleavage of protocatechuate leads to formation of 5-carboxy-2-hydroxy-muconate semialdehyde which is ultimately converted into acetyl-CoA and pyruvate, consuming 2 NAD and yielding 2 NADH (Kasai et al., 2009). The 3,4-cleavage of protocatechuate, widely distributed and the major aromatic degradation pathway among soil bacteria, involves catalysis of protocatechuate into 3-carboxy-*cis, cis*-muconate by protocatechuate 3,4-dioxygenase. This compound is then processed via β-ketoadipate pathway, yielding acetyl-CoA and succinyl-CoA (Iwagami et al., 2000). Protocatechuate 4,5-dioxygenase catalyses protocatechuate to 4-carboxy-2-hydroxy-muconate semialdehyde, consuming 1 NADP and ultimately resulting in production of 1 NADPH and 2 pyruvates (Masai et al., 2007).

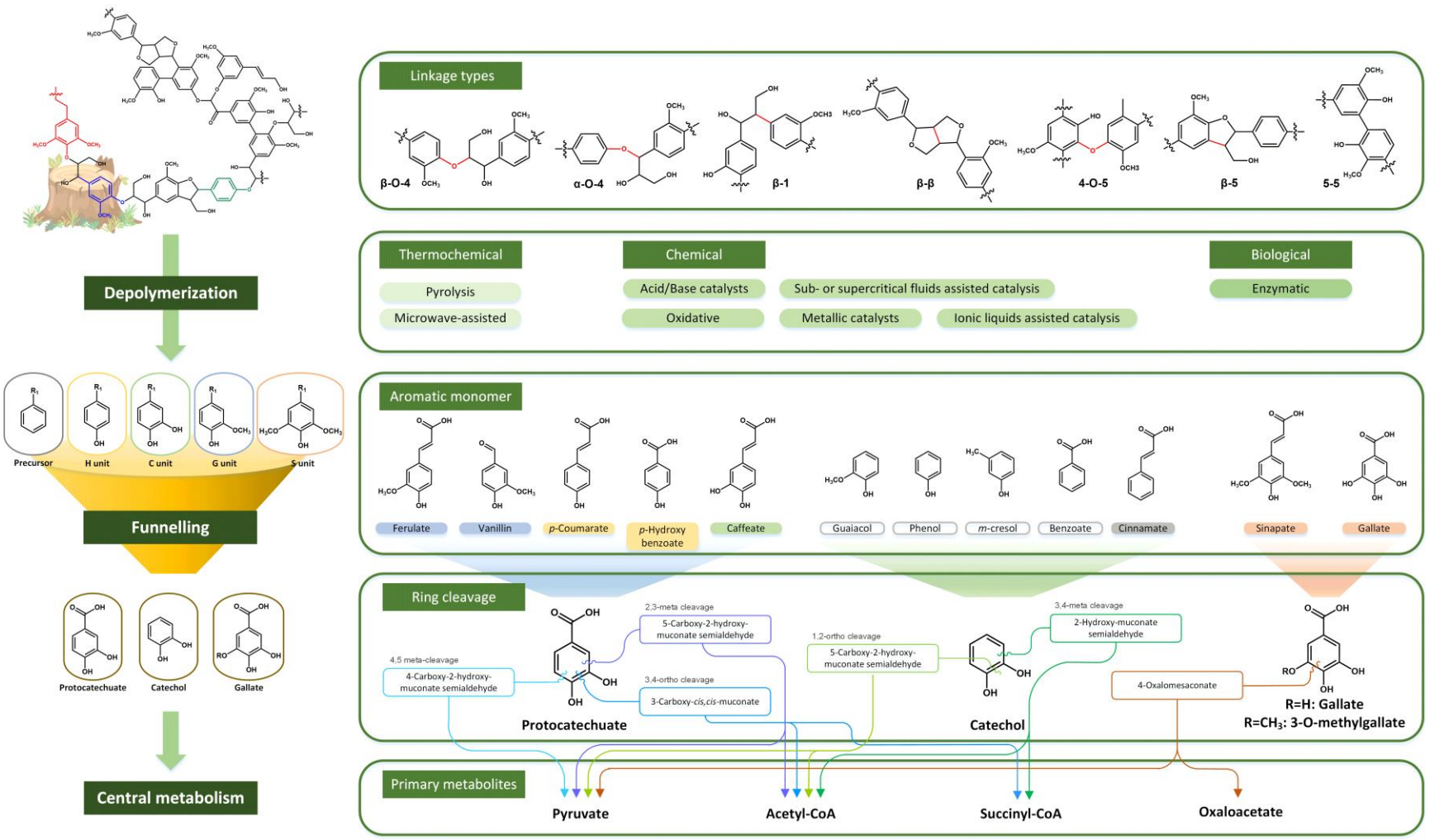

Figure 1. Biotechnological lignin valorisation using microbial cell factories. Lignin is a complex polymer composed of phenylpropanoids linked via diverse C-O and C-C bonds. Lignin undergoes depolymerization through thermochemical, chemical, and biological methods, yielding a variety of aromatic monomers. Microorganisms channel these aromatics into three main intermediates: protocatechuate, catechol, and gallate, which are further degraded via ring-opening processes and utilized in central metabolism.

In case of catechol, 1,2-(*ortho*) cleavage pathway provides a more efficient conversion of carbon to biomass while 2,3-(*meta*) cleavage of catechol is only feasible when 1,2-cleavage pathway is not available (Aghapour et al., 2013). By catechol 1,2-dioxygenase, catechol is converted to *cis, cis*-muconate, and is further processed to generate acetyl-CoA and succinyl-CoA through β-ketoadipate pathway. The 2,3-cleavage of catechol, initiated by catechol 2,3-dioxygenase, leads to production of acetyl-CoA and pyruvate, using 2 NAD and resulting in 2 NADH. Gallate and 3-*O*-methylgallate are exclusively observed in the degradation pathway of sinapyl alcohol, such as sinapate and syringate, resulting in the formation of 4-oxalomesaconate or 2-pyrone-4, 6-dicarboxynate, respectively. These compounds are intermediates in the protocatechuate 4,5-cleavage pathway, ultimately yielding 2 pyruvates.

On contrast, the conversion of primary lignin metabolites to main intermediates, often called the “upper pathway”, significantly differs depending on microorganisms. In general, the degradation of the lignin metabolites is classified into four categories: (1) CoA dependent β-oxidation pathway, (2) CoA dependent retro-aldol reaction, (3) CoA independent retro-aldol reaction and (4) CoA independent side chain reduction (Gallage & Møller, 2015; Priefert et al., 2001; Z. Xu et al., 2019).

Phenylpropanoids are first converted to their respective aromatic CoA thioesters by ligase in the CoA-dependent reaction (Fig. 2). These aromatic CoA thioesters are further hydrated to form 3-hydroxy-aromatic CoA thioesters, which are further oxidized to 3-oxo-aromatic CoA thioesters in β-oxidation pathway (1) or produce aldehydes by release of acetyl-CoA via retro-aldol reaction (2). In the CoA-independent pathways, the phenylpropanoids are converted to 3-hydroxy-molecules, then form aldehydes by removal of acetate on side chain (3) or simply reduced (4) to yield C_2-side chain shortened molecules before forming protocatechuate (Fig. 3).

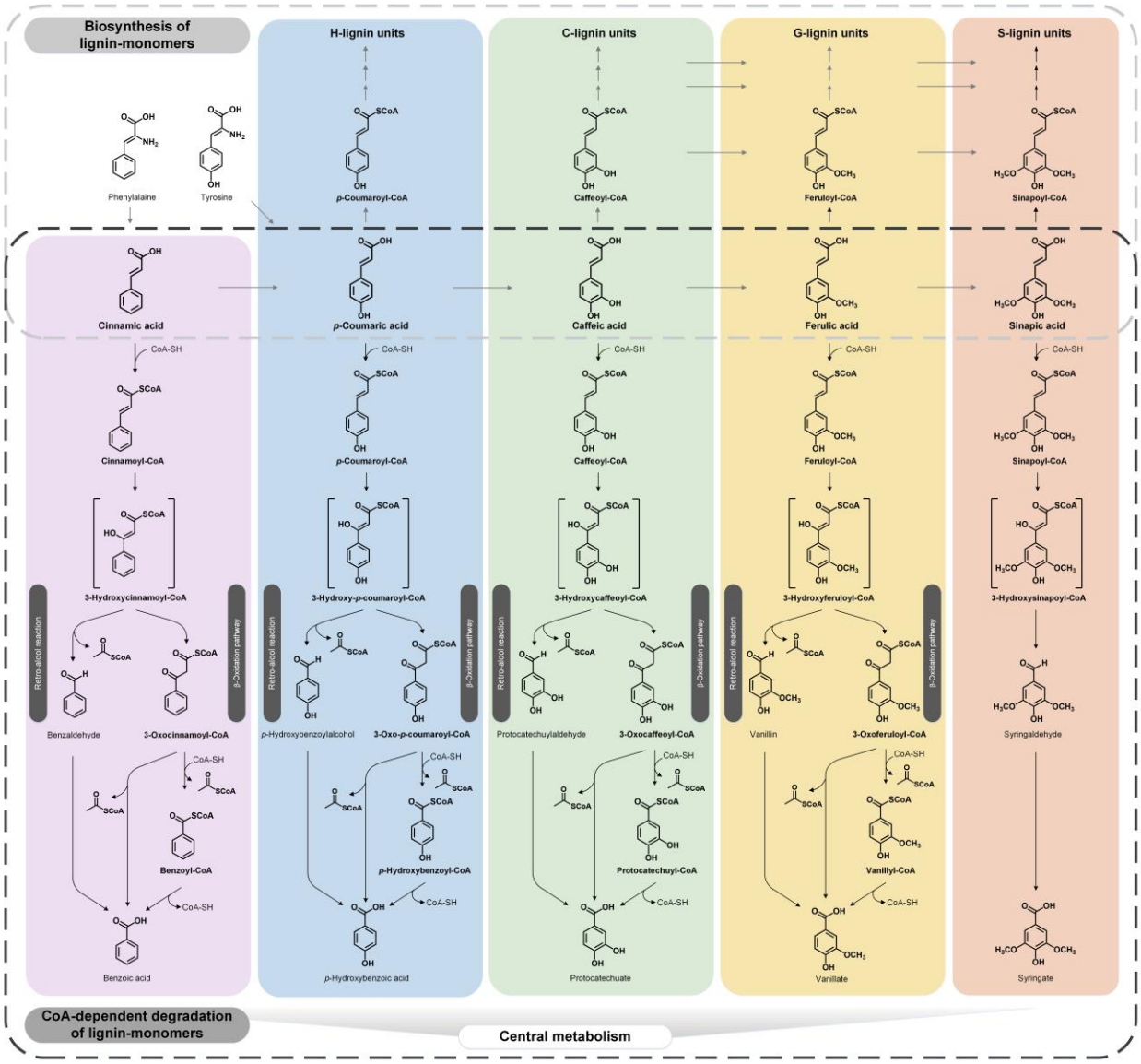

Figure 2. The CoA thioester-coupled metabolism of lignin monomers. The biosynthesis and degradation of lignin monomers extensively involve the formation of aromatic CoA thioesters. The biosynthesis of lignin monomers begins from phenylalanine or tyrosine, which are converted into cinnamate and *p*-coumarate, respectively. In the biosynthesis of lignin monomers (indicated with grey line), cinnamate is converted into *p*-coumarate, which is subsequently converted into caffeate, ferulate, and sinapate. All aromatic monomers are converted into their respective CoA thioesters, ultimately polymerized to form lignin structure. The CoA-dependent degradation of lignin monomers (indicated with black line) involves either a retro-aldol reaction or β-oxidation, which can optionally undergo *O*-demethylation depending on the presence of methoxy group, before entering central metabolism.

The β-oxidation cycle reaction has been extensively studied in fatty acid degradation (Kallscheuer et al., 2016). In general, the β-oxidation of fatty acid is initiated with CoA-activation and yield acyl-CoA thioesters by ATP-dependent ligase, and further catalysed to *trans*-enoyl-CoA via dehydration. Sequentially, 3-hydroxyacyl-CoA is formed by an addition of water molecule, then 3-hydroxyl group of the molecule is oxidized to form 3-oxoacyl-CoA. The 3-oxoacyl-CoA is cleaved into two molecules: acetyl-CoA and $acyl_{n-2}$-CoA by thiolase.

The β-oxidative degradation of aromatics is a branch of β-oxidation cycle reaction (Świzdor et al., 2012). For example, similar to fatty acid degradation, ferulate is catalysed to feruloyl-CoA using ATP and CoA-SH, and hydrated to 3-hydroxyferuloyl-CoA afterwards. Subsequently, the 3-hydroxyferuloyl-CoA is oxidized to yield 3-oxoferuloyl-CoA. The 3-oxoferuloyl-CoA is further divided into vanillyl-CoA ($acyl_{n-2}$-CoA) and acetyl-CoA by thiolase or to vanillate and acetyl-CoA by hydrolase.

The CoA-dependent β-oxidation of phenylpropanoids via hydrolysis has been reported in *R. jostii* RHA1 (Sainsbury et al., 2013), *A. fabrum* (Campillo et al., 2014), and *A. niger* (Lubbers et al., 2021) while *Rhodococcus* sp. I24 (Plaggenborg et al., 2006) encodes 3-ketoacyl thiolase, implying degradation through the formation of vanillyl-CoA.

The retro-aldol reaction during hydroxycinnamate degradation occurs both in the CoA-dependent and independent pathways. Analogous to the CoA-dependent β-oxidation pathway, hydroxycinnamates are CoA-activated as the first step of CoA-dependent retro-aldol reactions. In this pathway, the side chain of 3-hydroxyacyl-CoA is simply cleaved off, producing acetyl-CoA and an aldehyde. Conversely, the CoA-independent retro-aldol reactions occur in the same manner as CoA-dependent retro-aldol reactions but without CoA activation, resulting in the release of acetate instead of acetyl-CoA. Vanillin is a common intermediate of the retro-aldol reaction during ferulate degradation, formed by cleavage of the side chain of 3-hydroxy-feruloyl-CoA or 3-hydroxy-ferulate, producing of acetyl-CoA or acetate, respectively.

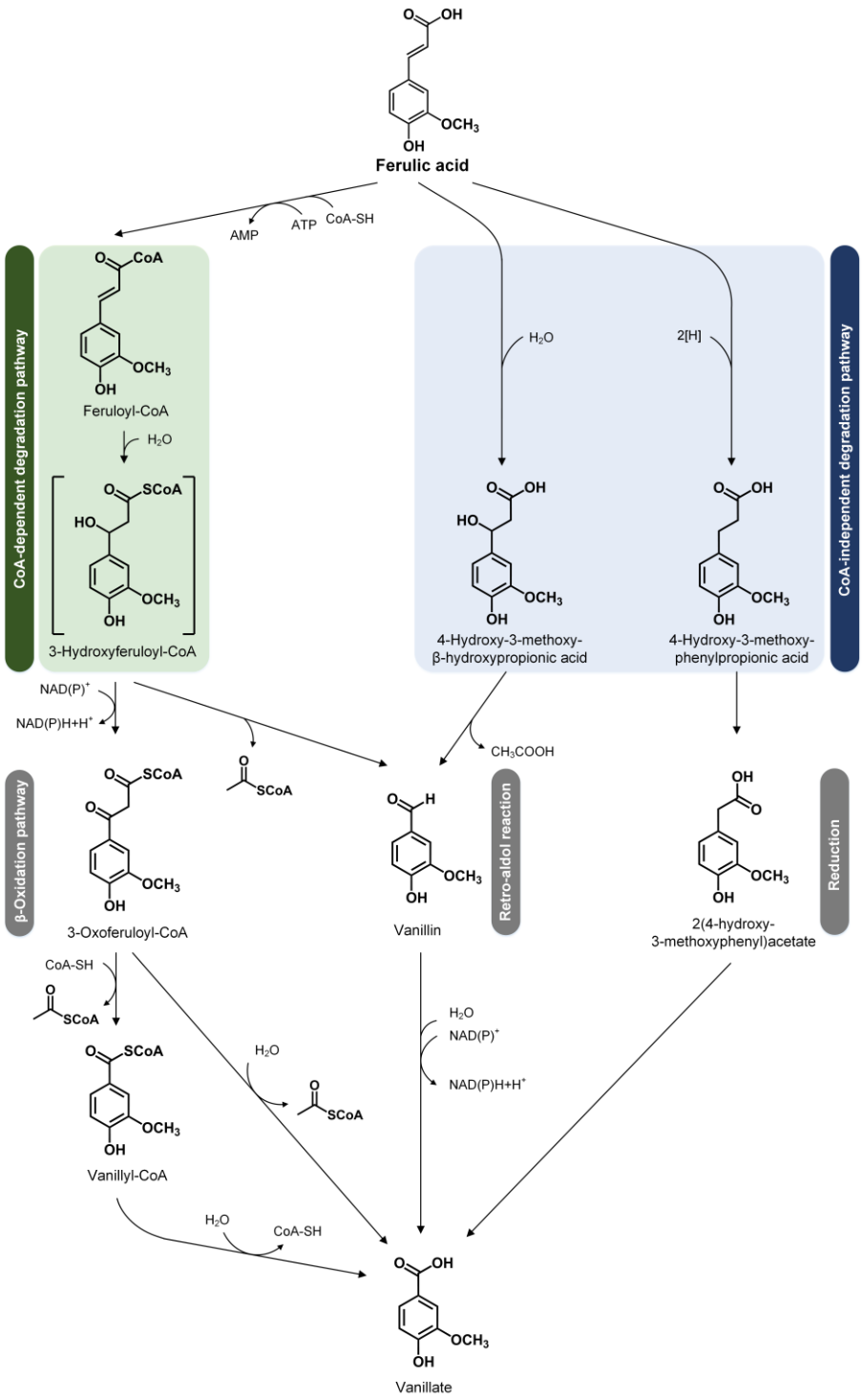

Figure 3. The degradation pathway of ferulate. The microbial degradation of ferulate can be achieved via CoA dependent β-oxidation pathway (1), CoA dependent retro-aldol reaction (2), CoA independent retro-aldol reaction (3), and CoA independent side chain reduction (4). In the CoA-dependent pathway, ferulate is first converted into feruloyl-CoA (highlighted with green), then further converted to vanillate via a β-oxidation pathway (1) or a retro-aldol pathway (2, non β-oxidation pathway). In CoA independent pathway (highlighted with blue), ferulate is degraded via retro-aldol reaction (3) or reduction (4).

The CoA-dependent retro-aldol reaction is the most abundant phenylpropanoid degradation pathway in bacteria (Priefert et al., 2001), identified in *P. fluorescens* (Narbad & Gasson, 1998), *Pseudomonas* sp. HR199 (Priefert et al., 1999), *Amycolatopsis* sp. strain HR167 (Achterholt et al., 2000), *D. acidovorans* (Plaggenborg et al., 2001), *S. paucimobilis* SYK-6 (Masai et al., 2002), *P. putida* KT2440 (Plaggenborg et al., 2003), *Streptomyces* sp. strain V-1 (Yang et al., 2013), and *N. aromaticivorans* DSM12444 (Cecil et al., 2018).

The CoA-independent retro-aldol reactions of phenylpropanoid degradation was identified in *P. acidovorans* (Toms & Wood, 1970), *B. subtilis* (Gurujeyalakshmi & Mahadevan, 1987), *S. cerevisiae*, *P. fluorescens* (Huang et al., 1993), and *P. mira* (Jurková & Wurst, 1993). Interestingly, *C. glutamicum* ATCC 13032 (Brinkrolf et al., 2006; Kallscheuer et al., 2016; Merkens et al., 2005), *R. opacus* PD630 (Cai et al., 2020), and *Amycolatopsis* sp. 39116 (F. Meyer et al., 2018) possess both β-oxidation and retro-aldol reactions, complementing each other.

Side chain reduction is exclusively observed under anaerobic conditions (Rosazza et al., 1995). The reaction is initiated by the hydride attack on a quinoid intermediate, resulting in the saturation of the side chain and formation of phenylpropionate. The reduction of hydroxycinnamate is catalysed in *P. cepacia* (Andreoni et al., 1984) and *W. succinogenes* (Ohmiya et al., 1986).

2.1.2 Seaweeds as a third-generation renewable feedstock

Marine macro-algae, commonly known as seaweeds, are multicellular, eukaryotic, and autotrophic chlorophyll-containing organisms, categorized into three main groups: Chlorophyta (green algae), Rhodophyta (red algae), and Phaeophyceae – Ochrophyta (Brown algae) (El Gamal, 2010). They are distributed horizontally in oceans depending on geometric, biotic, and abiotic conditions (Zhao et al., 2022). Green seaweeds, such as *Chaetomorpha*, *Codium, Enteromorpha, Ulva*, and *Caulerpa*, are located in intertidal zone whereas brown seaweeds including *Sargassum*, *Laminaria*, *Dictyota*, and *Turbinaria*, occupy tidal or upper subtidal zones and red seaweeds including

Gracilaria, *Ceramium*, *Acanthophora*, *Gelidiella*, and *Eucheuma*, are typically found in subtidal waters (Doty, 1946).

2.1.2.1 Production of Seaweeds

Seaweeds are acquired through both in ocean farming and wild harvest. The production of seaweeds has increased exponentially over the decades, from 0.56 million (wet) tonnes in 1950 to 35.8 million (wet) tonnes in 2019 (FAO, 2021). In 2021, over 97% of seaweed and microalgae production occurred in Asia countries, predominantly 56.8% in China, 27.8% in Indonesia and 5% in the Republic of Korea. Despite the presence of over 10,000 seaweed species in the marine environments, only 48 species are cultivated or harvested. Brown seaweeds, particularly *Laminaria*, *Saccharia* (Kombu), and *Undaria*, along with red seaweeds including *Kappaphycus*, *Eucheuma*, *Gracilaria*, *Porhyra* (Nori), and *Pyropia* dominate over 99% of total seaweed production, valued at 33.1 million USD (FAO, 2021). Over 70% of seaweeds is consumed as foods, while the remaining 30 % is utilized as feed, or processed for the extraction of ingredients such as polysaccharide, proteins, lipids, and pigments (Torres et al., 2019). In terms of wild collection, *Sargassum* grows freely from Caribbean and the north equatorial Atlantic to the west coast of Africa and Guinea, forming gigantic belts (Gower & King, 2019). Since 2011, an increase in the size and density of *Sargassum* mats has been observed, likely due to climate change. Despite of the natural formation of massive seaweed mats, the percentage of wild harvest seaweeds is limited to about 1 million (wet) tonnes, compared to 34.7 million (wet) tonnes of cultivated seaweeds (FAO, 2021).

2.1.2.2 Chemical Composition of Seaweeds

Seaweed biomass can vary intraspecies based on cultivation conditions such as temperature, light and seasons (Vilg et al., 2015). Seaweed biomass consists of mainly carbohydrates, mannitol, proteins, and minerals, constituting over 70% of total contents (Olsson et al., 2020). Particularly, brown seaweeds contain relatively high levels of phlorotannin and other phenolic compounds,

comprising up to 30 % of total dry weight (Stiger-Pouvreau et al., 2014). The carbohydrates and mineral contents in seaweeds varies by species (Olsson et al., 2020). Mannitol and protein concentrations also exhibit significant species-specific variations. For example, *Rhodophyta* (red seaweeds) contain high levels of proteins ranging from 100 to 200 g kg^{-1} dry weight and lacks mannitol, while *Phaeophyceae* (brown seaweeds) encompass approximately 59 to 120 g kg^{-1} dry weight of proteins and mannitol concentrations ranging 24 to 197 g kg^{-1} dry weight (Olsson et al., 2020). Apart from free carbohydrates like mannitol, seaweed carbohydrates are predominantly composed of monosaccharides bound by various glycosidic linkages, resulting in structurally diverse polysaccharides across different seaweed species (Salehi et al., 2019). Unlike terrestrial biomass, seaweeds contain either absence or very low amounts (less than 8% mass of dry biomass) of lignin, promoting efficient valorisation using microbial cell factories (Sadhukhan et al., 2019).

2.1.2.3 Applied and relevant use of seaweeds

Seaweeds are considered as a third-generation renewable feedstock due to their rapid grow rate, minimal interventions requirements (Poblete-Castro et al., 2020), and contribution to atmospheric carbon sink (Sayre, 2010). Apart from their traditional uses in food, biofertilizers, and medicine, seaweeds contain valuable industrial chemicals (Leandro et al., 2019) (Table 1). Phycocolloids such as agar, alginate, and carrageenan are polysaccharides that serve as gelling agents and find applications as food additives, cosmetic ingredients, and in pharmaceuticals (Lomartire & Gonçalves, 2023; Poblete-Castro et al., 2020). Besides polysaccharides, bioactive molecules including proteins, antioxidants, pigments, lipids, and polyunsaturated fatty acids are extracted from seaweeds.

Table 1. Industrially important seaweed-derived bioactive molecules beneficial for human health.

Type of compounds	Compound	Property and usage	Reference
Polysaccharides	Agar	Gelling agents/Food	(Lomartire & Gonçalves, 2023)
	Cellulose	Paper/Pulps/Textiles Pharmaceutical/Cosmetic/Food	(Baghel et al., 2021)
	Carrageenan	Anti-viral/Anti-tumour Pharmaceutical/Cosmetic/Food	(Lomartire & Gonçalves, 2023)
	Fucoidan	Anti-oxidant/Anti-viral/Anti-tumour Anti-inflammatory	(Song et al., 2020)
	Alginate	Anti-bacterial/Anti-inflammatory Thickener/Stabilizer/Colloidal agent	(Aliste et al., 2000)
	laminarin	Anti-bacterial/Anti-viral Antioxidant/Prebiotic	(Choudhary et al., 2021)
Proteins/ Amino acids	Lectin	Anti-viral Cancer biomarker/Drug delivery	(Bleakley & Hayes, 2017) (Choudhary et al., 2021)
	Phycobiliproteins	Natural dye/Anti-oxidant Anti-viral/Anti-tumour/ Anti-inflammatory	(Bleakley & Hayes, 2017) (Choudhary et al., 2021)
	Acidic amino acids	Dietary	(Aguilera-Morales et al., 2005)
Pigments	Fucoxanthin	Anti-obesity/Anti-proliferative	(Woo et al., 2009)
	β-Carotene	Anti-oxidant/Anti-inflammatory/ Anti-obesity/Anti-tumour	(Tan & Norhaizan, 2019)
	Chlorophyll *a*	Anti-oxidant/Anti-inflammatory/ Anti-obesity/Anti-cancer	(Chen et al., 2017)
Polyphenol	Phlorotannin	Anti-oxidant/Anti-inflammatory/ Anti-proliferative	(Dutot et al., 2012)
Fatty acids	Omega-3	Nutritional	(Choudhary et al., 2021)
	Omega-6	Nutritional	(Choudhary et al., 2021)

In terms of biorefinery processes, seaweeds require relatively mild pretreatment due to lignin-free nature. Research on seaweed biorefinery primarily aims to replace petrochemicals, particularly in energy (biofuel) production. The energy (biofuel) production from seaweeds has been extensively discussed (Torres et al., 2019). The electricity selling price from seaweeds is evaluated at USD 154 per MWh, which is relatively lower than existing thermal sources (USD 250 ± 10 MWh) (Yong et al., 2022). With the growth of aquaculture systems, it is projected that 0.3 billion wet tonnes of seaweeds can be generated alongside additional seafood harvesting (0.5 billion wet tonnes). Macroalgae-for-energy has the potential to generate a worth of USD 30 billion per year at USD 100 per dry tonnes (Capron et al., 2020). Regarding biofuels, anaerobic digestion of seaweeds has been explored for production of biomethane (Tabassum et al., 2017), ethanol (Chades et al., 2018; Sasaki et al., 2018; I. Sunwoo et al., 2019; Xia et al., 2015), biodiesel (X. Xu et al., 2014),

and butanol (X. Hou et al., 2017; Potts et al., 2012; I. Y. Sunwoo et al., 2018). However, the studies have been conducted on a laboratory scale, yet achieving optimal yields remains a challenge.

Currently, the size of the seaweed farms exclusively for biofuel production is not available, with the industry heavily dependent on high-value native products, including bioactive compounds derived from seaweeds (Yong et al., 2022). As seaweed biomass comprises predominantly carbohydrates, mannitol, and proteins, which are conventional substrates for microorganisms, allowing an option to valorise seaweeds for other high-value products from seaweeds and seaweed industry wastes using microbial cell factories (Poblete-Castro et al., 2020).

Despite of challenges including variation of carbohydrates, pre-requisition of polysaccharide degradation, or mixture of sugars, a cascaded valorisation of seaweed using microbial cell factories such as production of lactate (Mazumdar et al., 2014), L-lysine (Hoffmann et al., 2021), and riboflavin (Pérez-García et al., 2022) has been successfully demonstrated, opening up opportunities for utilizing industrial wastes from seaweed products.

2.1.2.4 Microbial utilization of mannitol

Mannitol, a six-carbon sugar alcohol, is utilized as a storage compound and can comprise up to 30% of the composition in brown seaweed (Peng et al., 2011; Reed et al., 1985). Typically, mannitol is used as a carbon source for cultivation of *Streptomyces* (Quinn et al., 2020) and in the production of natural products, including geosmin (Schrader & Blevins, 2001) and streptomycin (Dulaney, 1949).

Compared to glucose, which is a common substrate for microbial cell factories, the utilization of mannitol can lead to the relief of carbon catabolite repression (CCR). *In Pseudomonas* species, where glucose is the preferred carbon source, the presence of mannitol induces the binding of CrcZ, a small RNA, to the RNA-binding protein Crc. This interaction results in the release of mRNA from Crc-mediated translational repression, allowing for the expression of genes involved in

utilizing alternative carbon sources like mannitol (Sánchez et al., 2010). In *Streptomyces*, deletion of *bld* genes influenced on carbon-source dependent gene regulation as well as formation of secondary metabolites and aerial mycelium. When grown on mannitol instead of glucose, the repression of specific *bld* genes like *bldA*, *bldG*, and *bldH* is relieved differently. This shift can affect the formation of aerial mycelium and the production of secondary metabolites in *Streptomyces* strain(Sánchez et al., 2010).

Intriguingly, microbial catabolism and uptake of mannitol varies significantly depending on the microorganism involved. In bacteria, mannitol is taken up by three different types of transporters: phosphotransferase system (PTS), ATP-binding cassette (ABC) transporters, or major facilitator superfamily (MFS) transporter.

Mannitol is phosphorylated into mannitol 1-phophate during transportation to the cytoplasm through mannitol-specific PTS system. Once inside the cytoplasm, mannitol 1-phosphate is converted to fructose 6-phosphate by mannitol 1-phosphate dehydrogenase (Novotny et al., 1984), and further utilized in glycolysis. The mannitol-specific transporter has been discovered in *E. coli* (Postma et al., 1993), *B. subtilis* (Watanabe et al., 2003), *B. stearothermophilus* (Henstra et al., 2000), *A. baylyi* (Sand et al., 2013), *C. acetobutylicum* (Behrens et al., 2001), and *S. mutans* (Honeyman & Curtiss, 1992).

In case of *P. fluorescens* (Brünker et al., 1998), *P. inhibens* (Wiegmann et al., 2014), and *Z. galactanivorans* (Groisillier et al., 2015), mannitol is transported into the cytoplasm via ABC transporter and converted into fructose by mannitol 2-dehydrogenase. Subsequently, fructose is likely further converted into fructose 6-phosphate by fructokinase, with the corresponding gene located in the mannitol catabolic operon, then enters into glycolysis.

In contrast to other bacteria, mannitol is transported through the MFS mannitol transporter (*MtlT*) in *C. glutamicum*, and then oxidized to fructose by mannitol 2-dehydrogenase (*MtlD*). Interestingly,

fructose appears to be excreted outside the cell and subsequently re-uptaken by the fructose-specific PTS transporter (*PtsF*) and converted into fructose 1-phosphate, which is then phosphorylated into fructose 1,6-bisphosphate by 1-phosphofructokinase (*PfkB*) (Peng et al., 2011). Ultimately, fructose enters glycolytic metabolism through double phosphorylation by the fructose-specific PTS transporter and 1-phosphofructokinase, compensating for the absence of fructokinase (Dominguez & Lindley, 1996).

2.2 Products: From renewable feedstocks to natural products

Natural products (NPs) represent a diverse array of chemical structures with significant biological activities, synthesized through complex enzymatic systems. Importantly, they serve as major sources of therapeutics, including anti-cancer, anti-infection, anti-inflammation, and immunosuppressive agents, providing significant benefits to human health (D. Park et al., 2021; Pham et al., 2019).

The majority of NPs is produced by bacteria, especially family *Actonomycetaceae* (Bérdy, 2012). Currently, the production of NPs by microorganisms heavily relies on food-based feedstocks (Drescher & Kienberger, 2022; Ögmundarson et al., 2020). The food-based carbon substrates such as glucose and starch, as well as protein substrates including soybean, yeast extract, and peptones are commonly used in microbial cell factories for the production of NPs due to their availability and ability to support robust growth and metabolite production (Ahsan et al., 2017; Elibol, 2004; Lichtenthaler & Peters, 2004; Wang et al., 2011). However, despite high technological readiness levels of agricultural feedstocks (Ögmundarson et al., 2020), it has raised concerns about their impact on the competition for land-use (Jong et al., 2020; Straathof et al., 2019), demanding the development of sustainable alternative feedstock utilization.

The synthesis of NPs using renewable feedstocks is an emerging area of research that holds promise for sustainable production of high-value pharmaceuticals and other valuable compounds. While there has been significant progress in utilizing renewable feedstocks like lignin-derived monomers for green chemical synthesis of active pharmaceutical ingredients (APIs), such as paracetamol, aspirin, and amoxicillin (J. Park et al., 2021), the focus on microbial cell factories for NP synthesis from advanced renewable sources has been relatively limited.

Moving forward, expanding research efforts into microbial cell factories for NP synthesis, specifically focusing on two major classes — polyketides (PKs) and ribosomally synthesized and post-translationally modified peptides (RiPPs) — from renewable feedstocks, could lead to innovative processes addressing sustainability concerns in pharmaceutical production. This includes exploring the metabolic capabilities of microorganisms to efficiently convert renewable substrates into complex pharmaceuticals, thereby reducing reliance on traditional feedstocks and contributing to a more sustainable pharmaceutical industry.

2.2.1 Bottromycin as a promising antimicrobial peptide

In general, RiPPs are considered as a major class of NPs together with PKs, non-ribosomal peptides (NRPs), and isoprenoids (D. Park et al., 2021). The biosynthesis of RiPPs involves peptides ranging from ~20 to 110 residues of proteinogenic amino acids, which are then post-translationally modified by enzymes, resulting in a vast diversity of structures (Arnison et al., 2013). At the genomic level, the biosynthetic genes responsible for RiPPs in bacteria are typically clustered at a single locus. This biosynthetic cluster of RiPPs includes a gene for the precursor peptide and a series of genes encoding enzymes that facilitate post-translational modification. In most cases of RiPP biosynthesis, the precursor peptide consists of a core peptide that serves as the scaffold for the final product, along with a leader peptide located at the N-terminus of the core peptide. The leader peptide acts as a recognition signal for post-translational enzymes and is

eventually removed by proteases (Skinnider et al., 2016). RiPPs encompass a wide range of natural product such as lanthipeptides, proteusins, linear azol(in)e-containing peptides, cyanobactins, bottromycin, lasso peptides, microviridins, among others (Arnison et al., 2013)

Bottromycin

Bottromycin is a RiPP antibiotic effective against Gram-positive pathogens (Kobayashi et al., 2010; Waisvisz et al., 1957b) by inhibiting protein synthesis. In detail, bottromycin A_2 binds to aminoacyl-tRNA binding site (A site) of 50S ribosome in prokaryotes, thereby disrupting the correct positioning (Otaka & Kaji, 1976, 1981, 1983). The structure of bottromycin consists of a macrocycle heptapeptide formed from four amino acids via amidine linkage, C-methylated unnatural amino acids, D-aspartate, and an exo-thiazole (Franz et al., 2021). Bottromycin is naturally produced by several *Streptomyces* species including *S.* sp. BC16019 (Huo et al., 2012), *S. bottropensis* DSM 40262 (Gomez-Escribano et al., 2012), *S.* sp. WMMB272 (Y. Hou et al., 2012), and *S. scabies* (Crone et al., 2012), sharing a majority of the identical biosynthetic gene cluster (BGC) responsible for bottromycin production (Franz et al., 2021).

The BGC of bottromycin typically consist of 13 genes, including one precursor peptide (*botA*), MFS transporter (*botT*), regulatory protein (*botR*), *O*-methyltransferase (*botM*), cytochrome P450 (*botJ*), two YcaO-domains (*botC* and *botD*), three hydrolase-like proteins (*botH*, *botI*, *botP*), and three radical SAM methyltransferases (*botB*, *botG* and *botS*) (Crone et al., 2012; Franz et al., 2021; Huo et al., 2012) (Fig. 4B). Uniquely, the bottromycin precursor gene encodes a core peptide, (M)GPVVVFDC, and a follower peptide, which distinguishes it from other RiPP precursor peptides that consist of a leader peptide followed by a core peptide (Franz et al., 2021; Huo et al., 2012). The follower peptide acts as a recognition sequence, then is subsequently cleaved off with an act of amidohydrolase (BotI). The precursor peptide gene consists of 44 amino acids, 7 core peptides and 36 follower peptides in *S.* sp. BC16019, covering 14 amino acids in 20 canonical amino acids (Fig. 4A).

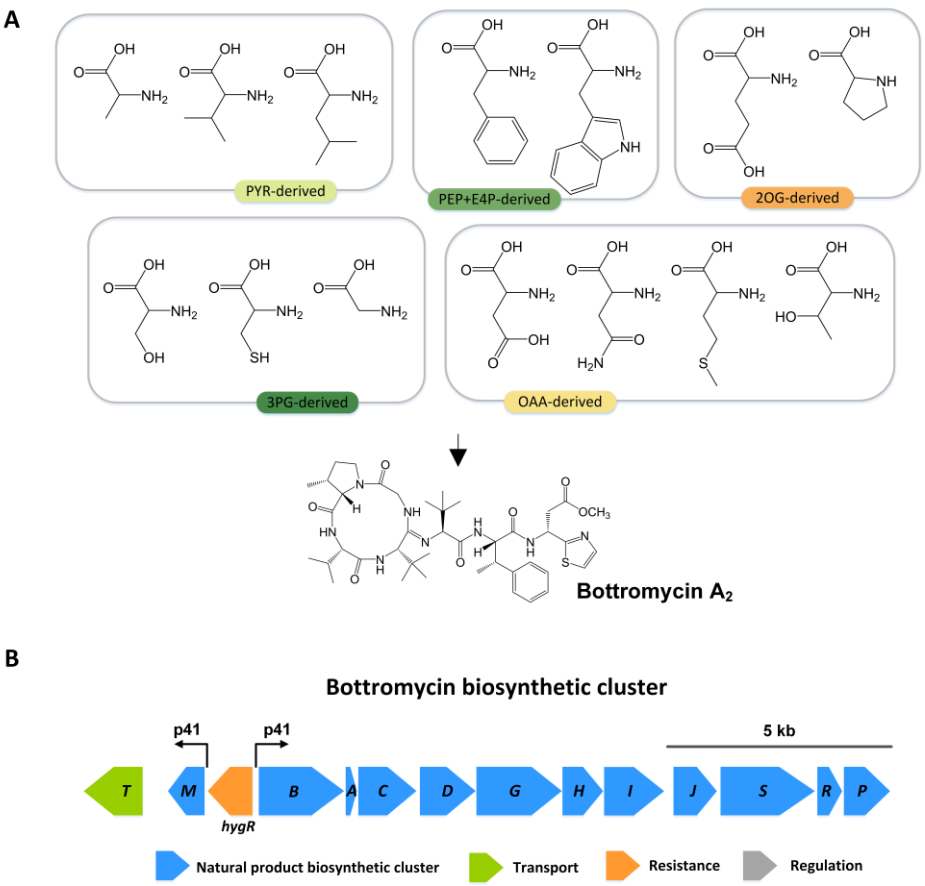

Figure 4. The origin and biosynthetic gene cluster (BGC) of bottromycin A_2. The biosynthesis of peptide antibiotic bottromycin requires 14 amino acids: alanine, valine, leucine (PYR-derived), phenylalanine, tryptophane (PEP+E4P derived), cysteine, glycine (3PG-derived), glutamate, proline (2OG-derived), and aspartate, asparagine, methionine, threonine (OAA-derived) (A). The bottromycin A_2 BGC used in this study, originally derived from *S.* sp. BC16019, was engineered by integrating P41 pair of synthetic promoters between *botM* and *botB* (Horbal et al., 2018) (B). The figure was modified from a previously published paper (Seo et al., 2023).

Despite of the early discovery of bottromycin in 1950s (Elgersma et al., 1955; Waisvisz et al., 1957a; Waisvisz et al., 1957b), its production in the lab-scale fermentation remains extremely low (Crone et al., 2012; Horbal et al., 2018; Huo et al., 2012), reaching approximately 20 µg L^{-1} in *S. coelicolor* A3(2) (Huo et al., 2012). Heterologous expression of bottromycin BGC has been explored in several studies to enhance the production of bottromycin.

The regulation of the bottromycin BGC was elucidated in *S. scabies*, revealing that transcriptional start sites are located in between *botM* and *botB*, with a transcriptional start site within *botB* (Vior et al., 2020). Heterologous expression of the bottromycin BGC from *S.* sp. BC16019 in *S. albus* J1024 and *S. coelicolor* A3(2) was demonstrated using a pOJ436-based cosmid library, successfully producing bottromycin A_2 (Huo et al., 2012). The cosmid library including the bottromycin BGC is further simplified by replacing a fragment of non-bot genes (5'-end) to a kanamycin resistance gene via Red/ET recombination (Gust et al., 2003), yielding a new cosmid termed DG2-kan (Huo et al., 2012). The DG2-kan derivate cosmids, containing random promoters mutated at the sequences of *ermE*p1 promoter, were employed for recombination in *S. lividans* TK24. As a result, the highest producer strain was named as *S. lividans* TK24 DG2-Km-P41hyg$^+$, proving bottromycin A_2 production at an average level of 3.3 fold higher than native *S.* sp. BC16019 and higher expression levels at 14 and 175 fold higher of *botT* and *botB*, respectively, compared to *S. lividans* TK24 DG2-Km$^+$ (Horbal et al., 2018). Besides extensive genomic modifications, medium optimization strategies were employed. For example, supplementation of microparticles into the cell culture successfully enhanced bottromycin production, leading to increases in yields by up to 13-fold (Kuhl et al., 2021).

2.2.2 Pamamycin – an antibiotic polyketide

Polyketides are synthesized through a series of decarboxylative Claisen condensation reactions with extender units, which consist of small carbon precursors such as malonyl-CoA, ethylmalonyl-CoA, and methylmalonyl-CoA, catalysed by polyketide synthases (PKSs). The mechanism of polyketide biosynthesis resembles that of fatty acid biosynthesis, both processes involving chain extension from simple acyl-CoA units through repetitive condensation reactions. The biosynthesis of PKs involves several modules, with the corresponding genes encoding enzymes typically clustered in the genome, forming a BGC (Cummings et al., 2014). The formation of polyketides scaffold includes several steps: initiation, chain extension, and product release. The backbone of

the polyketide is initiated by the selection and assembly of acyl-CoA units by the PKS, which consists of an acetyltransferase and an acyl carrier protein (ACP). Subsequently, the polyketide scaffold is extended with extender units that are loaded onto the acetyltransferase and ACP. Extender units are subsequently loaded onto the acyltransferase and ACP, facilitating backbone elongation. This process also employs ketosynthase, leading to the formation of a β-keto-acyl intermediate (Cummings et al., 2014). Other domains, such as dehydrogenase, enoylreductase, and ketoreductase, are accessory domains that increase the diversity of structures. Modules containing different domains are repeated, and the final product is ultimately released by thioesterase. The structural diversity of polyketides increases significantly during scaffold formation including choice of building blocks, chain length, modification of scaffold by reduction, cyclization, and alkylation, as well as rearrangements and secondary cyclization (Cummings et al., 2014).

Pamamycin

Pamamycins are a series of macrodiolide polyketide naturally produced by several *Streptomyces* species, including *S. alboniger* (Kondo et al., 1988). They exhibit antimicrobial activity against Gram-positive bacteria, including *Mycobacteria* and *Neurospora* (McCann & Pogell, 1979), as well as their specific inhibition of nucleoside uptake, adenine, uracil, and inorganic phosphate in *S. aureus* (Chou & Pogell, 1981). In addition, supplementation with pamamycins has been shown to induce the production of secondary metabolites in various *Streptomyces* spp. (Hashimoto et al., 2011). Chemically, pamamycins are characterized by 16-membered structures with varying side chains at six positions, leading to a range of molecular weights from 579 to 649 Da (Fig. 5A) (Hanquet et al., 2016; Kondo et al., 1988).

The BGC of pamamycin in *S. alboniger* consists of 18 genes, including a transporter gene (*pamW*), acyl-carrier protein (*pamC*), ketosynthases (*pamG*, *pamF*, *pamA*, *pamD*, *pamE*, *pamK*, and *pamJ*), acyltransferase (*pamB*), ketoreductase/dehydrogenases (*pamO*, *pamM*, *pamN*), CoA-ligase

(*pamL*), hydrolase (*PamH*), aminotransferase (*pamX*), methyltransferase (*pamY*), and hydratase (*pamS*) (Fig. 5B). PamA is involved in the initial condensation, utilizing succinyl-CoA with malonyl- or methylmalonyl-CoA to produce 3-oxoadipyl-CoA or methyl-3-oxoadipyl-CoA, which are the main intersection of primary metabolites and pamamycin biosynthesis (Rebets et al., 2015). The formation of pamamycin involves the incorporation of various extender units such as succinyl-CoA, malonyl-CoA, methylmalonyl-CoA, and ethylmalonyl-CoA, by PKSs (Rebets et al., 2015) (Fig. 5A). This diversifies the spectrum of pamamycin produced, enabling investigations into the pathways involved in CoA thioester-related pathways (Gummerlich et al., 2021). The deletion of genes responsible for precursor formation influences intracellular CoA thioester pools, thereby affecting the spectrum of pamamycins produced (Gummerlich et al., 2021).

Due to its intriguing chemical properties, pamamycin synthesis has been extensively explored both chemically and biologically. However, chemical synthesis is time-intensive and complex, while biological synthesis has shown low levels of pamamycin production, with the exception of pamamycin 607 (Hanquet et al., 2016). Recently, successful improvement in the fermentative production of pamamycin has been reported. The supplementation of microparticles to liquid culture of recombinant strain *S. albus* J1074/R2 has demonstrated an elevated production of pamamycins, approximately 3-fold higher (Kuhl et al., 2020). Moreover, targeted production of heavy pamamycins (Pam 635, Pam 649, and Pam 663) was achieved by enhancing the overall CoA thioesters content through the addition of L-valine (Gläser et al., 2021).

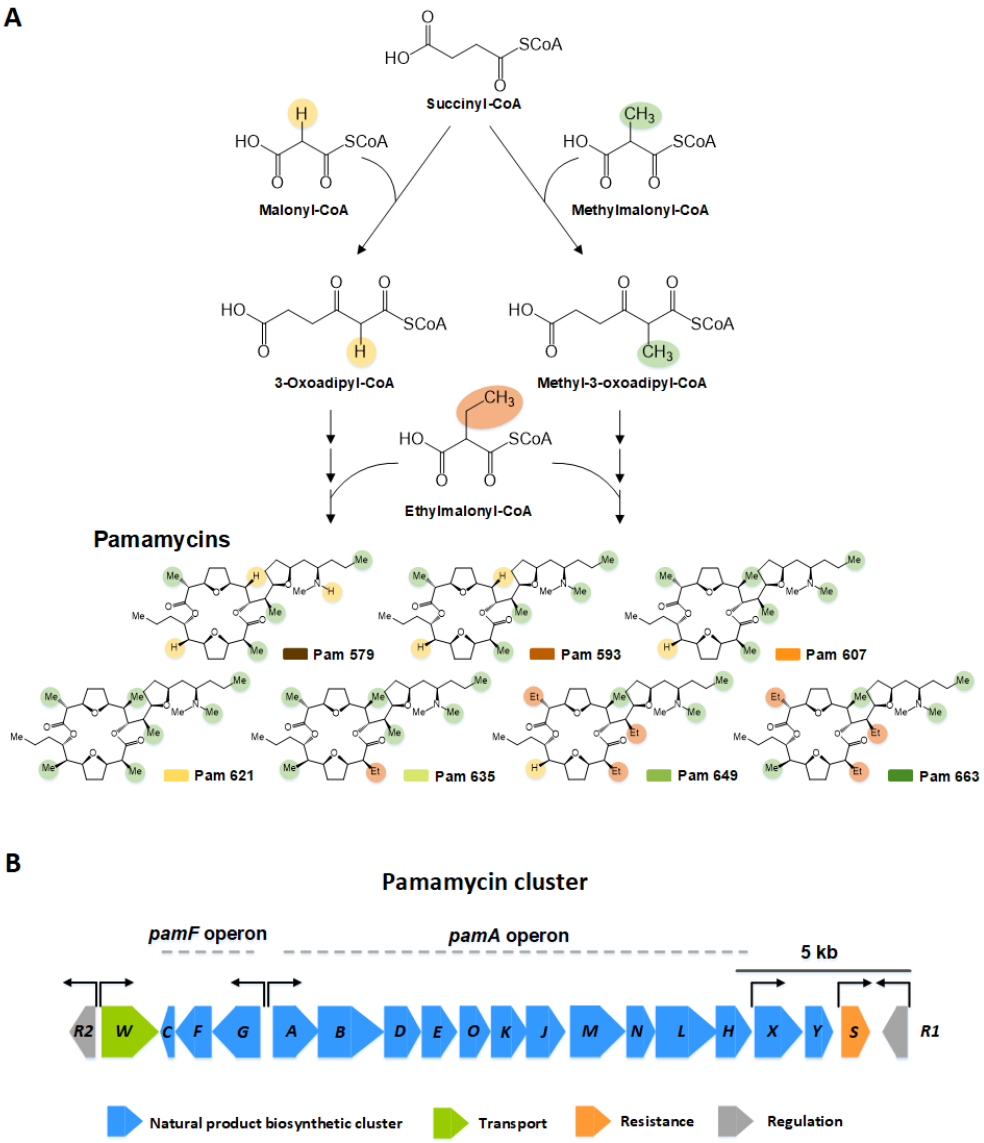

Figure 5. The microbial synthesis of pamamycin derivatives and biosynthetic cluster of pamamycin. Pamamycins are biosynthetically synthesized from 4 different CoA thioesters, including succinyl-CoA, malonyl-CoA, methylmalonyl-CoA, and ethylmalonyl-CoA (Rebets et al., 2015). During the synthetic process, the use of malonyl-CoA, methylmalonyl-CoA, and ethylmalonyl-CoA results in the incorporation of various side chains, producing pamamycin derivatives with molecular weights ranging from 579 to 663 Da (A). The pamamycin BGC, used in this study, was derived from *Streptomyces alboniger* DSMZ 40043 under control of native promoter (Rebets et al., 2015) (B) The figure was modified from a previously published paper (Seo et al., 2023).

2.3 Metabolic pathway analysis and microbial hosts

2.3.1 LC-MS/MS based acyl-CoA metabolism analysis

Acyl-CoA thioesters, such as acetyl-CoA, acetoacetyl-CoA, succinyl-CoA, and malonyl-CoA, are crucial intermediates in numerous biological pathways, including TCA cycle, fatty acid degradation, and ethylmalonyl-CoA pathway. Acetyl-CoA, in particular, serves as a vital C_2 precursor in central metabolism within biological systems. It is primarily produced from pyruvate, acetate, and fatty acid degradation and is consumed as an intermediate in the TCA cycle and fatty acid biosynthesis. Additionally, acetyl-CoA is also converted into acetate and ethanol, and assimilated into glyoxylate shunt (Krivoruchko et al., 2015). Biotechnologically, acetyl-CoA is a major precursor for fatty acids (Marella et al., 2018), polyhydroxyalkanoates (PHA) (Sagong et al., 2018), polyketides (Liu et al., 2019), and isoprenoids (Krivoruchko et al., 2015), leading extensive research on analysis and engineering on acyl-CoA metabolism (Alber, 2011).

Given the extensive utilization of LC-MS in metabolomic studies (B. Zhou et al., 2012), the profiling of acyl-CoA relies heavily on LC-MS analytics. Various extraction and separation methods have been devised to analyse acyl-CoA thioesters in different types of biological samples (Rivera & Bartlett, 2018). When applying positive mode $[M+H]^+$, multiple reaction monitoring (MRM) of acyl-CoA thioesters results in a neutral loss of 507 $[M+H-507]^+$, enabling selective analysis of CoA thioesters (Li et al., 2014; Palladino et al., 2012). The patterned fragmentation allows for untargeted screening and targeted analysis, facilitating the identification of anaerobic bacterium *Aromatoleum* sp. strain HxN1 and experimental proof of CoA thioester metabolism including fatty acid degradation, amino acid degradation, ethylmalonyl-CoA, and 3-hydroxypropanoyl-CoA pathways (Cakić et al., 2021). In addition, the intracellular acyl-CoA thioester pool have been analysed in diverse microorganisms, including *M. elsdenii* (Neubauer et al., 2015), *M. smegmatis*, *M. bovis*, *C. glutamicum*, and *S. coelicolor* (Cabruja et al., 2016).

As example, the intracellular CoA thioester pool was measured, providing evidence of improved production of polyketide based on acetyl-, butyryl-, and propionyl-CoA in heterologous production in engineered *E. coli* (Armando et al., 2012). Moreover, absolute quantification of the CoA thioester pool has been demonstrated to support improvement of pamamycin production by enhancing the precursor pool through modulation of branched-chain amino acid metabolism (Gläser et al., 2021) and the addition of microparticles (Kuhl et al., 2020).

Specific to the analysis of acyl-CoA thioesters related to the utilization of renewable feedstocks, aromatic CoA thioesters serve as key intermediates in bacterial aromatic degradation pathway, exhibiting wide chemical diversity depending on the availability of aromatic compounds and the specific catabolic pathways involved (Fig. 2). While genomic approaches have been extensively utilized to elucidate these pathways, metabolomic investigations have been relatively underexplored. One primary challenge in metabolomic studies of aromatic CoA thioesters is the lack of commercial availability of these molecules and their inherent chemical instability (Siegel et al., 2014).

Previously, a series of attempts to synthesize and detection in several organisms were performed. For example, feruloyl-CoA, cinnamoyl-CoA, caffeoyl-CoA, *p*-coumaroyl-CoA, and sinapoyl-CoA were synthesized using plant *p*-coumarate:CoA ligase (CL) and confirmed the mass of synthesized products via ESI-MS (Beuerle & Pichersky, 2002; Rautengarten et al., 2010). More recently, a broader range of aromatic CoA thioesters, including 4-hydroxybenzoate, anthranilate, and salicylate, were synthesized under mild conditions using bacterial aromatic CoA ligases (Chaudhury et al., 2023).

In terms of intracellular analysis, aromatic CoA thioesters have been investigated primarily in plants. In detail, aromatic CoA thioesters, particularly benzoyl-CoA, feruloyl-CoA, cinnamoyl-CoA, and *p*-coumaroyl-CoA, were extracted from petunia flower petals, and analysed using LC-MS/MS in negative ion mode, with a common fragment (m/z 408) shared among all acyl-CoAs (Qualley et

al., 2012a). Additionally, 3-oxocinnamoyl-CoA, an intermediate of β-oxidative pathway, was enzymatically synthesized and analysed using LC TOF/MS, suggesting that other unknown intermediates could be potentially detected. However, 3-hydroxycinnamoyl-CoA, an intermediate between cinnamoyl-CoA and 3-oxocinnamoyl-CoA, was not observed due to the bifunctionality of cinnamoyl-CoA hydratase-dehydrogenase (PhCHD) from petunia, which likely does not release 3-oxocinnamoyl-CoA (Qualley et al., 2012b).

2.3.2 *Corynebacterium glutamicum*

C. glutamicum is a gram-positive *Actinomycete* bacterium isolated from soil samples (Abe et al., 1967), and notably, it is a well-established strain for industrial production of amino acids, including L-lysine and L-glutamate (Becker & Wittmann, 2012), as well as organic acids and biopolymers (Wendisch et al., 2016). Beyond its applications in feed, food, and chemical production (Becker et al., 2018b), *C. glutamicum* is also utilized for the assimilation of toxic materials and soil/water bioremediation (Mateos et al., 2017), and is employed for inexpensive renewable feedstocks such as lignocellulose (Becker et al., 2018a), owing to its native substrate spectrum.

As *C. glutamicum* is an outstanding workhorse for industrial applications, its metabolic pathways have been extensively investigated, alongside multiple sequencing efforts of its genome by independent laboratories (GenBank NC_006958) (Kalinowski et al., 2003), Kyowa Hakko Kogyo Co., Ltd. (GenBank NC_003450), and Ajinomoto Co. (GenBank NC_004369) (Ray et al., 2022).

Based on its extensive genomic sequencing, the central metabolism of *C. glutamicum* has been well-characterized, encompassing glycolysis, the pentose phosphate pathway, the TCA cycle, the glyoxylate shunt, and gluconeogenesis (Kalinowski et al., 2003). As for the anaphoretic reaction of TCA cycle, carboxylation is facilitated by pyruvate carboxylase and phosphoenolpyruvate (PEP) carboxylase while decarboxylation is mediated by malic enzyme, PEP carboxykinase, and oxaloacetate decarboxylase (Wittmann, 2010). When growing on C_2 carbon sources such as

acetate, the glyoxylate shunt is activated. Specifically, isocitrate lyase converts isocitrate to glyoxylate and succinate, and malate synthase further catabolize glyoxylate to malate (Wendisch et al., 1997).

Interestingly, *C. glutamicum* lacks three key enzymes of β-oxidation: 3-ketoacyl-CoA thiolase (FadA), 3-hydroxyacyl-CoA dehydrogenase (FadB), and acyl-CoA dehydrogenase (FadE), indicating its incapability of fatty acid β-oxidation (Takeno et al., 2013). On the other hand, phenylpropanoid degradation is achieved through a CoA-dependent β-oxidative pathway in *C. glutamicum* via 3-hydroxyacyl-CoA intermediates (Kallscheuer et al., 2016).

In-depth investigation of *C. glutamicum* has enabled extensive engineering of the strain, broadening its substrate spectrum for the utilization of renewable feedstocks. *C. glutamicum* demonstrates the ability to consume lignocellulosic biomass components such as xylose, arabinose, mannose, mannitol, as well as aromatics, converting them into valuable chemicals including ethylene glycol, succinate, 3-hydroxypropionic acid, xylitol, and *cis*, *cis*-muconate (Becker et al., 2018a; B. Zhang et al., 2020).

2.3.3 *Streptomyces lividans*

S. lividans is a prominent filamentous *Actinomycete* bacterium in the field of natural product synthesis due to its exceptional genetic manipulability, low endogenous protease activity, compatibility with methylated DNA, strong secondary metabolic pathways, and capacity to secrete large quantities of proteins (Myronovskyi & Luzhetskyy, 2019). *S. lividans* TK24 has been instrumental to derive heterologous producers for natural products, such as tunicamycin, griseorhodin, and deoxycoformycin (Ahmed et al., 2020) as well as for the production of proteins including cellulase (Daniels et al., 2018) and human proteins (Bender et al., 1990).

As typical for the field, production relied on first generation substrates such as glucose, starch, yeast extract, and soytone (Horbal et al., 2018; Kuhl et al., 2021). Towards valorisation of next

generation raw materials, the microbe beneficially has a broad capable pathway available in its genome (GenBank CP009124) (Rückert et al., 2015). The closely related strain, *S. coelicolor,* has at least 53 potential carbohydrate uptake system including cellobiose, xylose, and maltose (Bertram et al., 2004). Furthermore, *S. lividans* contains the β-ketoadipate pathway, a key route in aromatic catabolism, though its role in growth on these substrates has not been experimentally investigated. Although not specifically tested for *S. lividans* before, mannitol appears as a generally well-accepted substrate for *Streptomyces* (Gläser et al., 2021; Kieser et al., 2000; Vicente et al., 2016). However, despite intensive usage of the strain, understanding of renewable substrates uptake and catabolic system in *S. lividans* remained limited.

3 CoA-thioester coupled aromatic degradation in *C. glutamicum*

3.1 Materials and Methods

3.1.1 Microorganisms and plasmids

E. coli BL21(DE3) (Thermo Fisher Scientific, Waltham, MA, USA) was used as a host strain for protein expression, utilizing plasmids pET-21a (Invitrogen, Carlsbad, USA) and pET-28a (Invitrogen) as expression vectors. *C. glutamicum* ATCC 13032 (WT) (Becker et al., 2011) and the MA-2 strain, a *cis, cis*-muconate producing strain (Becker et al., 2018a), were obtained from previous work used for cultivation and gene amplification. *N. aromaticivorans* DSM12444 (Cecil et al., 2018) and *P. putida* KT2440 (Parales & Harwood, 1992) were utilized for gene amplification. All strains were stored in 20% glycerol at -80°C prior to use. All strains and plasmids are listed in Table 2.

3.1.2 Media

LB medium (Becton & Dickinson, Heidelberg, Germany) and terrific broth (TB) medium were utilized for the cultivation of *E. coli* strains. The TB medium contained the following components: 24 g L^{-1} of yeast extract (Sigma-Aldrich, Taufkirchen, Germany), 12 g L^{-1} of tryptone (Fluka, Buchs, Switzerland), 5 g L^{-1} of glycerol, 12.5 g L^{-1} of K_2HPO_4, and 2.3 g L^{-1} of KH_2PO_4. The *C. glutamicum* strains were cultivated in BHI medium (brain heart infusion, 37 g L^{-1}, Becton & Dickinson) and a modified minimal medium. The modified medium contained the components as previously described (Weiland et al., 2023), except for the inclusion of 5 g L^{-1} of glucose and 0.1 g L^{-1} of EDTA, and the exclusion of protocatechuate. Aromatic compounds including ferulate, *p*-coumarate, and caffeate were added when needed. Filter-sterilized ampicillin (100 µg mL^{-1}) or kanamycin (50 µg mL^{-1}) was added according to the plasmid used.

Table 2. Strains and plasmids.

Strains and plasmids	Description	Reference
Strains		
E. coli BL21 (DE3)	Strain for high-level expression of recombinant proteins	Thermo Fisher Scientific
E. coli p21pcaI	Derivative of *E. coli* BL21 (DE3) harbouring p21pcaI plasmid	This study
E. coli p21pcaJ	Derivative of *E. coli* BL21 (DE3) harbouring p21pcaJ plasmid	This study
E. coli p21At4CL4	Derivative of *E. coli* BL21 (DE3) harbouring p21At4CL4 plasmid	This study
E. coli p28phdA	Derivative of *E. coli* BL21 (DE3) harbouring p28phdA plasmid	This study
E. coli p28phdE	Derivative of *E. coli* BL21 (DE3) harbouring p28phdE plasmid	This study
E. coli p28ferA	Derivative of *E. coli* BL21 (DE3) harbouring p28ferA plasmid	This study
C. glutamicum ATCC13032	Wild-type, native aromatic degrading bacterium	(Becker et al., 2011)
C. glutamicum MA-2	Derivative of *C. glutamicum* ATCC13032. Deletion of *catB* (CGL_RS11905) and overexpression of *catA* (CGL_RS11910) under control of *Ptuf* (CGL_RS02540).	(Becker et al., 2018a)
C. glutamicum MA-10	Derivate of *C. glutamicum* MA-2. Deletion of *phdR* (CGL_RS01495), integration of native *aroY* (Ecl_01944), *ecdB* (Ecl_04083), *ecdD* (Ecl_04081) from *E. cloacae* under control of *Ptuf* into the *pcaG* locus	This study
N. aromaticivorans DSM12444	Wild-type, native aromatic degrading bacterium	DSMZ
P. putida KT2440	Wild-type, native aromatic degrading bacterium	DSMZ
Plasmids		
pET-21a	Vector for protein overexpression	Invitrogen
pET-28a	Vector for protein overexpression	Invitrogen
p21pcaI	Derivative of pET21a plasmid. Protein expression vector for *pcaI* (PP_3951) gene of *P. putida* KT2440	This study
p21pcaJ	Derivative of pET21a plasmid. Protein expression vector for *pcaJ* (PP_3952) gene of *P. putida* KT2440	This study
p21At4CL4	Derivative of pET21a plasmid. Protein expression vector for At4CL4 (AAM19949) enzyme of *A. thaliana*	This study
p28phdA	Derivative of pET-28a plasmids. Protein expression vector for *phdA* (CGL_RS01490) gene of *C. glutamicum* ATCC 13032	This study
p28phdE	Derivative of pET-28a plasmids. Protein expression vector for *phdE* (CGL_RS01520) gene of *C. glutamicum* ATCC 13032	This study
p28ferA	Derivative of pET-28a plasmids. Protein expression vector for *ferA* (SARO_RS03365) gene of *N. aromaticivorans* DSM12444	This study

3.1.3 Genetic engineering

Software SnapGene (GSL Biotech LLC, San Diego, USA) was utilized for strain, plasmid, and primer design. To obtain aromatic CoA thioesters by enzymatic synthesis, *E. coli* strains for relevant enzyme production were generated.

For production of 3-oxoadipyl-CoA, two genes, *pcaI* and *pcaJ* encoding 3-oxoadipate:succinyl-CoA transferase subunits A and B from the genome of *P. putida* KT2440 (Parales & Harwood, 1992), were selected. To produce vanilloyl-CoA, cinnamoyl-CoA, and sinapoyl-CoA, *At4CL4* encoding 4-coumarate:CoA ligase (Hamberger & Hahlbrock, 2004) was chosen. The *Pseudomonas* genes were separately amplified from genomic DNA (Q5 HotStart Polymerase, New England Biolabs, Frankfurt am Main, Germany), while *At4CL4* was synthesized based on

amino acid sequences in *A. thaliana*. The backbone of the vector was digested with FastDigest NdeI and HindIII (Thermo Fisher Scientific) as per the manufacturer's protocol. Following gene amplification, each gene was cloned into linearized pET-21a expression vector (Gibson Assembly MasterMix, New England Biolabs). Subsequently, the plasmids were transformed into *E. coli* DH5α, amplified, isolated, and verified by sequencing. *E. coli* BL21 (DE3) was then transformed with the expression plasmids using heat shock.

For the production of aromatic CoA thioesters, the backbone of pET-28a expression vector was linearized with FastDigest NcoI and XhoI (Thermo Scientific) according to the manufacturer's protocol. Two genes in *C. glutamicum* ATCC 13032 - *phdA* encoding acyl:CoA ligase and *phdE* encoding enoyl-CoA hydratase (Kallscheuer et al., 2016) - were respectively amplified using Phusion High-Fidelity PCR Master Mix with HF Buffer (Thermofisher Scientific). Additionally, *ferA* encoding acetate-CoA ligase from the genomic DNA of *N. aromaticivorans* DSM 12444 (Cecil et al., 2018) was amplified using Phusion High-Fidelity PCR Master Mix with GC Buffer (Thermofisher Scientific). Each gene was then assembled into the linearized pET-28a vector using Gibson assembly. The plasmids were subsequently transformed into *E. coli* BL21(DE3) via heat shock and verified by sequencing.

The design of plasmid, production, and purification of 3-oxoadipyl-CoA and vanilloyl-CoA were carried out in collaboration with Dr. Patrick D. Gerlinger at the Max Planck Institute for Terrestrial Microbiology (Marburg, Germany). All *C. glutamicum* strains used in this study, including engineered MA strains, were offered by Fabia Weiland at Institute of Systems Biotechnology (Saarland, Germany).

3.1.4 Cultivation

For cell growth observation, all *C. glutamicum* strains were cultivated in 250 mL baffled flask with 10% of filling volume on an orbital shaker (230 rpm, 30 °C, 5 cm shaking diameter, Multitron, Infors

AG, Bottmingen, Switzerland). For CoA thioester sampling, the cultivations were conducted separately in 500 mL baffled flask with 50 mL of medium. In general, the first preculture was conducted in a 100 mL baffled flask with 10 mL of BHI medium and incubated overnight. Afterwards, cells were collected (6,000 rpm, 3 min, 25 °C), transferred to 50 mL minimal medium containing 10 g L^{-1} of glucose, and then incubated overnight. Subsequently, cells were harvested (6,000 rpm, 3 min, 25 °C) and transferred to the main culture containing 5 g L^{-1} of glucose and the aromatic compounds of interest. The cultivations for cell growth were carried out in triplicate, while those for CoA thioester samples were conducted in duplicate.

3.1.5 Quantification of cell concentration, substrates, and products

The cell concentration was measured spectrophotometrically at optical density 660 nm. (OD_{660}). Cell dry weight (CDW) was calculated using the correlation from a previous study: CDW [g L^{-1}] = 0.32 x OD_{660} (Rohles et al., 2016).

Sugars were analysed by HPLC (1260 Infinity Series, Agilent, Waldbronn, Germany) using a column (NUCLEOGEL SUGAR Pb, 300 × 7.8 mm, Macherey-Nagel, Düren, Germany) at 80 °C as the stationary phase with deionized water as the mobile phase (0.4 mL min^{-1}). Refraction index was measured.

Aromatics were separated on a C18 column at 25 °C (Nucleodur C18 Isis, 100 × 3 mm, Macherey-Nagel) using a gradient of 0.025% H_3PO_4 and acetonitrile (1 mL min^{-1}) (Barton et al., 2018). The analytes were detected by UV absorbance at compound-specific wavelengths (210 nm for protocatechuate, 220 nm for vanillate, 260 nm for 4-hydroxybenzoate and *cis, cis*-muconate, 310 nm for *p*-coumarate, and 325 nm for ferulate and caffeate).

External standards were used for substrate and product quantification.

3.1.6 Protein production and purification

In general, *E. coli* BL21 (DE3) cells harbouring the respective pET-21a or pET-28a derivate plasmids were plated on LB agar supplemented with ampicillin for pET-21a vector or kanamycin for pET-28a. A single colony was picked from overnight incubated plates (37°C) and inoculated into 10 mL of LB medium containing the appropriate antibiotic in a 100 mL shake flask, followed by incubation on an orbital shaker (37°C, 160 rpm).

Subsequently, 10 mL of the grown culture was transferred to 300 mL of TB medium (1 L shake flask) with the corresponding antibiotic concentration. When the OD reached 0.7, 0.5 mM of IPTG was added for protein induction, and the culture continued to incubate at 28°C overnight.

After inoculation, the culture was collected (5,000 × *g*, 4°C, 10 min) and resuspended in buffer A (450 mM NaCl, 50 mM HEPES-KOH, 15% (v/v) glycerol, pH 7.6) at a ratio of 2:1 (v/w), followed by sonication. Cell debris was clarified by centrifugation (10,000 × *g*, 4°C, 45 min). The supernatant was filtered (0.45 µm), loaded onto Ni-NTA agarose beads (Protino, Macherey-Nagel), and washed with 10 mL of buffer C (350 mM NaCl, 50 mM HEPES, 15 % (v/v) glycerol, pH 7.8). The protein was eluted using buffer B (20 mM NaCl, 50 mM HEPES, 10% glycerol, 500 mM imidazole, pH 7.6). The protein size was calculated from nucleotide sequence and verified via SDS-Page. The protein concentration was determined spectroscopically at 280 nm calculated by ProtParam (Wilkins et al., 1999) (Table 3).

Table 3. Size and extinction coefficients of heterologously produced enzymes used in this study. The size and extinction coefficient of each enzyme were calculated based on their amino acid sequence using ProtParam (Wilkins et al., 1999). The concentration of enzymes was determined using the calculated extinction coefficients.

Protein	Size (kDa)	Extinction coefficient (M^{-1} cm^{-1}) at 280 nm
PhdA	56.4	45840
PhdE	17.2	19480
FerA	73.3	45755
PcaI	26.6	14440
PcaJ	24.7	11585

3.1.7 Synthesis of CoA thioesters

For the enzymatic synthesis of 3-oxoadipyl-CoA, 30 mg of succinyl-CoA (8.25 mM final concentration, 1 eq.) was dissolved in 25 mM ammonium formate (pH 4.2) and added to a mixture containing 33 mM 3-oxoadipic acid (4 eq.), 20 mM $MgCl_2$, 100 mM $KHCO_3$, and 100 mM HEPES-KOH (pH 7.5) to a final volume of 4 mL. After brief equilibration at 30°C, 10 µM of PcaI and PcaJ were added, and the mixture was further incubated (30°C, 200 rpm). After 3 hours, the assay was quenched with a final concentration of 10 % (v/v) formic acid, centrifuged (4500 × g, 25 °C, 20 min), and filtered (0.45 µm) for further purification.

Aromatic CoA thioesters, including feruloyl-CoA, *p*-coumaroyl-CoA, and caffeoyl-CoA, were synthesized using FerA enzyme whereas sinapoyl-CoA, cinnamoyl-CoA, and vanilloyl-CoA were produced using At4CL4 enzyme. All aromatics (6.52 mM final concentration, 3 eq) were respectively dissolved in deionized water and mixed with CoA trillium salt (2.17 mM final concentration, 1 eq, Sigma-Aldrich) and ATP (6.52 mM final concentration, 3 eq). The assay was performed with a total volume of 3 mL containing 20 mM $MgCl_2$, 50 mM $KHCO_3$, and 50 mM HEPES buffer (pH 7.5). The reaction was initiated with the addition of FerA or At4CL4 (10 µM) and incubated for 1 hour (30°C, 230 rpm). After incubation, the reaction was quenched with a final concentration of 10 % (v/v) formic acid.

The synthesis of 3-hydroxy-feruloyl-CoA, 3-hydroxy-*p*-coumaroyl-CoA, and 3-hydroxy-caffeoyl-CoA was performed under identical condition as mentioned above, except using both PhdA and PhdE enzymes.

3.1.8 Purification of CoA thioesters

The aromatic CoA thioesters were purified using an 1260 Infinity prep-LC system (Agilent) with a reversed phase column (Gemini 10 µm NX-C18 110 Å, 100 x 21.2 mm AXIA packed column,

Phenomenex, Aschaffenburg, Germany). The purification process involved a gradient of solvent A (25 mM NH_4HCO_2, pH 5.5) and solvent B (methanol) at a flow rate of 1 mL min^{-1}: 5 % - 50 % B in 15 min, followed by 2 min wash with 95% B, and subsequent re-equilibration of the column for 2 min (5 % B). Fractions containing each product were pooled, flash frozen in liquid nitrogen, lyophilized, and stored at -20 °C.

The concentrations of purified CoA thioesters were determined photometrically, utilizing the following known extinction coefficients: saturated acyl-CoA for 3-oxoadipyl-CoA ($\varepsilon_{260\ nm}$ = 16.4 mM^{-1} cm^{-1}) (Dawson et al., 2002; Peter et al.) and each aromatic CoA thioester separately (ε_{346}=19 $mM^{-1}cm^{-1}$ for feruloyl-CoA, ε_{333}=21 $mM^{-1}cm^{-1}$ for *p*-coumaroyl-CoA, ε_{346}=18 $mM^{-1}cm^{-1}$ for caffeoyl-CoA, ε_{352}=20 $mM^{-1}cm^{-1}$ for sinapoyl-CoA) (Rautengarten et al., 2010).

Table 4. Extinction coefficients and absorption maximum wavelengths of aromatic CoA thioesters used in this study.

Compound	Wavelength [nm]	Extinction coefficient [mM^{-1} cm^{-1}]	Reference
Feruloyl-CoA	346	19	(Rautengarten et al., 2010)
p-Coumaroyl-CoA	333	21	(Rautengarten et al., 2010)
Caffeoyl-CoA	346	18	(Rautengarten et al., 2010)
Sinapoyl-CoA	352	20	(Rautengarten et al., 2010)
Cinnamoyl-CoA	311	22	(Gaid et al., 2012)
Benzoyl-CoA	261	21.1	(Schnell & Schink, 1991)
3-Oxoadipyl-CoA	260	16.4	(Peter et al., 2016)

For the hydroxy-aromatic CoA thioesters, fractions exhibiting peaks at 260 nm were collected and confirmed using LC-MS with the calculated masses: 3-hydroxyferuloyl-CoA ($[M+H]^+$ = 962.2), 3-hydroxy-*p*-coumaroyl-CoA ($[M+H]^+$ = 932.2), and 3-hydroxycaffeoyl-CoA ($[M+H]^+$ = 948.1).

3.1.9 LC-MS based analysis of aromatic CoA thioesters

All aromatic CoA thioesters tested were synthesized as described above, while benzoyl-CoA was purchased from Sigma-Aldrich. The synthesis and purification of cinnamoyl-CoA and sinapoyl-CoA were conducted by Dr. Patrick D. Gerlinger at the Max Planck Institute for Terrestrial Microbiology (Marburg, Germany). The aromatic CoA-thioesters were analysed using LC-ESI-

MS/MS (Agilent Infinity 1290; AB Sciex QTrap 6500, Darmstadt, Germany) with separation on a reversed phase column (Kinetex 2.6 µ XB-C18 100 Å, 100 × 2.1 mm, Phenomenex) at 40 °C and a gradient of eluent A (50 mM formic acid, adjusted to pH 7.7 with 25% ammonium hydroxide) and eluent B (methanol) at a flow rate of 300 µL min^{-1}. The initial acquisition method was adapted from prior work (Gläser et al., 2020; Seo et al., 2023), incorporating additional MRM methods to scan both aromatic CoA thioesters and central metabolic CoA thioesters. The gradient of the initial acquisition method proceeded as follows: 0 – 7 min, 100 – 90 % A; 7 – 10 min, 90 – 0 % A, with 1 min rinsing and 2 min re-equilibrium. For the separation of aromatic CoA thioesters, gradient was adjusted as follows: 0-3 min, 100 – 85% A; 3-8 min, 85%-75% A; 8 – 10 min, 70 – 0 % A; with 1 min rinsing and 2 min re-equilibrium. Multiple reaction monitoring (MRM) was used for detection of CoA thioesters.

In general, analysis was operated in positive ion mode $[M+H]^+$, and specific values for the curtain gas (35 psi), collision gas flow rate (medium), ion spray voltage (4.5 kV), temperature (400 °C); ion source gas (60 psi), entrance potential (10 V). For the analysis of aromatic CoA thioesters, the optimized parameters were described in Supplementary data: Table S2. Other CoA esters were referenced from previous work (Gläser et al., 2020; Peter et al., 2016).

Intracellular CoA thioesters were prepared using a recently established protocol (Gläser et al., 2020; Kuhl et al., 2020; Seo et al., 2023) with a slight modification. In general, 45 mL of cell broth was centrifuged (5 min, 4 °C, 6,500 × *g*). The pellet was then resuspended in 25 mL of quenching solution (95% acetonitrile with 25 mM formic acid, -20 °C) and incubated on ice (10 min). Cell debris were clarified by centrifugation (10 min, 4 °C, 10,000 × *g*), and the supernatant was collected. The cell debris was subsequently washed with super cooled deionized water (5 ml), and clarified again. The obtained supernatants were combined, quick-frozen in liquid nitrogen, further underwent lyophilization. The freeze-dried samples were resuspended in 700 µL of resuspension buffer (25 mM ammonium formate, 2% methanol, pH 5.6, 4°C) before LC-MS/MS analysis.

3.1.10 Preparation of ^{13}C-labelled aromatic CoA thioesters

C. glutamicum MA10 strain was cultivated using 99% [$^{13}C_6$] D-glucose (Cambridge Isotope Laboratories, Tewksbury, MA, USA). The preculture was prepared as described in 3.1.4, substituting non-labelled glucose with 99% [$^{13}C_6$] D-glucose. After overnight cultivation, cells were harvested (6,000 rpm, 3 min, 25 °C), and transferred to the main culture contained 5 g L^{-1} of 99% [$^{13}C_6$] D-glucose and 5 mM ferulate.

3.2 Results and Discussion

3.2.1 Metabolism of aromatics in the wild-type of *C. glutamicum*

To produce *cis, cis*-muconate from aromatic compounds using *C. glutamicum*, the medium contained both glucose to promote biomass formation and aromatic compounds to enable product formation, respectively (Weiland et al., 2023). At the start, the wild-type (WT) strain was cultivated on glucose and three different aromatics: ferulate, *p*-coumarate, and caffeate, respectively (Fig. 6).

C. glutamicum naturally degraded ferulate, *p*-coumarate, and caffeate. All tested aromatics were consumed once glucose was completely depleted, indicating catabolic repression by glucose (Brinkrolf et al., 2006). Interestingly, the strain exhibited the different capabilities to utilize ferulate (Fig. 6A), *p*-coumarate (Fig. 6B), and caffeate (Fig. 6C). The growth was slower on *p*-coumarate than on ferulate and caffeate.

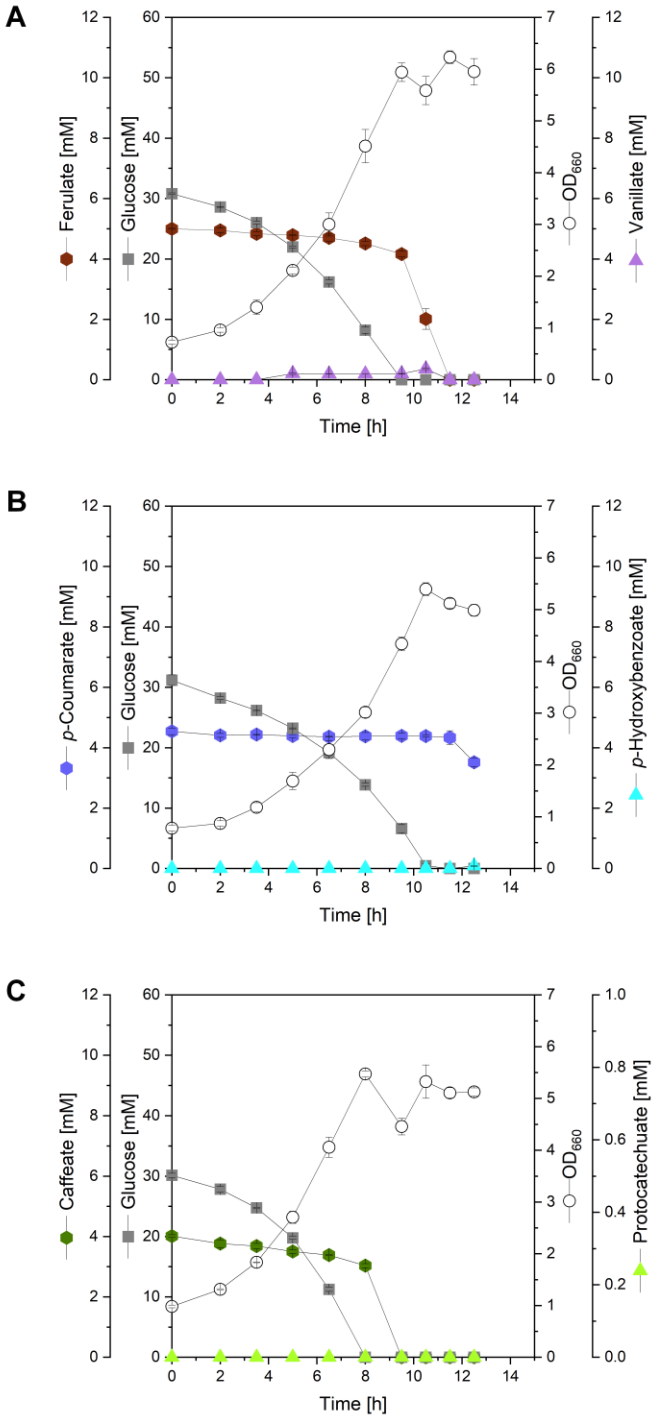

Figure 6. Cultivation of *C. glutamicum* ATCC 13032 on glucose and ferulate, *p*-coumarate, or caffeate. The wild-type strain was grown in minimal medium containing 5 g L^{-1} of glucose along with 5 mM of ferulate (A), *p*-coumarate (B), caffeate (C). The data represent mean values and standard deviations from three biological replicates (n=3).

3.2.2 Enzymatic synthesis of aromatic-derived CoA thioesters

In the process of degrading ferulate, *p*-coumarate, and caffeate, *C. glutamicum* converts these compounds into their respective aromatic CoA thioesters (Kallscheuer et al., 2016). Since commercial sources for these aromatic CoA thioesters were unavailable, the metabolites were enzymatically synthesized prior to analysis, including LC-MS based structural validation and purification via preparative HPLC.

The CoA-dependent ligases, required for the enzymatic synthesis, were expressed heterologously in *E. coli* BL21(DE3). Given that the spectrum of each ligase varies, multiple CoA-dependent ligases from different hosts were utilized to derive the CoA thioesters of interest (Table 2).

First, 3-oxoadipyl-CoA, an intermediate of the degradation pathway of protocatechuate and catechol (Z. Xu et al., 2019), was enzymatically synthesized using 3-oxoadipate:succinyl-CoA transferase (PcaI and PcaJ) from *P. putida* KT2440 (Parales & Harwood, 1992). The synthesis of 3-oxoadipyl-CoA achieved approximately 40% yield, as determined by absorption at 260 nm. Feruloyl-CoA, *p*-coumaroyl-CoA, and caffeoyl-CoA were synthesized using acetate-CoA ligase (FerA) from *N. aromaticivorans* (Cecil et al., 2018) with over 90% yield, verified by Ellmann's reaction. Sinapoyl-CoA, cinnamoyl-CoA, and vanilloyl-CoA were synthesized using At4CL from *A. thaliana* (Hamberger & Hahlbrock, 2004). In addition to obtaining aromatic CoA thioesters, 3-hydroxy-aromatic CoA thioesters were synthesized through a combined enzymatic reaction involving acyl:CoA ligase (PhdA) and enoyl-CoA hydratase (PhdE) from *C. glutamicum*. In this regard, acyl:CoA ligase (PhdA) in *C. glutamicum* (Kallscheuer et al., 2016) was found capable of converting ferulate, *p*-coumarate, and caffeate into their respective CoA thioesters. The process successfully yielded 3-hydroxyferuloyl-CoA and 3-hydroxy-*p*-coumaroyl-CoA. However, the synthesis of 3-hydroxycaffeoyl-CoA failed, likely due to oxygen sensitivity of the product.

Table 5. Properties of the expected spectrum of CoA-thioesters involved in lignin-based aromatics degradation. The predicted molecular formula and monoisotopic masses were obtained from PubChem (S. Kim et al., 2023). The mass of the proton adduct of each CoA thioester was manually calculated to be utilized for analytical verification.

Lignin type	Compound	Molecular formula	Monoisotopic mass [Da]	$[M+H]^+$
Coniferyl alcohol	Feruloyl-CoA	$C_{31}H_{44}N_7O_{19}P_3S$	943.16	944.2
	3-Hydroxyferuloyl-CoA	$C_{31}H_{46}N_7O_{20}P_3S$	961.17	962.2
	3-Oxoferuloyl-CoA	$C_{31}H_{44}N_7O_{20}P_3S$	959.15	960.2
	Vanillyl-CoA	$C_{29}H_{42}N_7O_{19}P_3S$	917.15	918.1
p-Coumaryl alcohol	*p*-Coumaroyl-CoA	$C_{30}H_{42}N_7O_{18}P_3S$	913.15	914.2
	3-Hydroxy-*p*-coumaroyl-CoA	$C_{30}H_{44}N_7O_{19}P_3S$	931.13	932.1
	3-Oxo-*p*-coumaroyl-CoA	$C_{30}H_{42}N_7O_{19}P_3S$	929.11	930.1
	p-Hydroxybenzoyl-CoA	$C_{28}H_{40}N_7O_{18}P_3S$	887.14	888.1
Caffeoyl alcohol	Caffeoyl-CoA	$C_{30}H_{42}N_7O_{19}P_3S$	929.15	930.1
	3-Hydroxycaffeoyl-CoA	$C_{30}H_{44}N_7O_{20}P_3S$	947.12	948.1
	3-Oxocaffeoyl-CoA	$C_{30}H_{42}N_7O_{20}P_3S$	945.12	946.1
	Protocatechuyl-CoA	$C_{28}H_{40}N_7O_{19}P_3S$	903.13	904.1
Sinapyl alcohol	Sinapoyl-CoA	$C_{32}H_{46}N_7O_{20}P_3S$	973.14	974.1
	3-Hydroxysinapoyl-CoA	$C_{32}H_{48}N_7O_{21}P_3S$	991.14	992.1
	3-Oxosinapoyl-CoA	$C_{32}H_{46}N_7O_{21}P_3S$	989.14	990.1
	Syringyl-CoA	$C_{30}H_{44}N_7O_{20}P_3S$	947.14	948.1
Cinnamoyl alcohol	Cinnamoyl-CoA	$C_{30}H_{42}N_7O_{17}P_3S$	897.16	898.2
	3-Hydroxycinnamoyl-CoA	$C_{30}H_{44}N_7O_{18}P_3S$	915.16	916.2
	3-Oxocinnamoyl-CoA	$C_{30}H_{42}N_7O_{18}P_3S$	913.15	914.2
	Benzoyl-CoA	$C_{28}H_{40}N_7O_{17}P_3S$	871.14	872.1
Degradation intermediate	3-Oxoadipyl-CoA	$C_{27}H_{42}N_7O_{20}P_3S$	909.14	910.1

After synthesizing the CoA thioesters, the enzymes in the mixture were denatured and removed by filtration. The products were subjected to mass verification using LC-MS. The chromatographic separation of the obtained metabolites was conducted using a previously established acquisition method (Gläser et al., 2020). Upon detection of the corresponding masses using LC-MS (Table 5), the CoA thioesters were purified, considering the known absorption maximum wavelengths (Table 4) for detection of fractions contained the analytes of interest. For hydroxylated aromatic CoA thioesters, for which absorption properties were not available, it was noted that the adenine moiety in the CoA structure exhibits maximum absorbance at 260 nm. Consequently, all fractions showing absorbance at 260 nm were pooled and subjected to mass verification. All purified CoA thioesters were freeze-dried. The samples were dissolved in resuspension buffer and stored at -80 °C for future use. Subsequently, they were utilized to tune the LC-MS/MS for optimum analysis and served as external standards.

3.2.3 Establishment of a data-based MS/MS method for aromatic CoA thioesters

In the next step, the fragmentation patterns of the isolated CoA thioesters were compared to the predicted pattern, characterized by neutral loss of the 3'-phosphate-5'-diphosphate moiety, using LC-MS/MS in the positive mode (Table 5). The experimental values favourably matched the experimental data (Table 6), indicating that the synthesized and purified metabolites exhibited the correct structure.

Table 6. Theoretical and experimental fragmentation patterns of aromatic CoA thioesters. The synthetized CoA thioesters were analysed using LC-MS/MS. The masses of the obtained proton adduct were compared to the theoretical values, calculated from the chemical structure.

	Theoretical fragmentation		Practical fragmentation	
	Q1 [Da]	**Q3 [Da]**	**Q1 [Da]**	**Q3 [Da]**
Feruloyl-CoA	944.2	437.2	944.2	437.2
3-Hydroxyferuloyl-CoA	962.2	455.2	962.2	455.0
Vanillyl-CoA	918.1	411.1	918.1	411.1
p-Coumaroyl-CoA	914.2	407.2	914.1	407.2
3-Hydroxy-*p*-coumaroyl-CoA	932.1	425.1	932.3	425.3
Caffeoyl-CoA	930.1	423.1	930.1	423.2
Sinapoyl-CoA	974.1	467.1	974.0	467.2
Cinnamoyl-CoA	898.2	391.2	898.1	391.2
Benzoyl-CoA	872.1	365.1	872.1	365.2
3-Oxoadipyl-CoA	910.1	403.1	910.3	403.1

The agreement suggested the feasibility of using the fragmentation pattern for analysing aromatic CoA thioesters even without having a pure standard available. However, in a such case, a tuning of the LC-MS/MS would not be possible, eventually limiting sensitivity.

After successful verification of the structure of the synthesized metabolites, the chromatographic separation of the compounds was refined to facilitate their analysis in the expected complex mixtures of cell extracts. For this purpose, all pure CoA thioesters analysed using LC-MS/MS the MRM mode to obtain the corresponding retention time (Fig. 7). The optimization of the elution gradient enabled the separation of all nine different aromatic CoA thioesters (Table 7).

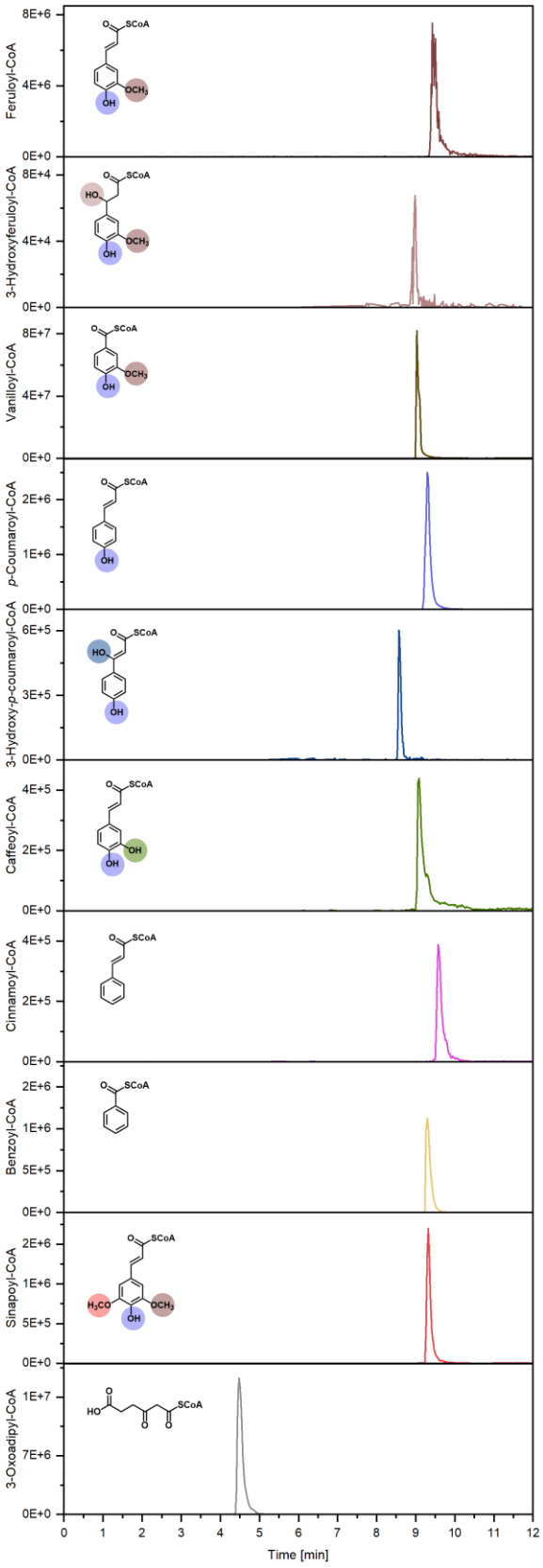
Feruloyl-CoA
8E+6
4E+6
0E+0
3-Hydroxyferuloyl-CoA
8E+4
4E+4
0E+0
Vanilloyl-CoA
8E+7
4E+7
0E+0
p-Coumaroyl-CoA
2E+6
1E+6
0E+0
3-Hydroxy-p-coumaroyl-CoA
6E+5
3E+5
0E+0
Caffeoyl-CoA
4E+5
2E+5
0E+0
Cinnamoyl-CoA
4E+5
2E+5
0E+0
Benzoyl-CoA
2E+6
1E+6
5E+5
0E+0
Sinapoyl-CoA
2E+6
1E+6
5E+5
0E+0
3-Oxoadipyl-CoA
1E+7
7E+6
0E+0
0 1 2 3 4 5 6 7 8 9 10 11 12
Time [min]

Figure 7. LC-MS/MS analysis of aromatic CoA thioesters. The aromatic CoA thioesters were analysed via MRM in positive mode using LC-MS/MS, demonstrating molecular-specific detection characterized by the neutral loss of 507 Da (Table 6). The gradient of eluents was obtained from previous work (Gläser et al., 2020), with an addition of the MRM spectrum for aromatic CoA thioester. The corresponding tuning parameters, optimized for each analyte are given in the supplement (Supplementary data: Table S2).

Table 7. Retention time of aromatic CoA thioesters using LC-MS/MS. The acquisition method was obtained from previous work (Gläser et al., 2020). All analytes were detected using MRM.

	Retention time [min]	
	Initial	**Adapted**
Feruloyl-CoA	9.42	8.81
3-Hydroxyferuloyl-CoA	8.98	5.80
Vanillyl-CoA	9.03	7.07
p-Coumaroyl-CoA	9.23	8.43
3-Hydroxy-*p*-coumaroyl-CoA	8.67	4.68
Caffeoyl-CoA	9.06	7.19
Sinapoyl-CoA	9.28	
Cinnamoyl-CoA	9.58	
Benzoyl-CoA	9.28	
3-Oxoadipyl-CoA	4.60	

After the targeted detection and separation of aromatic CoA thioesters, external standards were prepared. The concentrations of CoA standards were determined using their extinction coefficients (Table 4), except for 3-hydroxyferuloyl-CoA and 3-hydroxy-*p*-coumaroyl-CoA, for which no extinction coefficients were available.

Table 8. Detection range of aromatic CoA thioesters used in this study.

Compound	Tested detection range [fmol]
Feruloyl-CoA	2.9 – 2.60E+04
p-Coumaroyl-CoA	2.5 – 1.31E+05
Caffeoyl-CoA	5.8 – 3.28E+05
Sinapoyl-CoA	6.5 – 3.67E+05
Cinnamoyl-CoA	2.8 – 1.60E+05
Benzoyl-CoA	2.2 – 1.27E+03
3-Oxoadipyl-CoA	44.7 – 5.30E+03

Subsequently, the threshold for detection and the dynamic range for quantification was estimated. For this purpose, a dilution series of the analytes was prepared and tested (Table 8). Generally, concentrations ranging from very low (fmol) to high (nmol) levels were detectable, enabling the coverage of a wide range of concentrations in biological samples (Fig. 8). All CoA thioesters, except 3-oxoadipyl-CoA were detected at the fmol level, indicating high analytical sensitivity.

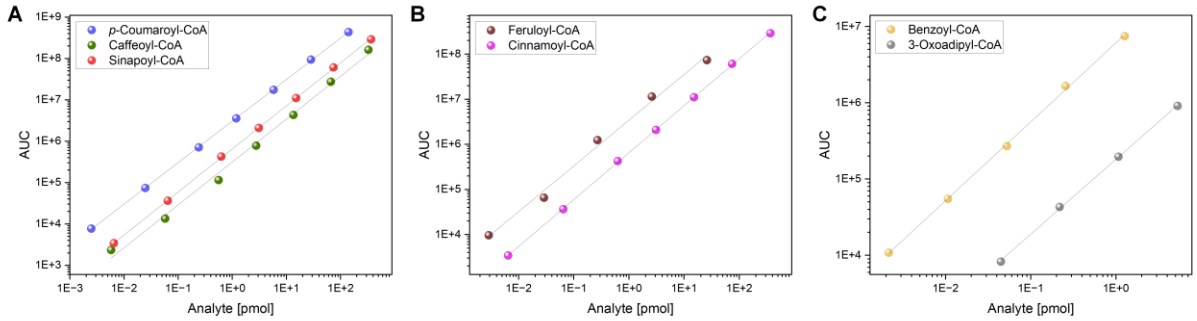

Figure 8. LC-MS/MS analysis of CoA thioesters using MRM. The exact concentrations of the aromatic CoA thioesters in the differently diluted standards were determined (Table 8) using photometric analysis and the known extinction coefficients (Table 4). The known concentrations were plotted against the measured signal intensity (AUC) in log-scale.

3.2.4 Targeted analysis of intracellular aromatic CoA thioesters in *C. glutamicum*

In the next step, the developed approach was applied for investigating biological samples. For this purpose, ferulate-grown *C. glutamicum* was employed. The catabolic ferulate pathway yields feruloyl-CoA as first metabolic intermediate, which is then converted into 3-hydroxyferuloyl-CoA (Fig. 3) (Kallscheuer et al., 2016). The aromatic CoA thioester intermediates are funnelled towards protocatechuate, which is subsequently converted into acetyl-CoA and succinyl-CoA, ultimately entering the TCA cycle (Brinkrolf et al., 2006). Because it could not be excluded that other metabolic intermediates in the complex cell extract would interfere with the measurement, the analytical approach was advanced. To this end, a set-up was chosen that should provide ^{13}C-labelled CoA-thioesters during growth of *C. glutamicum* on ferulate. Particularly, the use of ^{13}C-labelled glucose plus naturally labelled ferulate in the growth medium of *C. glutamicum* should result in partially ^{13}C-labelled feruloyl-CoA, enabling the comparison of non-labelled and ^{13}C-labelled molecules (Fig. 9A). The backbone of the CoA-ester should largely result from the ^{13}C-glucose, although a small fraction of ^{12}C-carbon was expected from the release of acetyl-CoA during the conversion of 3-oxoferuloyl-CoA into vanillin (Fig. 3). This approach promised to yield advanced information on the fragmentation pattern and provide an extra level of confidence for detecting the compounds in cell extracts. Additionally, considering that feruloyl-CoA was finally catabolized into acetyl-CoA and succinyl-CoA, also emerging from glucose-based carbon, the origin of these two central CoA-thioesters from ferulate and glucose, respectively, was expected to become better distinguishable.

To address this, *C. glutamicum* MA10 was selected. This strain was capable of co-consuming glucose and aromatics due to the removal of the *phdR* gene, which regulates the aromatic upper degradation pathway (Fabia Weiland, Institute of Systems Biotechnology, Saarland University).

Due to heterologous expression of *aroY* the strain could accumulate *cis, cis*-muconate from ferulate (Weiland et al., 2023).

C. glutamicum MA10 was cultured under three conditions: on glucose, a mixture of glucose and ferulate, and a mixture of 99% [U-$^{13}C_6$] glucose plus ferulate. Assuming that the CoA-thioester backbone was formed from glucose and therefore ^{13}C-labelled, while the side chain of feruloyl-CoA was derived from non-labelled ferulate, predicted a partially ^{13}C-enriched structure (Fig. 9A). The detectable ions of this partially ^{13}C-enriched metabolite in the Q1 and the Q3 of the LC-MS/MS were expected to exhibit masses of 965.2 and 448.0 Da, different to the non-labelled metabolite (Q1 944.2, Q3 437.2 Da). During the co-consumption phase of ferulate and glucose after about 9 hours (Fig. 9B), CoA-esters were sampled, processed, and analysed by LC-MS/MS. The culture on the non-labelled substrates yielded a clear signal for the masses 944.2 (Q1) and 437.2 Da (Q3), eluting after 8 minutes (Table 7), and corresponding to non-labelled ferulate. The signal was not present, when cells were grown on glucose alone, as expected. Interestingly, no signal also resulted for growth on the isotopic tracer mixture, containing [U-$^{13}C_6$] glucose. The findings revealed that there were no matrix effects that could have corroborated the feruloyl-CoA analytics. More importantly, ion fragments of 965.2 Da (Q1) and 448.2 Da (Q3) were detected exclusively in the culture supplemented with ^{13}C-enriched glucose and ^{12}C ferulate, identifying the metabolite as feruloyl-CoA.

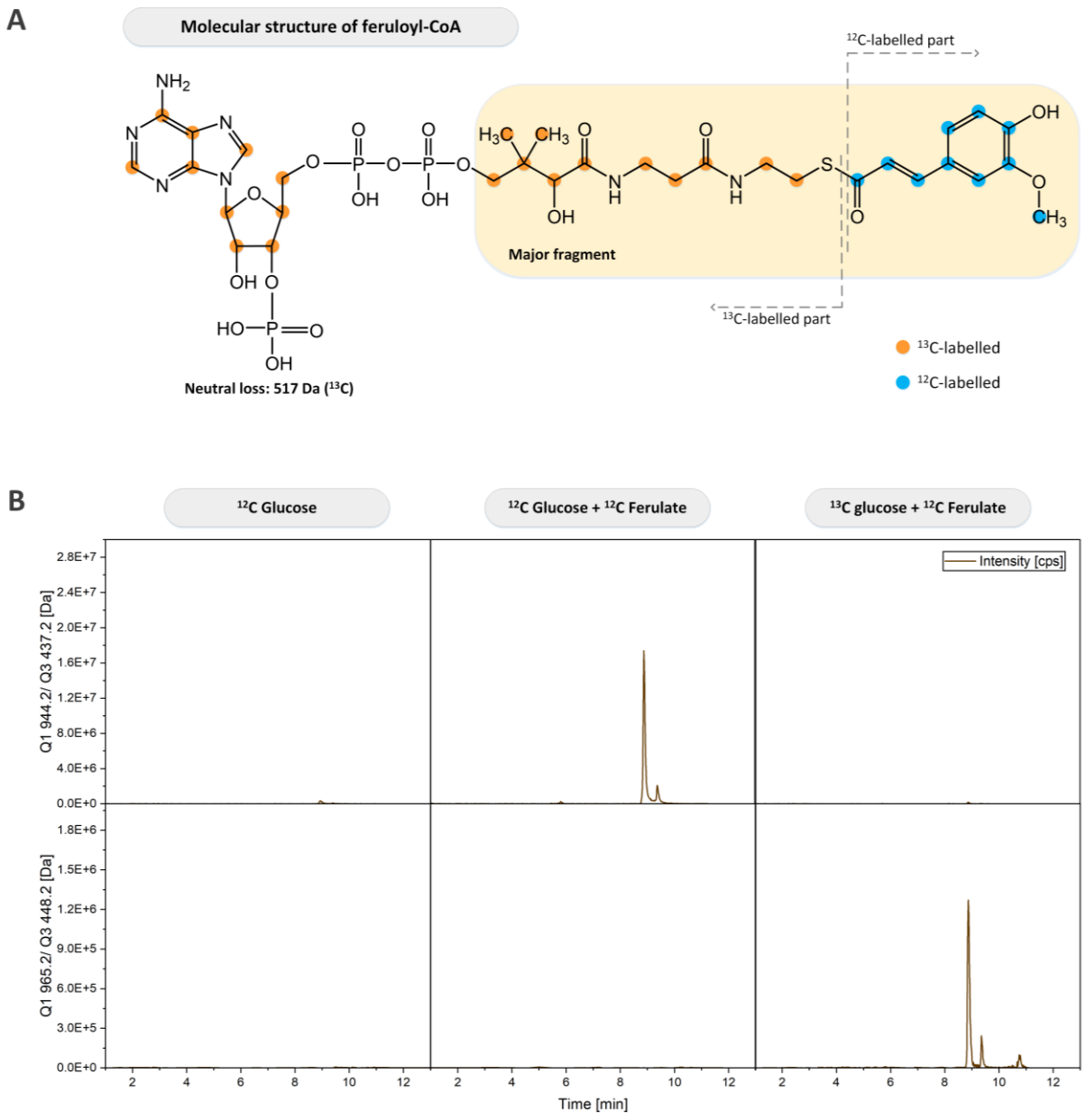

Figure 9. Molecular structure of the partially ^{13}C-labelled metabolite expected from growth of the microbe on [U-$^{13}C_6$] glucose and ferulate (A) and MRM analysis of non-labelled and ^{13}C-labelled feruloyl-CoA (B). *C. glutamicum* MA10 was cultivated on glucose, a mixture of ^{12}C glucose and ^{12}C ferulate and on a mixture of [U-$^{13}C_6$] glucose and non-labelled ferulate. All samples were collected at an OD_{600} of 2.5. In the given structure, the ^{13}C-labelled (^{13}C glucose-derived) carbon is highlighted in orange whereas ^{12}C is shown in blue. The major fragment (Q3) is marked with yellow (A). The molecular weights considered for the analysis were as follows: non-labelled feruloyl-CoA (Q1 944.2/ Q3 437.2 Da) and ^{12}C-^{13}C feruloyl-CoA (Q1 965.2/ Q3 448.2).

3.2.5 Intracellular dynamics on aromatic mixtures

In *C. glutamicum*, the *phd* gene cluster is involved in aromatic degradation through the β-oxidative pathway. It consists of 7 genes: a MarR-type repressor (*phdR*), 5 degrading enzymes (*phdA*, acyl:CoA ligase; *phdB*, 3-hydroxyacyl-CoA dehydrogenase; *phdC*, 3-oxoacyl-CoA ketohydrolase (acetyl-CoA forming); *phdD*, acyl-CoA dehydrogenase; *phdE*, enoyl-CoA hydratase), and a transporter (*phdT*) (Kallscheuer et al., 2016), enabling the degradation of ferulate, *p*-coumarate, and caffeate (Fig. 6). As shown, the pathway involves several CoA-thioester intermediates. Their intracellular presence and dynamics were assessed using metabolomic analysis.

C. glutamicum MA10, cultivated on glucose, as well as mixtures of glucose supplemented with single aromatics (ferulate, *p*-coumarate, caffeate) and a combination of all three aromatics (Fig. 10). The strain exhibited different growth, depending on the aromatic. Compared to glucose-only cultivation (Fig. 10A), the addition of ferulate (Fig. 10C) or *p*-coumarate (Fig. 10E) enhanced cell growth, while caffeate seemed inhibiting (Fig. 10G). Despite the genes encoding the caffeate-degrading enzymes (*phdA-E*) were still contained in the mutant, it exhibited retarded degradation of caffeate, differently to the wild type (Fig. 6C). This suggested the presence of an additional factor influencing caffeate degradation that remains to be elucidated. When a combination of all aromatics was added, the inhibitory effect of caffeate on cell growth was mitigated by the other aromatics, resulting in recovered growth (Fig. 10I). Notably, caffeate remained untouched while other aromatics were utilized. After the depletion of ferulate and *p*-coumarate, caffeate was consumed, implying a substrate preference among the aromatics in the cell.

Subsequently, using the newly developed approach, the aromatic CoA thioesters were analysed. No aromatic CoA thioester was observed in the glucose-only cultivation (Fig. 10B), while the different aromatic CoA thioesters were well detected in the respective aromatic-amended cultivations (Fig. 10D, F, H). The engineered strain was able to co-utilize the three aromatics, as evidenced by the simultaneous detection of all aromatic CoA thioesters in the culture (Fig. 10J).

To obtain a detailed view of the degradation of the aromatic combination by engineered strain, various other CoA-based degradation intermediates were analysed (Fig. 2 and 11). This, enabled to observe different sequential intermediates. For example, the concentration of *p*-coumaroyl-CoA increased as that of *p*-coumarate decreased. Subsequently, the concentration of *p*-coumaroyl-CoA decreased with a corresponding increase in 4-hydroxybenzoate. Ultimately, all intermediates were depleted, ending up in *cis, cis*-muconate.

In addition, the analysis provided insights into the substrate preference of *C. glutamicum*. As observed in Fig. 10, *p*-coumarate and ferulate were immediately consumed whereas caffeate consumption was delayed. The concentration of caffeate decreased after the depletion of other aromatics, suggesting a sequential uptake of substrates. However, aromatic CoA thioester analysis revealed caffeoyl-CoA concentration did not increase while the caffeate concentration decreased in the culture, which may imply that caffeoyl-CoA is not solely derived from caffeate. MA10 produced *cis, cis*-muconate from a mixture of aromatics. Given that lignin is a heterogeneous aromatic complex in nature, the ability to degrade multiple aromatic compounds simultaneously is crucial for microbial cell factories involved in lignin valorisation. The analysis of aromatic CoA thioesters exhibited that *C. glutamicum* utilizes multiple aromatic compounds via the β-oxidative pathway.

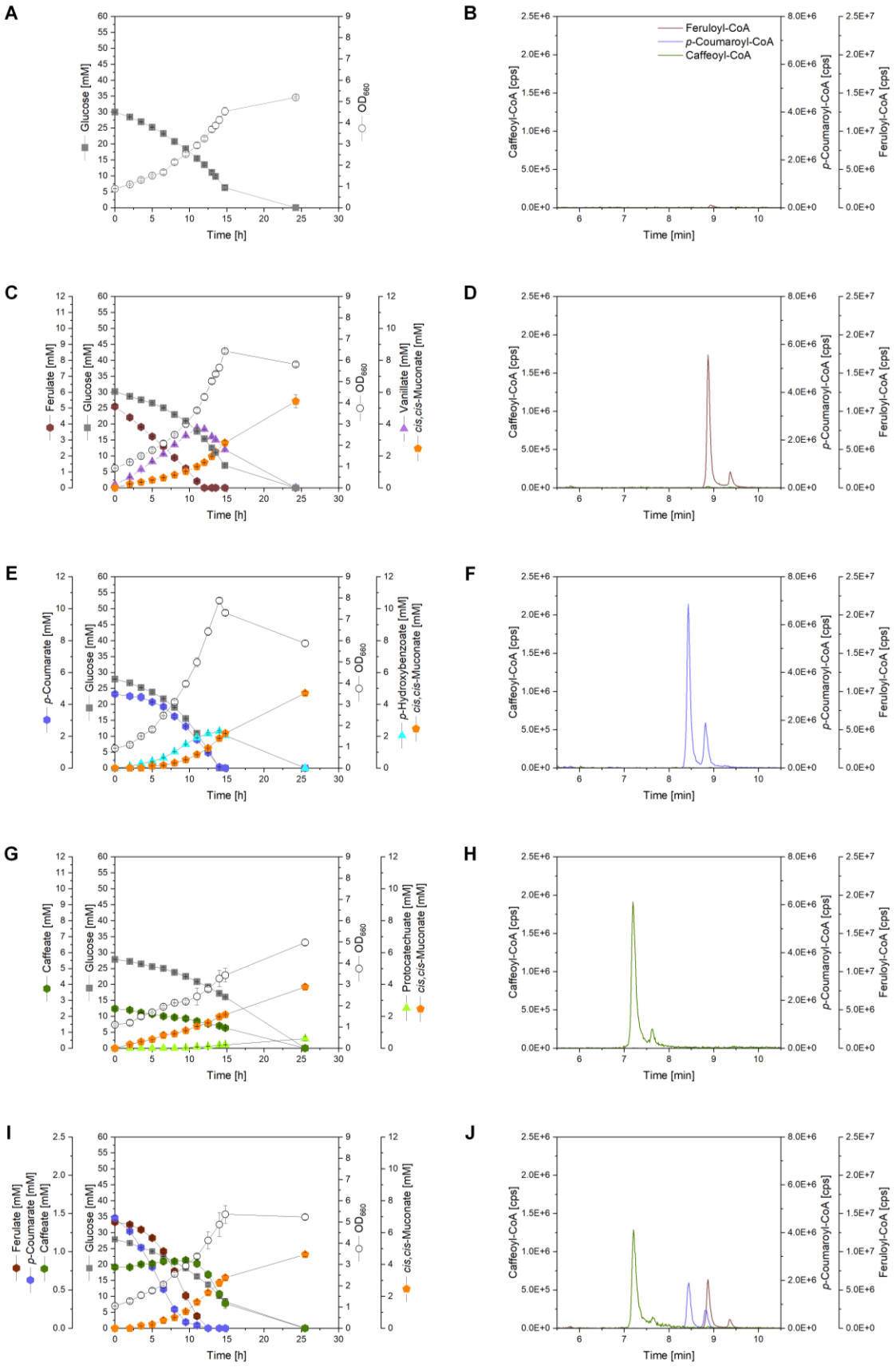
A
Glucose [mM]
OD660
Time [h]
B
Feruloyl-CoA
p-Coumaroyl-CoA
Caffeoyl-CoA
Caffeoyl-CoA [cps]
p-Coumaroyl-CoA [cps]
Feruloyl-CoA [cps]
Time [min]
C
Ferulate [mM]
Glucose [mM]
OD660
Vanillate [mM]
cis,cis-Muconate [mM]
Time [h]
D
Caffeoyl-CoA [cps]
p-Coumaroyl-CoA [cps]
Feruloyl-CoA [cps]
Time [min]
E
p-Coumarate [mM]
Glucose [mM]
OD660
p-Hydroxybenzoate [mM]
cis,cis-Muconate [mM]
Time [h]
F
Caffeoyl-CoA [cps]
p-Coumaroyl-CoA [cps]
Feruloyl-CoA [cps]
Time [min]
G
Caffeate [mM]
Glucose [mM]
OD660
Protocatechuate [mM]
cis,cis-Muconate [mM]
Time [h]
H
Caffeoyl-CoA [cps]
p-Coumaroyl-CoA [cps]
Feruloyl-CoA [cps]
Time [min]
I
Ferulate [mM]
p-Coumarate [mM]
Caffeate [mM]
Glucose [mM]
OD660
cis,cis-Muconate [mM]
Time [h]
J
Caffeoyl-CoA [cps]
p-Coumaroyl-CoA [cps]
Feruloyl-CoA [cps]
Time [min]

Figure 10. Cultivations and aromatic CoA thioester profiles in metabolically engineered *C. glutamicum* MA10 strain. The MA10 strain was cultivated in minimal medium containing various aromatic compounds: glucose alone (A), glucose with ferulate (C), glucose with *p*-coumarate (E), glucose with caffeate (G), and glucose with all aromatics (I). The aromatic CoA thioester profiles for each cultivation condition was analysed using LC-MS/MS: glucose (9.5 h) (B), ferulate (8 h) (D), *p*-coumarate (6.5 h) (F), caffeate (12 h) (H), all aromatics (8 h) (J). The CoA thioester samples were collected when the OD_{660} reached 2.5. All cultivation was conducted in triplicate (n=3) whereas CoA thioester samples were taken in duplicate (n=2). The data represent mean values and standard deviations.

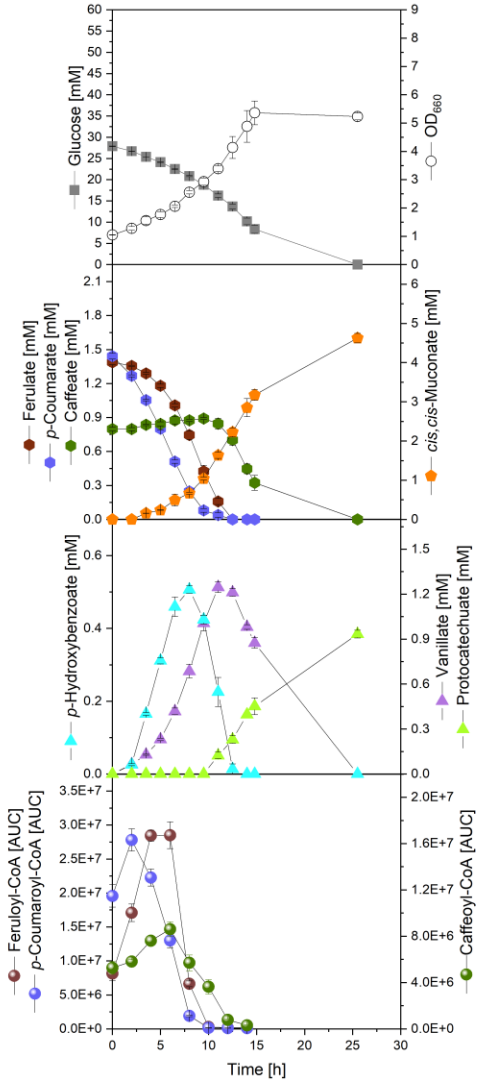

Figure 11. Cultivation of *C. glutamicum* MA10 strain on a combination of aromatics. The MA10 strain was cultivated in minimal medium containing a combination of 5 g L^{-1} of glucose, 1.5 mM each of ferulate, *p*-coumarate and caffeate. All cultivation was performed in triplicate (n=3) while the CoA thioester samples were taken in duplicate (n=2). The data represent mean values and standard deviations.

3.2.6 Cross-pathway interaction during degradation of ferulate

In order to understand why caffeate remained unutilized, targeted analysis of various aromatic CoA thioesters in the wildtype and the MA-10 strain was performed using the MRM method.

When caffeate was supplied to the medium, feruloyl-CoA was not detected. Intriguingly, caffeoyl-CoA was observed in the ferulate-amended culture. When both the wild type and the mutant strains were cultivated in the ferulate-amended culture, caffeoyl-CoA was detected (Fig. 12).

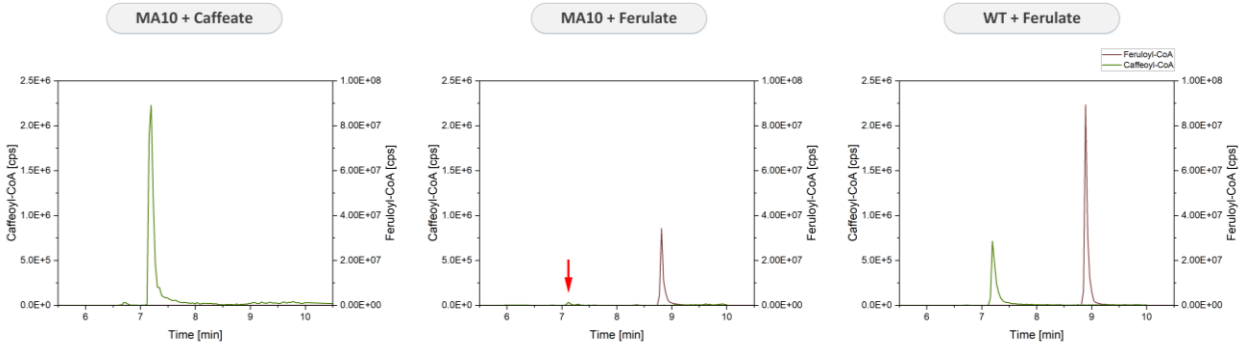

Figure 12. Targeted analysis of caffeoyl-CoA and feruloyl-CoA in *C. glutamicum* strains using LC-MS/MS. The caffeoyl-CoA and feruloyl-CoA content in the CoA thioester extraction from caffeate-amended and ferulate-amended cultures were analysed using LC-MS/MS. The samples were taken from the experiments described in Fig. 6A (WT) and Fig. 10C, G (MA10). The initial acquisition method was used for detection of all CoA thioesters, and the retention time of peaks was adjusted to the second acquisition method.

The conversion of phenylpropanoids in *C. glutamicum* is conducted by the same enzymes (PhdA-E). Consequently, degradation was expected to proceed in a unidirectional manner, such as from ferulate to feruloyl-CoA, to 3-hydroxyferuloyl-CoA, to 3-oxoferuloyl-CoA, and finally to vanillate, without cross-interaction (Fig. 2). However, in this study, caffeoyl-CoA was detected in the ferulate-amended culture, suggesting that the presence of ferulate might induce the formation of caffeoyl-CoA, possibly due to enzymatic conversion or metabolic pathway overlap.

Considering the biosynthesis of ferulate (Fig. 2), ferulate is produced from caffeate by caffeate *O*-methyltransferase (COMT) (Ma & Xu, 2008). *C. glutamicum* lacks COMT, requiring additional functional expression of plant-derived *O*-methyltransferase to produce methylated plant polyphenols, including pterostilbene, kaempferol, and quercetin (Kallscheuer et al., 2017). The absence of feruloyl-CoA formation from caffeoyl-CoA supports previous studies with metabolomic evidence. In contrast, the degradation of ferulate involves *O*-demethylation. In a previous study, ferulate was converted to vanillate, which was then *O*-demethylated by vanillate *O*-demethylase (VanAB) (Merkens et al., 2005). However, this observation indicates that *C. glutamicum* may possess an additional *O*-demethylase capable of converting ferulate in an earlier step of the pathway.

Because the Phd enzymes were responsible for both caffeoyl-CoA and feruloyl-CoA conversion, the substrate preference of these enzymes determined the substrate preference of the strain. Additionally, ferulate could be converted to caffeate by *O*-demethylation, leading to the occupation of the caffeate degradation pathway. As a result, caffeate remained untouched (Fig. 11). This discovery suggests a competitive interaction between the degradation pathways of ferulate and caffeate, likely due to the shared enzymatic machinery.

This cross-pathway interaction indicates a more complex metabolic network in *C. glutamicum* than previously understood, where the presence of one aromatic compound can influence the metabolism of another. The detection of caffeoyl-CoA in the ferulate-amended culture suggests intricate interactions between different aromatic compounds in *C. glutamicum* metabolism. Specifically, it indicates that ferulate might play a role in influencing the metabolic fate of caffeate or vice versa. This finding highlights the need to consider such interactions when engineering microbial strains for lignin valorisation or other biotechnological applications involving complex aromatic substrates.

Understanding these interactions could lead to more efficient metabolic engineering strategies by taking into account the competitive and synergistic effects between different pathways. This could enhance the microbial conversion of lignin-derived aromatic compounds into valuable bioproducts, thereby improving the feasibility and efficiency of lignin valorisation processes.

3.2.7 Extension of the accessible CoA thioester spectrum

To analyse the impact of genetic modifications on catabolic pathway flux, the wild type and the metabolically engineered strain *C. glutamicum* MA10 were cultivated in minimal medium containing glucose and ferulate, and harvested, during the ferulate consumption phase. The CoA-thioester samples were harvested in the stationary phase (11 h) for the wild-type strain (Fig. 6A), whereas the mutant, capable of co-consuming glucose and ferulate, had its CoA samples harvested in the exponential phase at an OD of 2.5 (7 h) (Fig. 10C). Both strains were actively consuming ferulate at their respective sampling time points.

The concentrations of intermediates in the upper pathways were strongly altered compared to those in the wild type (Fig. 13).

In the *phd* cluster, 3-oxoacyl-CoA ketohydrolase (PhdC) is responsible for the conversion from 3-oxoferuloyl-CoA to vanillate by cleaving acetyl-CoA. Although, there is an alternative route to vanilloyl-CoA via 3-ketoacyl thiolase (Fig 3). However, 3-ketoacyl thiolase is not present in the *phd* cluster, and *C. glutamicum* naturally lacks 3-ketoacyl-CoA thiolase, yet it still produced a minor amount of vanilloyl-CoA. Given the minor amounts observed of vanilloyl-CoA, it seemed to originate likely from an unspecific reaction catalysed by other thiolases.

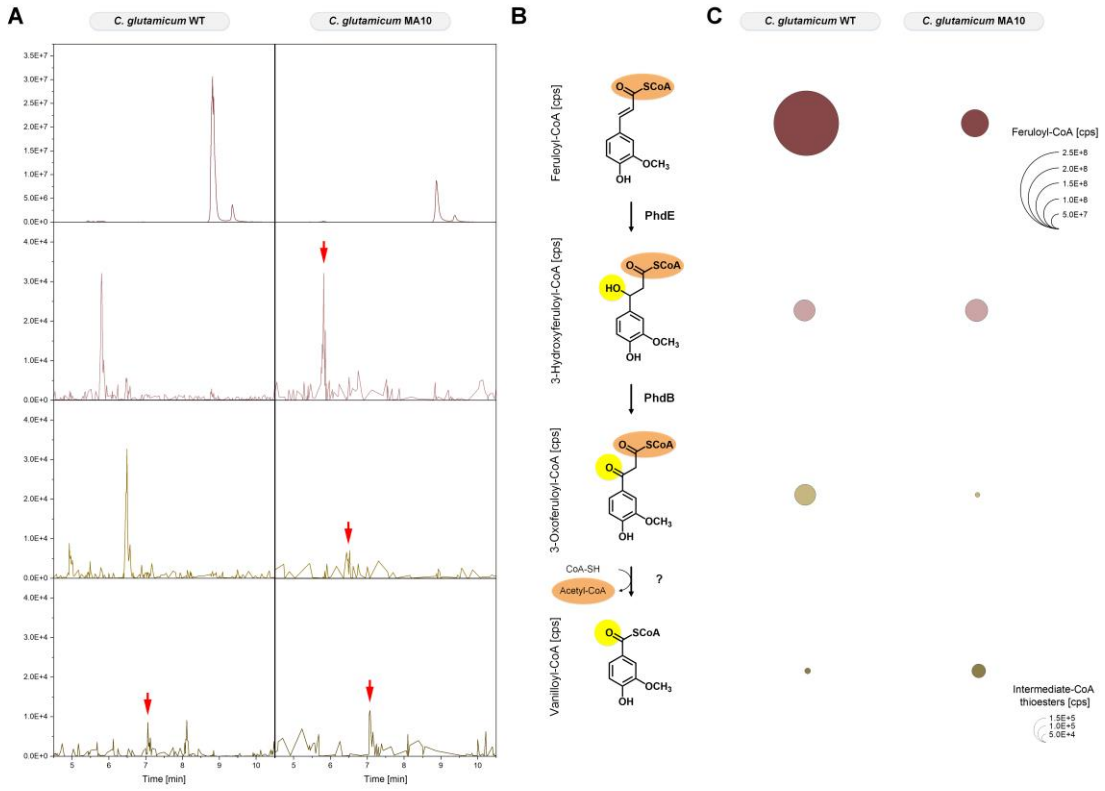

Figure 13. Targeted analysis of CoA-thioester intermediates in ferulate degradation pathway in *C. glutamicum* using LC-MS/MS. *C. glutamicum* strains were cultivated in minimal medium containing 5 g L^{-1} of glucose and 5 mM of ferulate. The CoA thioester samples were harvested as the aromatic compound was consumed. The chromatogram from the MRM analysis of intracellular metabolites using LC-MS/MS is shown (A). The degradation pathway is illustrated (B), with the converted part highlighted in colours. The concentration of each intermediate is displayed, with the circle size indicating the intensity of each metabolite. All LC-MS/MS quantitative values were normalized to the OD_{660} value of 2.5.

A significant difference in the intracellular feruloyl-CoA pools between the wild type and the mutant strain was observed (Fig. 13C). Notably, the wild type consumed ferulate within 2 hours and therefore than the mutant, which required 12 hours to degrade the aromatic. The resulting high consumption rate in the wild type as compared to the mutant, might explain its higher feruloyl-CoA concentration. However, the huge accumulation of feruloyl-CoA indicates a bottleneck in the functionality of enoyl-CoA hydratase (PhdE). On the other hand, 3-hydroxyferuloyl-CoA was present at similar level in both strains, implying that the mutant strain was capable of efficiently

converting feruloyl-CoA. This suggests that the mutant strain was capable of processing aromatics efficiently up to this intermediate stage likely due to the consistent expression of the Phd cluster.

In general, CoA thioesters are recognized as unstable molecules prone to spontaneous hydrolysis and thiol-disulfide bond formation (Siegel et al., 2014). However, feruloyl-CoA was found to be very stable in aqueous conditions at pH 5.7 (Supplementary data: Fig. S1), suggesting that feruloyl-CoA can act as a storage molecule for carbon sources.

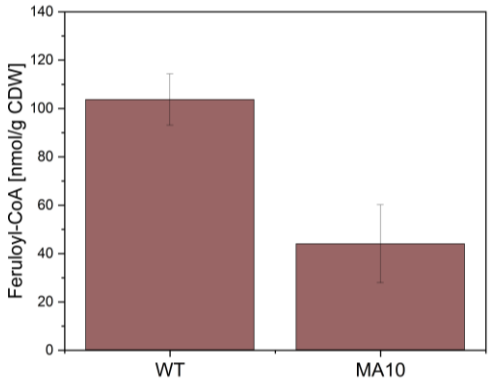

Figure 14. Absolute quantification of intracellular feruloyl-CoA in *C. glutamicum*. *C. glutamicum* strains were cultivated in minimal medium containing 5 g L^{-1} of glucose and 5 mM of ferulate. The CoA thioester samples were harvested when ferulate was actively consumed. The absolute concentration of intracellular feruloyl-CoA was calculated assuming no degradation while quenching and analysis. The value was normalized based on CDW of each sample. The data represent mean values and standard deviations of duplicate (n=2).

Based on the given stability of feruloyl-CoA, intracellular feruloyl-CoA was absolutely quantified, assuming that no degradation occurred during the quenching and analysis process (Fig. 14). The intracellular feruloyl-CoA concentration was determined as 103.6 nmol g^{-1} in the wild type and 43.9 nmol g^{-1} in MA10 strain.

Considering the concentrations of CoA thioesters involved in central metabolism in *C. glutamicum* (Gläser et al., 2020), with methylmalonyl-CoA and succinyl-CoA concentrations at 750 and 110 nmol g^{-1}, respectively, the accumulated amount of feruloyl-CoA in the wild-type strain is notably significant, reaching levels comparable to that of succinyl-CoA.

3.2.8 Ferulate metabolization affects the intracellular acetyl-CoA pool

When analysing different masses for feruloyl-CoA, ranging from Q1 934.2/ Q3 427.2 to Q1 975.2/ Q3 468.2 Da (Fig. 15A), the compound, analysed from the cultivation of *C. glutamicum* MA10 grown on ^{13}C glucose and ^{12}C ferulate, exhibited a bimodal distribution, due to the release of acetyl-CoA during the conversion of 3-oxoferuloyl-CoA into vanillin. (Fig. 15C).

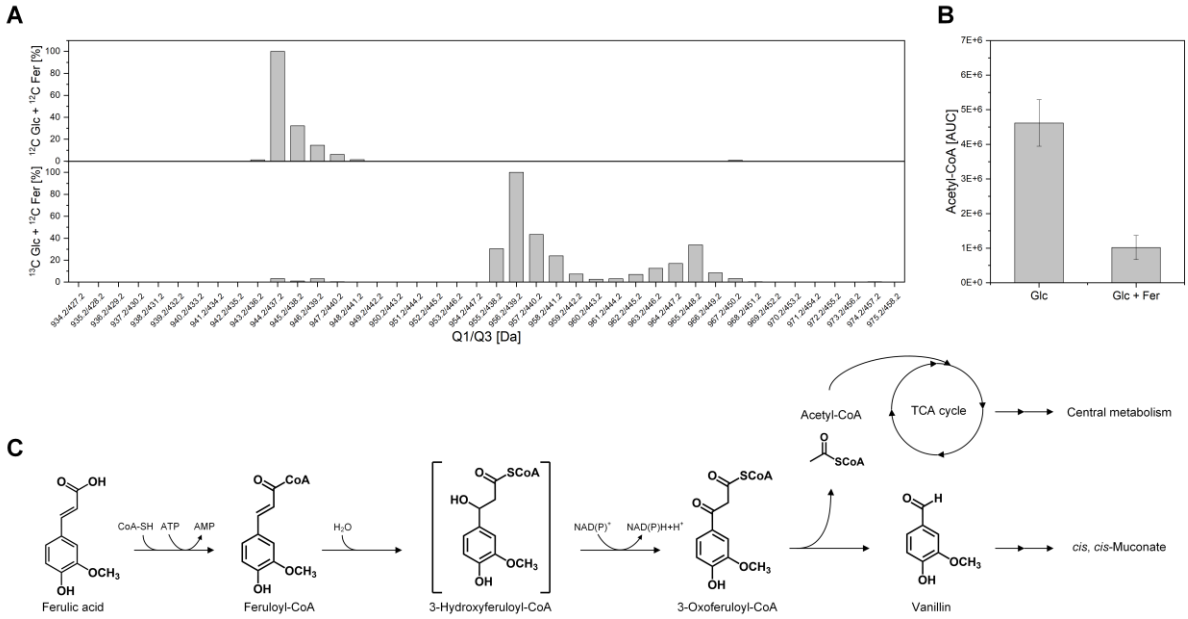

Figure 15: The distribution of feruloyl-CoA isotopes, comparison of acetyl-CoA contents, and β-oxidative degradation pathway of ferulate. The isotope distribution of feruloyl-CoA was examined by MRM scanning from Q1 934.2/ Q3 427.2 to Q1 975.2/ Q3 468.2 Da (A). The comparison of acetyl-CoA contents from cell extracts cultivated solely on glucose and those from glucose and ferulate-amended culture. The CoA thioester samples were prepared when the OD reached 2.5. Data represent mean values and standard deviations from three biological replicates (n=3) (B). The ferulate degradation in *C. glutamicum* MA10 produces acetyl-CoA, subsequently assimilated into the central metabolism (C).

To further explore the effects of ferulate utilization on central carbon metabolism, the intracellular acetyl-CoA level from glucose-grown cells was compared to cells cultivated on a mixture of glucose and ferulate. The acetyl-CoA concentration was significantly lower in the presence of

ferulate (Fig. 15B). The acetyl CoA-supplying consumption of ferulate together with glucose mimics the co-consumption of acetate and glucose. Previous analysis of the co-consumption of glucose and acetate in *C. glutamicum* revealed that glucose primarily served as precursor for glycolytic intermediates, while acetyl-CoA was predominantly supplied from acetate (Wendisch et al., 2000). It seems that also aromatics have an impact on the central catabolic routes. Further research is required to clarify this relationship.

The main strategy for producing *cis, cis*-muconate from aromatic compounds involves the deletion of downstream pathways (Becker et al., 2018a; Salvachúa et al., 2020; Weiland et al., 2023). When producing *cis, cis*-muconate from funnelled intermediates such as catechol, benzoate, and guaiacol, there is no direct interaction between central metabolism and aromatic catabolism. However, utilizing ferulate, *p*-coumarate, and caffeate, which involve the upper degradation pathway, results in the cleavage of acetyl-CoA. This cleavage impacts the central metabolism by altering the acetyl-CoA pool. Therefore, a detailed examination of central metabolism through metabolomic studies is required, along with careful consideration of genetic modifications.

To produce *cis, cis*-muconate effectively from these substrates, it is essential to understand how the introduction of ferulate, *p*-coumarate, and caffeate affects the acetyl-CoA levels and overall metabolic flux. The cleavage of acetyl-CoA from these compounds leads to changes in the central metabolic pathways, influencing the balance and availability of key metabolites. Further metabolomic studies would provide a comprehensive view of the metabolic changes that occur when these aromatic compounds are utilized, revealing any potential bottlenecks or imbalances in the metabolic network. This information is crucial for designing targeted genetic modifications to optimize the production process.

4 From waste to health molecules: Biosynthesis of natural products from lignin-, plastic-, and seaweed-based monomers using metabolically engineered *S lividans*

The results of this work have been published and re-written in this thesis.

Kyoyoung Seo, Wei Shu, Christian Rückert-Reed, Patrick Gerlinger, Tobias J. Erb,

Jörn Kalinowski & Christoph Wittmann

Microbial Cell Factories volume 22, Article number: 262 (2023)

https://doi.org/10.1186/s12934-023-02266-0

4.1 Materials and Methods

4.1.1 Microorganisms and plasmids

Streptomyces lividans ΔYA8 was gained from previous work (Ahmed et al., 2020). Plasmids were amplified using *Escherichia coli* DH5α (Invitrogen) while *E. coli* ET12567/pUZ8002 was employed for conjugal gene transfer (Kieser et al., 2000). Cosmids, DG2-Km-P41hyg (bottromycin biosynthetic gene cluster under synthetic promoter control) (Horbal et al., 2018) and R2 (pamamycin biosynthetic gene cluster under synthetic promoter control) (Rebets et al., 2015), respectively, were taken from previous work. All strains were stored in 20% glycerol at -80°C. All strains and plasmids are listed in Table 9.

Table 9. Strains and plasmids.

Strains and plasmids	Description	Reference
Strains		
E. coli DH5α	Strain for plasmid amplification	Invitrogen
E. coli ET12567	Strain harbouring pUZ8002 for conjugal gene transfer	(Kieser et al., 2000)
E. coli BL21 (DE3)	Strain for high-level expression of recombinant proteins	Thermo Fisher Scientific
S. lividans ΔYA8	Derivative of *S. lividans* TK24, 8 secondary metabolite gene clusters were removed from genomic DNA.	(Ahmed et al., 2020)
S. lividans ΔYA8-DG2	Derivative of *S. lividans* ΔYA8 containing bottromycin biosynthetic cluster	This work
S. lividans ΔYA8-R2	Derivative of *S. lividans* ΔYA8 containing pamamycin biosynthetic cluster	This work
Plasmids		
DG2-Km-P41hyg	Derivative of integrative DG2-cosmid with Km^R marker and P41 promoter pairs, contains bottromycin biosynthetic cluster	(Horbal et al., 2018)
R2	An Integrative cosmid containing pamamycin biosynthetic gene cluster	(Rebets et al., 2015)

4.1.2 Media

S. lividans were grown on mannitol soy (MS) flour agar, containing followings per liter: 20 g of mannitol, 20 g of soy flour (Schoenenberger Hensel, Magstadt, Germany), and 20 g of agar (Becton & Dickinson). Liquid cultures of *S. lividans* involved two sequential precultures, followed by the main culture. Tryptic soy broth (30 g L^{-1}, TSB, Sigma-Aldrich) was used for the first

precultivation. The second precultivation and the main cultivation were conducted in minimal medium, containing per liter: 200 mM potassium phosphate buffer (pH 7.8): 15 g of $(NH_4)_2SO_4$, 1 g of NaCl, 200 mg of $MgSO_4 \cdot 7H_2O$, 55 mg of $CaCl_2$, 20 mg of $FeSO_4 \cdot 7H_2O$, 2 mg of $FeCl_3 \cdot 6H_2O$, 2 mg of $MnSO_4 \cdot H_2O$, 0.5 mg of $ZnSO_4 \cdot H_2O$, 0.2 mg of $CuCl_2 \cdot 2H_2O$, 0.2 mg of $Na_2B_4O_7 \cdot 10H_2O$, 0.1 mg of $(NH_4)_6Mo_7O_{24} \cdot 4H_2O$, 1 mg of riboflavin, 1 mg of nicotinamide, 0.5 mg of thiamine hydrochloride, 0.5 mg of pyridoxine hydrochloride, 0.2 mg of biotin, and 0.1 mg of *p*-aminobenzoate. Mannitol, protocatechuate (PCA), and 4-hydroxybenzoate (4HB), respectively, were added as carbon source, as given below. When needed, kanamycin (50 µg mL^{-1}), apramycin (20 µg mL^{-1}), phosphomycin (200 µg mL^{-1}), and ampicillin (100 µg mL^{-1}), respectively, were added from filter sterilized stocks when needed.

4.1.3 Genetic engineering

For strain and primer design, the software SnapGene (GSL Biotech LLC, San Diego, USA) was utilized. Transformation and conjugation of S. *lividans* ΔYA8 was based on standard methods (Kieser et al., 2000). The site-specific integration of biosynthetic gene clusters into genomic DNA of S. *lividans* ΔYA8 was carried out using the phiC31 integrase system (Horbal et al., 2018). In detail, the corresponding cosmid was transformed into *E. coli* DH5α using heat shock, amplified, isolated (QIAprep Spin MiniPrep Kit, Qiagen, Hilden, Germany), and transformed into *E. coli* ET12567/pUZ8002 by electroporation. The resulting mutant served as a donor for conjugal transfer. The mutant was mixed with spores of *S. lividans* ΔYA8 and plated on MS agar and incubated at 30 °C overnight. To obtain positive transconjugants, the agar was overlayed with phosphomycin and a selective antibiotic. Subsequently, the plates were further incubated until sporulation. The obtained transformants were verified for correctness of the desired genetic change by PCR (Phire Green Hot Start II PCR Mastermix, Thermo Scientific) and by sequencing.

4.1.4 Preparation of brown seaweed hydrolysate

Himanthalia elongate, a brown seaweed, was chosen to prepare mannitol-rich hydrolysate. In brief, 50 g of dried *Himanthalia elongata* (PureRaw, Klötze, Germany) was blended into powder, and suspended in 500 mL of deionized water, and extracted (121 °C, 18 min) (Hoffmann et al., 2021). The extract was adjusted to pH 5.5, then depolymerized by adding Celluclast 1.5 L and Viscozyme L (Sigma-Aldrich) at a level of 0.01 g of the enzyme mix per g of dry biomass, followed by incubation over 48 hours. Sequentially, the hydrolysate was centrifuged (4500 x g, 15 min, 4 °C) and re-adjust to pH 7.0 (6 M NaOH). The obtained solution was autoclaved prior to further use. Preparation of seaweed hydrolysate was conducted by Wei Shu at Institute of Systems Biotechnology (Saarland, Germany).

4.1.5 Batch cultivation of Streptomyces strains on defined media

Cultivations were conducted in 500 mL baffled shake flasks, filled with 50 mL medium and 30 g soda-lime glass beads (5 mm, Sigma-Aldrich) on an orbital shaker (230 rpm, 28 °C, 75% relative humidity, 5 cm shaking diameter, Multitron, Infors AG). For bottromycin production, 10^7 spores of the bottromycin producing strain were inoculated into TSB medium and incubated for 48 hours. Following the incubation, cells were collected (8000 × *g*, 2 min, 25 °C), and transferred to the second preculture in minimal medium, containing 10 g L^{-1} of mannitol as carbon source. After 72 hours incubation, the culture was harvested, and inoculated to the main culture containing either mannitol, PCA or 4HB, as described below. For pamamycin production, 10^7 spores of the pamamycin producer were inoculated into TSB medium. The cells were incubated for 24 hours. Then, either 10 mM of mannitol or 4HB was added to the preculture for adaptation, followed by an additional 24 hours of incubation. Subsequently, the cells were harvested by centrifugation (8000 × g, 2 min, 25 °C) and inoculated into the main culture in minimal medium containing either mannitol or 4HB. Routinely, the main cultures were inoculated to a starting optical density (OD_{600}) = 0.5. All cultivations were performed in triplicate.

4.1.6 Batch cultivation on seaweed hydrolysate

The seaweed hydrolysate was mixed with 2M MOPS buffer (pH 7.0) at a volume ratio of 9:1 (v/v). As described above, 10^7 spores of the pamamycin producing strain were inoculated into TSB medium and incubated for 48 hours. Afterwards, the cells were collected by centrifugation (8000 × *g*, 2 min, 25 °C) and inoculated to seaweed hydrolysate containing 200 mM MOPS buffer.

4.1.7 Fed-batch cultivation in shake flasks

The first and second preculture of bottromycin producing mutant was prepared, harvested, and transferred to the second preculture as described in 4.1.5. The main culture contained 30 mM of 4HB as an initial concentration. When the concentration of 4HB is depleted, concentrated 4HB (500 mM , pH 7.0) was added to the main culture to restore the 4HB level to 30 mM.

4.1.8 Quantification of cell concentration and substrates

Cell growth was measured spectrophotometrically by optical density at 600 nm (OD_{600}). For correlation of OD-cell dry weight (CDW), cells were centrifuged (10,000 × *g*, 4 °C, 10 min), washed with 15 mL deionized water, lyophilized, and weighed (Kuhl et al., 2020). The substrate specific correlation between OD_{600} and CDW is as follows: CDW (g L^{-1}) = 0.946 × OD_{600} (mannitol, 4HB), CDW (g L^{-1}) = 0.474 × OD_{600} (PCA). The correlation between OD600 and CDW is plotted in Supplementary data: Fig. S7. The concentrations of mannitol and aromatic were quantified as described in 3.1.5.

4.1.9 Quantification of intracellular amino acids

Intracellular amino acids were quantified as previously described (Bolten et al., 2007; Schwechheimer et al., 2018). In detail, 2 mg of biomass was harvested by vacuum filtration (cellulose nitrate, 0.2 µm pore size, 47 mm, Sartorius, Göttingen, Germany). The filter with the cells was washed (15 mL 2.5% NaCl, 25 °C), and quickly transferred into 2 mL of a 200 µM *α*-aminobutyrate solution. Afterwards, amino acids were extracted in boiling water (15 min, 100°C),

followed by cooling down on ice and removal of debris (20,000 × *g*, 5 min, 4°C). The amino acid contents in the solution was separated on a reversed phase column (Gemini 5 µm C18 110 Å, 150 x 4.6 mm, Phenomenex) by HPLC after precolumn derivatization with *o*-phthaldialdehyde and fluorenylmethyloxycarbonyl chloride (Rohles et al., 2016). The Quantification was based on *α*-aminobutyrate as internal standard.

4.1.10 Analysis of absolute quantification of intracellular CoA thioesters

Intracellular CoA thioesters were quantified using a previously established protocol (Gläser et al., 2020; Kuhl et al., 2020) as described in 3.1.9 with minor adaptations. In brief, cell culture, containing approximately 8 mg CDW, was transferred into a quenching solution (95% acetonitrile with 25 mM formic acid, -20 °C) at a volume ratio of 1:2, mixed and kept on ice for 10 min. Cell debris was clarified by centrifugation (10 min, 4 °C, 10,000 × *g*). The supernatant was combined with 5 mL of super cooled deionized water. The pellet was washed once with 5 mL of super cooled deionized water, followed by collection of all supernatants, freezing in liquid nitrogen, and lyophilization. The extract powder was resuspended in 1 mL of resuspension buffer (25 mM ammonium formate, pH 5.6, 2% methanol, 4°C). Subsequently, CoA thioesters were analysed using LC-ESI-MS/MS with separation on a reversed phase column. Multiple reaction monitoring (MRM) was employed for detection of CoA thioesters. The external standards were obtained from previous work (Gläser et al., 2020) whereas internal standard was prepared using 99% 4-hydroxybenzoic acid-[phenyl-$^{13}C_6$] (Sigma-Aldrich) following by the established method (Gläser et al., 2020).

4.1.11 Analysis of bottromycin and pamamycin

In brief, 300 µL of culture broth was mixed with an equal volume of acetone and shaken for 10 min at 25 °C (1,000 rpm, Thermomixer F1.5, Eppendorf, Wesseling, Germany). Afterwards, 300 µL of ethyl acetate was added, followed by an additional incubation under the same condition for 10 min. The mixture was centrifuged (20,000 × *g*, room temperature, 10 min). Then, organic phase

was collected and evaporated under nitrogen. The extract was resuspended in 300 µL of methanol, followed by removal of debris (20,000 × *g*, 4 °C, 10 min). The obtained extract was analysed by LC-ESI-MS (Agilent Infinity 1290; AB Sciex QTrap 6500, Darmstadt, Germany) (Gläser et al., 2020; Horbal et al., 2018; Kuhl et al., 2021). The analytes were separated on a reversed phase column (Vision HT C18 HighLoad, 100 × 2 mm, Dr. Maisch, Ammerbuch-Entringen, Germany) at 45 °C. Pamamycins were separated using an isocratic gradient of eluent A (8 mM ammonium formate in 92% acetonitrile) at a flow rate of 0.3 mL min^{-1}. Bottromycin was separated using an identical column, with a flow rate of 0.55 mL min^{-1}. The gradient of eluents was described as follows: 0.1% formic acid in deionized water (A) and 0.1% formic acid in acetonitrile (B): 0-11 min, 95 - 5% A, 5 - 95% B.

4.1.12 Transcriptomic analysis

Samples were collected (20,000 × *g*, 1 min, 4 °C) during the exponential phase, specifically 12 hours after inoculation, followed by quick-freeze in liquid nitrogen. Sample preparation, RNA extraction, and RNA sequencing were conducted in biological triplicate and technological quintuplicate as described previously (Gläser et al., 2021; Kuhl et al., 2020; Kuhl et al., 2021). The extraction of RNA was conducted using Qiagen RNA Mini kit (Qiagen) according to the manufacturer's instructions. The removal of residual DNA was performed by digestion with 10 U RNase-free DNase I (Thermo Scientific) for 1 h in the presence of RiboLock RNase inhibitor (Thermo Scientific), followed by re-purification of RNA with the same kit. The quality of RNA was verified by Trinean Xpose (Gentbrugge, Belgium) and the Agilent RNA 6000 Nano Kit on an Agilent 2100 Bioanalyser (Agilent Technologies, Böblingen, Germany). The removal of ribosomal RNA (rRNA) was conducted from the total RNA with the Ribo-Zero rRNA Removal Kit (Illumina, San Diego, USA) and verified with the Agilent RNA 6000 Pico Kit on an Agilent 2100 Bioanalyser (Agilent Technologies). The preparation of cDNA libraries was carried out with the TruSeq Stranded mRNA Library Prep Kit (Illumina), followed by sequencing of the resulting cDNA in a

paired-end fashion on an Illumina NextSeq 500 system with 2x75 bp read length. The reads underwent alignment to the *S. lividans* TK24 ΔYA8-DG2 genome sequence (CP111182.1) using Bowtie2 (Langmead & Salzberg, 2012), with adjustments such as increasing the maximum allowed distance for paired reads to 600 bases. Read alignments and raw read count calculation were visualized using ReadXplorer 2.2.3 (Hilker et al., 2014). DESeq2 (Love et al., 2014) was then utilized for quality control, including principal component analysis (Supplementary data: Fig. S3) and sample-to-sample distance calculation (Supplementary data: Fig. S4), as well as for generating differentially expressed gene (DGE) datasets. Both raw (sequenced reads) and processed (input matrix & normalized read counts from DESeq2) datasets are accessible from GEO (GSE246798). Statistical analysis involved a Student's t-test, filtering genes based on a $\log_2$fold change ≥ 1 (adjusted p value ≤ 0.05). Hierarchical clustering was performed using the gplots software package (R core team 2014; Warnes et al., 2016). The entire process of RNA extraction and sequencing was conducted three times for biological replicate. RNA extraction, sequencing, and data processing were performed by Dr. Christian Rückert-Reed at Cebitec (Bielefeld, Germany).

4.2 Results and Discussion

4.2.1 Heterologous production of bottromycin in *S. lividans* on renewable monomer

To verify the native capability of *S. lividans* to utilize sustainable monomers, *S. lividans* TK24, the wild type strain, was incubated on minimal media agar plate containing mannitol, protocatechuate, or 4-hydroxybenzoate, respectively (Supplementary data: Fig. S2). The *S. lividans* TK24 was capable of growing on all substrates as a sole carbon source. To minimize the interference caused by the production of native natural products, *S. lividans* ΔYA8, a genetically modified strain of *S. lividans* TK24 in which eight natural biosynthetic clusters were deleted (Ahmed et al., 2020), was used. Then, DG2-Km-P41hyg (Horbal et al., 2018), a cosmid for bottromycin biosynthesis under control of P41 synthetic promoters, was integrated into the genomic DNA of *S. lividans* ΔYA8 at the attB site (locus tag, SLIV_19310) using Int-phiC31 recombinase system, resulting in the generation of a novel bottromycin producer strain named *S. lividans* ΔYA8-DG2.

To evaluate its production performance, the same minimal media was used as in the initial growth tests. *S. lividans* ΔYA8-DG2 successfully formed bottromycin from mannitol as sole carbon source with concentrations of 10, 20, and 30 mM. Overall, both the titre of bottromycin and the biomass yield increased with cultivation time, resulting in the highest production of bottromycin from 30 mM of mannitol.

In addition to mannitol, a potential of production from protocatechuate and 4-hydroxybenzoate was explored. The initial concentrations of substrates were increased up to 30 mM. The cultivations on aromatics have proven that the strain catabolizes protocatechuate and 4-hydroxybenzoate efficiently. The concentration of protocatechuate in the culture decreased faster than mannitol at 10 mM and 20 mM, in contrast, 30 mM of 4-hydroxybenzoate results in extension of lag phase and cultivation period. In general, biomass yielded from aromatic was lower than the

biomass from mannitol. A possible explanation is that decreased energy was yielded from aromatics compared to sugars (Becker et al., 2018a; Weiland et al., 2023).

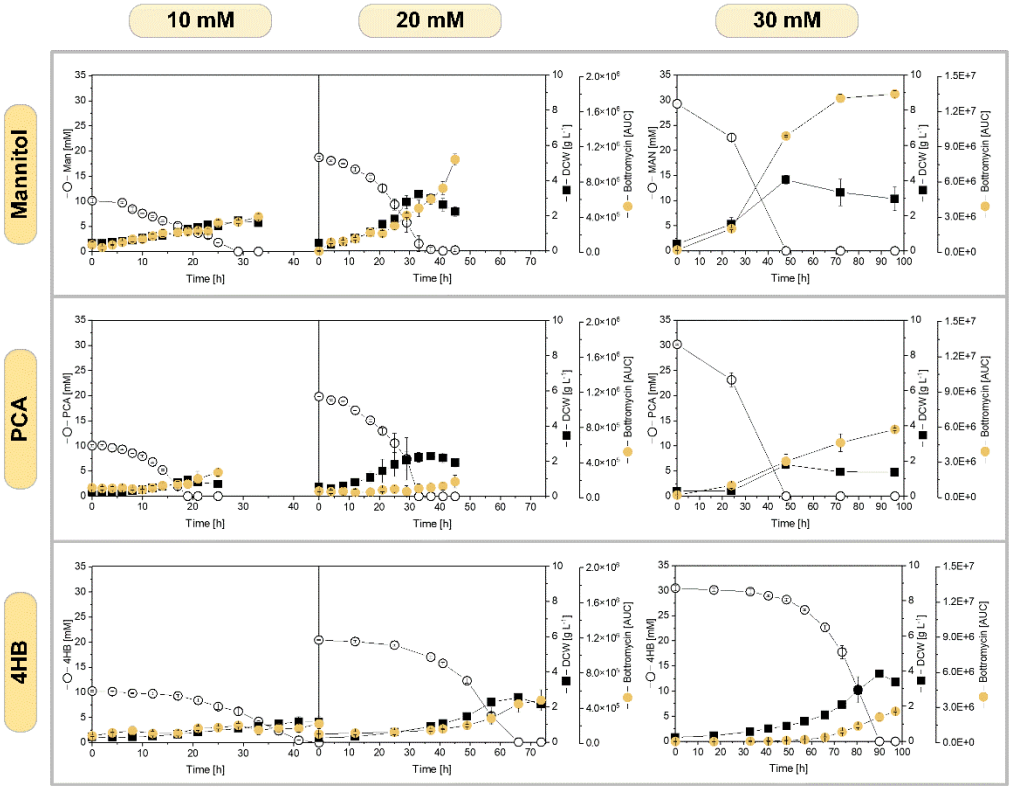

Figure 16. Production of biomass and bottromycin from sustainable monomers. The engineered strain was cultivated on mannitol, protocatechuate (PCA), and 4-hydroxybenzoate (4HB) with 10 mM, 20 mM, and 30 mM of concentrations. The data represent mean values and standard deviations of triplicate (n=3). The figure was obtained from a previously published paper (Seo et al., 2023).

Bottromycin was produced from all tested substrates despite deviations of bottromycin and biomass levels depending on substrates, proving the potential of robustness of *S. lividans* in next-generate substrates utilization, including toxic compounds. The production of bottromycin was initiated from early stage of cultivation and maintained steady independent of the presence of substrate and growth phase, likely due to synthetic promoter regulating the bottromycin gene cluster (Horbal et al., 2018; Kuhl et al., 2021).

4.2.2 Fed-batch cultivation on 4-hydroxybenzoate

As stated above, *S. lividans* ΔYA8-DG2 is highly resistant to 4-hydroxybenzoate. To enhance the production of bottromycin, the strain was cultivated in a fed-batch process with a repeat feeding of 4-hydroxybenzoate, showing the highest toxicity among tested substrates.

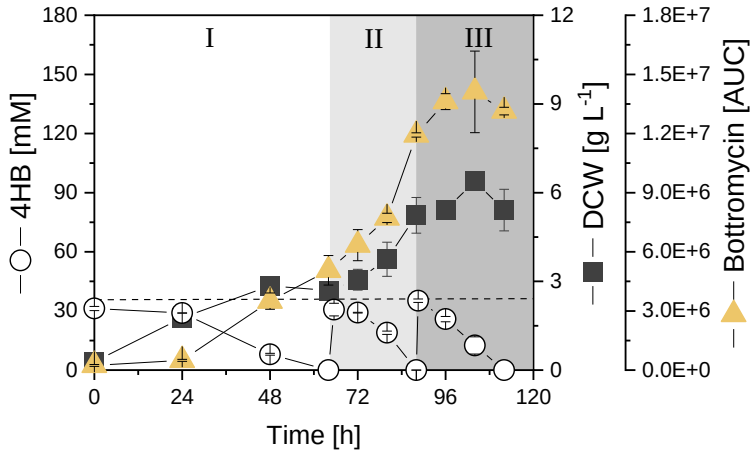

Figure 17. The fed-batch cultivation of *S. lividans* ΔYA8-DG2 on 4-hydroxybenzoate (4HB). The substrate was repeatedly fed to the culture when completely consumed. The data represent mean values and standard deviations of three biological replicates (n=3) (A). The figure was obtained from a previously published paper (Seo et al., 2023).

The initial concentration of 4-hydroxybenzoate was 30 mM, as shown in Fig. 17, and was monitored in real time throughout the process. When the substrate was depleted, the concentrated stock was added to the culture to bring the concentration back up to 30 mM. Compared to the initial substrate consumption rate, the substrate was consumed after in an additional supply and produce bottromycin constantly. Furthermore, it catabolizes a third supply 4-hydroxybenzoate, resulting in consumption of 90 mM of substrate in total. In conclusion, bottromycin was 3-times higher titre than the batch culture, demonstrating that *S. lividans* is able to convert aromatics to bottromycin in a fed-batch procedure. Afterwards, bottromycin A_2 was extracted from the culture broth. The ethyl acetate extract from the culture broth was analysed by LC-MS, which showed that the product is identical to the commercial product.

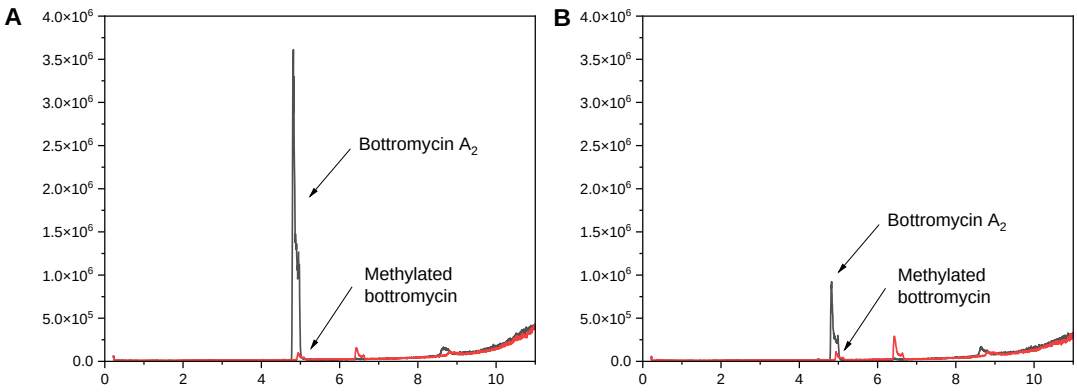

Figure 18. LC-MS analysis of ethyl acetate extract. The culture broth was harvested and extracted using ethyl acetate to verify formation of bottromycin A_2 ($[M+H]^+$ = 823.453) and methylated bottromycin $[M+H]^+$ = 837.453) (A). The extract was compared to commercial product (B) The figure was obtained from a previously published paper (Seo et al., 2023).

4.2.3 Transcriptomic analysis

To gain a comprehensive understanding of metabolism, gene expression levels were compared between mannitol-amended cultures and aromatic-amended cultures. This comparison allows for a systemic analysis of metabolic changes in response to different substrates. As described above, *S. lividans* ΔYA8-DG2 was cultivated on 10 mM of three distinct substrates: mannitol, protocatechuate, or 4-hydroxybenzoate. In middle of exponential phase (12 h), RNA samples were taken, extracted and sequenced. The PCA plot of RNA sequencing confirmed reliable statistical quality (Supplementary data: Fig. S3). Metabolic changes were observed at the level of global gene expression by substrate, with separate sample sets clustered (Supplementary data: Fig. S4). Compared to the culture on mannitol, the culture based on protocatechuate changes the expression level of 387 genes (5.2 % of the total of 7497 genes), while the culture based on 4-hydroxybenzoate alters the expression level of 1,786 genes (23.8 %). Between the two aromatics, 1,373 genes (18.3%) were differentially expressed (adjusted p-value < 0.05, $\log_2$ fold change ≥1). The most significantly up-regulated and down-regulated genes belonged to different functional categories (Table 10 and 11).

Table 10. The genes up-regulated in *S. lividans* ΔYA8-DG2 on aromatic-amended culture. The 40 genes most up-regulated on protocatechuate compared to mannitol (adj $p < 0.05$, log_2fold change> 2.0) were listed. The genes encoding enzymes of the TCA cycle (●), the EMP pathway, gluconeogenesis (●), aromatic catabolism (●), and the ethylmalonyl-CoA pathway (●). Further genes encode other enzymes (M) and regulators (R), as well as proteins of unknown function (U). (Fig. 19). n=3. The table was obtained from a previously published paper (Seo et al., 2023).

Function	Annotation	Gene	PCA	4HB
R	Two component histidine kinase	SLYA8N_18305	10.2	6.3
●	Cytochrome B subunit	SLYA8N_33310	8.7	8.5
M	Glycosyl transferase	SLYA8N_18300	8.1	3.4
M	ABC transporter, ATP-binding protein	SLYA8N_13690	8.0	1.1*
●	Succinate dehydrogenase/fumarate reductase iron-sulfur subunit	SLYA8N_33320	7.6	8.5
●	Hypothetical protein	SLYA8N_33325	7.4	8.3
M	Protease	SLYA8N_17590	7.3	0.2*
●	Succinate dehydrogenase flavoprotein subunit	SLYA8N_33315	7.1	7.6
●	Benzaldehyde dehydrogenase	SLYA8N_02130	6.7	8.4
R	Transcriptional regulatory protein	SLYA8N_18310	6.4	2.8
●	4-Carboxymuconolactone decarboxylase	SLYA8N_05020	6.4	6.2
●	Crotonyl-CoA reductase	SLYA8N_06060	6.3	3.6
●	β-Ketoadipyl-CoA thiolase	SLYA8N_05000	6.1	6.2
U	Integral membrane protein	SLYA8N_13695	6.0	0.3*
●	Succinyl-CoA:3-ketoacid coenzyme A transferase subunit A	SLYA8N_04990	6.0	6.3
U	Hypothetical protein	SLYA8N_18295	6.0	0.5*
●	3-Carboxy-*cis*, *cis*-muconate cycloisomerase	SLYA8N_05015	5.9	5.8
●	Succinyl-CoA:3-ketoacid coenzyme A transferase subunit B	SLYA8N_04995	5.9	6.2
●	Protocatechuate 3,4-dioxygenase subunit B	SLYA8N_05005	5.8	5.0
●	Pyruvate phosphate dikinase	SLYA8N_25215	5.7	6.1
●	Transmembrane transporter	SLYA8N_02135	5.7	7.3
●	Protocatechuate 3,4-dioxygenase subunit A	SLYA8N_05010	5.7	5.3
R	Response regulator	SLYA8N_17595	5.5	-0.1*
●	Benzoylformate decarboxylase	SLYA8N_02125	5.4	6.6
M	Transport integral membrane protein	SLYA8N_13895	4.8	1.5
●	β-Ketoadipyl-CoA thiolase	SLYA8N_04415	4.5	3.8
M	Alcohol dehydrogenase	SLYA8N_29215	4.3	3.8
●	Transcriptional regulator	SLYA8N_04985	4.3	4.3
●	Protein MeaA	SLYA8N_06065	4.3	3.4
M	Long-chain-fatty-acid-CoA ligase	SLYA8N_04410	4.2	3.6
M	Aldehyde dehydrogenase	SLYA8N_29210	4.0	3.5
M	Exopolysaccharide phosphotransferase	SLYA8N_08030	3.9	2.0
●	Oxidoreductase	SLYA8N_06050	3.9	3.3
U	Hypothetical protein	SLYA8N_34285	3.8	3.7
M	Acyl-CoA dehydrogenase	SLYA8N_29235	3.7	3.5
M	Hypothetical protein	SLYA8N_32305	3.6	6.1
M	Iron-sulfur oxidoreductase subunit beta	SLYA8N_05120	3.5	1.9
M	Membrane protein	SLYA8N_03150	3.4	2.4
●	Phosphoenolpyruvate carboxykinase	SLYA8N_13500	3.3	3.3
●	4-Hydroxybenzoate hydroxylase	SLYA8N_22275	3.2	9.0

* Genes not significant (Benjamini-Hochberg FDR > 0.05) but included for completeness.

Table 11. The genes down-regulated in *S. lividans* ΔYA8-DG2 on aromatic amended culture. The 40 genes most down-regulated on protocatechuate compared to mannitol (adj p < 0.05, log_2fold change> 2.0) were listed. The genes encoding enzymes of the EMP pathway, linked to glycolysis and gluconeogenesis (●), mannitol catabolism (●), pigment biosynthesis (●). Further genes encode other enzymes (M) and regulators (R), as well as proteins of so far unknown function (U). (Fig. 19). n=3. The table was obtained from a previously published paper (Seo et al., 2023).

Function	Annotation	Gene	PCA	4HB
M	Monooxygenase	SLYA8N_19810	-5.7	-0.9*
M	Heavy metal reductase	SLYA8N_19790	-5.5	-0.7
M	Arsenite resistance protein *ArsB*	SLYA8N_19800	-5.2	-2.0
R	Transcriptional regulator	SLYA8N_19795	-5.0	-2.4
●	Substrate binding protein, *smoE*	SLYA8N_28225	-4.6	-5.3
●	Integral membrane sugar transport protein, *smoF*	SLYA8N_28220	-4.6	-5.7
●	Hypothetical protein	SLYA8N_28205	-4.6	-5.0
●	Transcriptional regulator, *smoR*	SLYA8N_28230	-4.5	-4.2
●	DNA-binding protein	SLYA8N_19785	-4.4	-0.6
●	Integral membrane sugar transporter, *smoG*	SLYA8N_28215	-4.4	-4.3
●	Zinc-binding dehydrogenase, *smoD*	SLYA8N_28210	-4.3	-3.3
U	Hypothetical protein	SLYA8N_36995	-4.2	-5.2
U	Hypothetical protein	SLYA8N_36990	-4.1	-5.3
U	Hypothetical protein	SLYA8N_36975	-4.1	-5.3
M	Oxidoreductase	SLYA8N_36985	-4.0	-5.0
M	Methyltransferase	SLYA8N_36945	-4.0	-5.6
M	Endoglucanase	SLYA8N_01130	-3.9	-3.0
M	Methylesterase	SLYA8N_36955	-3.9	-5.5
●	Enolase 2	SLYA8N_01125	-3.8	-3.4
●	Deoxyribodipyrimidine photo-lyase	SLYA8N_36980	-3.7	-5.3
●	Phytoene dehydrogenase	SLYA8N_36965	-3.7	-4.9
●	Geranylgeranyl pyrophosphate synthase	SLYA8N_36970	-3.7	-4.2
●	Lycopene cyclase	SLYA8N_36940	-3.7	-4.7
●	Lipoprotein	SLYA8N_36920	-3.5	-3.7
●	Fructose-specific permease	SLYA8N_21710	-3.5	-2.4
M	Secreted protein	SLYA8N_01030	-3.4	-0.4*
●	DeoR family transcriptional regulator	SLYA8N_21700	-3.4	-2.4
●	Phytoene synthase	SLYA8N_36960	-3.3	-5.2
M	Sigma factor	SLYA8N_36925	-3.2	-1.4
●	Glyceraldehyde-3-phosphate dehydrogenase	SLYA8N_01755	-3.2	-2.6
M	Dehydrogenase	SLYA8N_36950	-3.2	-4.8
M	Integral membrane lysyl-tRNA synthetase	SLYA8N_20785	-3.2	-1.5
●	1-Phosphofructokinase	SLYA8N_21705	-3.1	-2.8
U	Hypothetical protein	SLYA8N_36915	-2.8	-3.8
M	Secreted protein	SLYA8N_19820	-2.6	0.1
●	Fructokinase	SLYA8N_27935	-2.6	-1.8
U	Hypothetical protein	SLYA8N_20790	-2.5	-0.9
M	Neutral zinc metalloprotease	SLYA8N_11275	-2.5	0.3*
M	Lipoprotein	SLYA8N_17715	-2.4	-2.9
R	MarR family regulatory protein	SLYA8N_01120	-2.4	-2.6

* Genes not significant (Benjamini-Hochberg FDR > 0.05) but included for completeness.

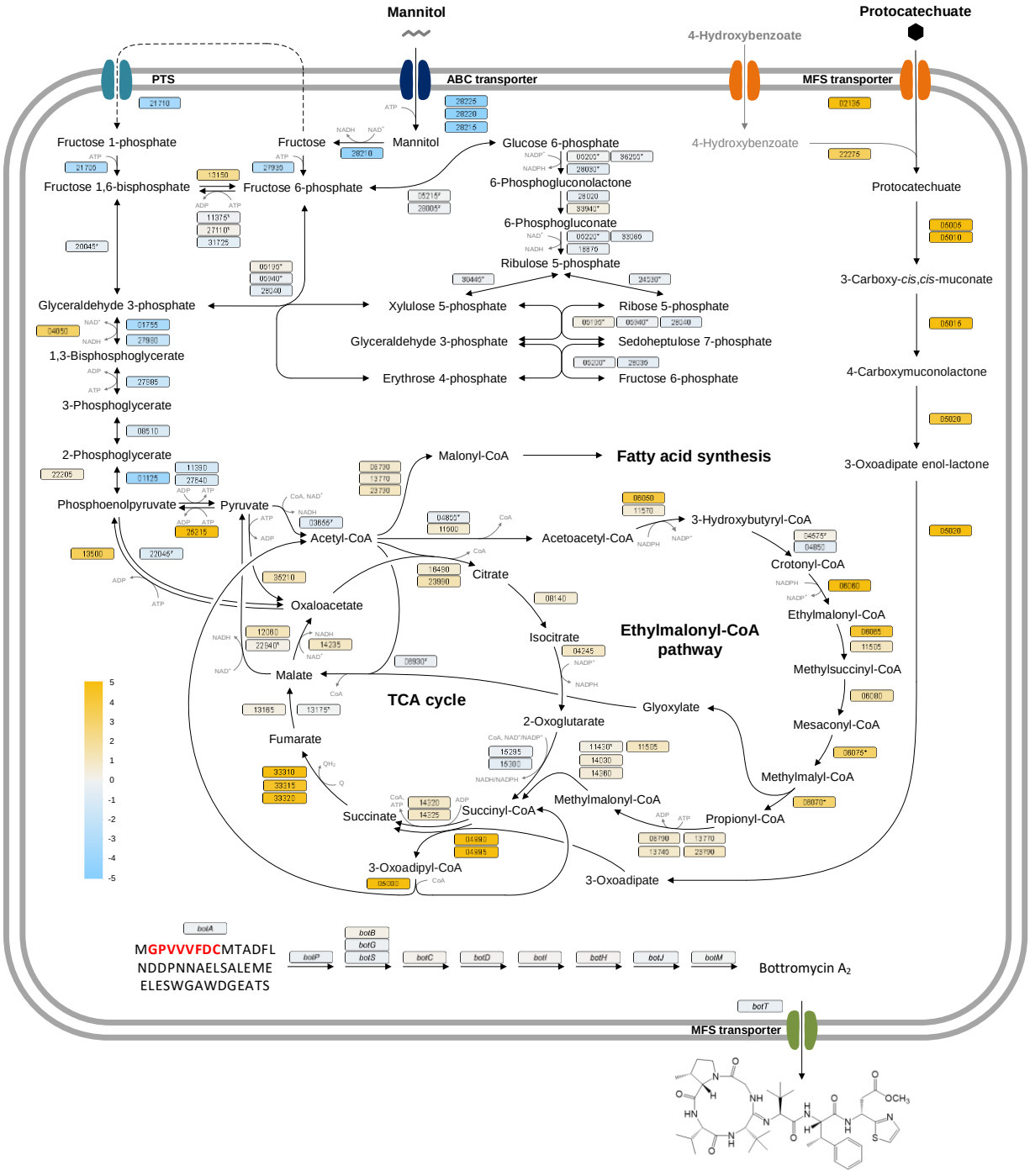

Figure. 19. Gene expression levels of central carbon metabolism in response to substrates in *S. lividans* ΔYA8-DG2. The data show the differences in gene expression levels between cells cultured with mannitol and protocatechuate (10 mM, 12 h) and are highlighted in colour (blue, downregulated on protocatechuate; yellow, upregulated on protocatechuate). The metabolic network was compiled from the KEGG database and manually curated. The genes responsible for the mannitol uptake system were adapted from *C. glutamicum* as template (Hoffmann et al., 2018; Peng et al., 2011). The cofactors refer to *S. lividans* TK24 (Daniels et al., 2018) unless stated. The cofactor specificity of phosphoenolpyruvate carboxykinase (PEPCk) and pyruvate

carboxylase (PC) was taken from *S. coelicolor* M145 (Llamas-Ramírez et al., 2020) whereas succinate-dehydrogenase was inferred to *E. coli* (Cecchini et al., 2002). $^{+}$, Putative genes; *, Genes not significant (Benjamini-Hochberg FDR > 0.05) but included for completeness. The figure was obtained from a previously published paper (Seo et al., 2023).

Despite its frequent use in the synthesis of natural products and enzymes (Dulaney, 1949; Quinn et al., 2020; Schrader & Blevins, 2001), the utilization of mannitol in *S. lividans* has been less explored. Through the analysis of differentiated gene expression levels, identification of mannitol and aromatic uptake systems in *S. lividans* TK24 were conducted. In the aromatic-amended cultures, the expression of ABC sugar transporter genes and fructose related genes were downregulated (Table 12 and Fig. 19). The sugar transport system consists of zinc-binding dehydrogenase, membrane sugar transporter, membrane sugar transport protein, and substrate binding protein.

Table 12. The influence of substrates on genes related to mannitol uptake and degradation pathways in *S. lividans* ΔYA8-DG2. The strain was cultivated on minimal medium containing either 10 mM mannitol, protocatechuate (PCA), or 4-hydroxybenzoate (4HB) as the sole carbon source. Samples were collected from the cultures after 12 hours. (Fig. 19). The expression levels are normalized to the mannitol-amended culture and are given as $\log_2$ fold change. The significance level (Benjamini-Hochberg, FDR) was set to < 0.05, n=3. The table was obtained from a previously published paper (Seo et al., 2023).

Gene	Annotation	PCA	4HB
SLYA8N_09400	Phosphocarrier protein HPr	-1.48	-0.87
SLYA8N_17190	Trehalose import ATP-binding protein SugC	-1.43	-1.13
SLYA8N_21700	DeoR family transcriptional regulator	-3.40	-2.42
SLYA8N_21705	1-Phosphofructokinase	-3.07	-2.75
SLYA8N_21710	Fructose-specific permease	-3.47	-2.43
SLYA8N_28205	Hypothetical protein	-4.56	-5.01
SLYA8N_28210	Zinc-binding dehydrogenase	-4.28	-3.31
SLYA8N_28215	Integral membrane sugar transporter	-4.35	-4.28
SLYA8N_28220	Integral membrane sugar transport protein	-4.57	-5.71
SLYA8N_28225	Substrate binding protein	-4.61	-5.28
SLYA8N_28230	Transcriptional regulator deoR-type	-4.54	-4.20

In terms of mannitol transporter system, this downregulation was observed in a six-gene operon in protocatechuate-fed cells. This operon appears to encode components of an ABC transporter for mannitol intake, based on BLASTN comparison with the *S. coelicolor* A3(2) genome (Table 13) (Bertram et al., 2004). Although genome analysis suggested the presence of an ABC-type membrane protein for sugar alcohols (potentially including mannitol), the *smo* operon was not activated when mannitol was added to the culture medium in the previous study. However, in this study, a significant induction of a five-gene operon in *S. lividans* TK24 that closely resembles the proposed mannitol operon in *S. coelicolor* A3(2), was observed particularly when mannitol was the sole carbon source (Fig. 19 and Table 11). This indicates that these genes likely form the mannitol absorption system in both *S. lividans* TK24 and *S. coelicolor* A3(2).

Table 13. Nucleotide sequence comparison of genes up-regulated during growth of *S. lividans* ΔYA8-DG2 on mannitol, against the genome of *S. coelicolor* A3(2). The BLASTN analysis exhibited that six genes including a sugar ABC transporter showed high similarity to mannitol transporter (Bertram et al., 2004). The table was obtained from a previously published paper (Seo et al., 2023).

Gene	Annotation	Reference	Coverage/Identity (%)
SLYA8N_28205	Hypothetical protein	SCO1902	100/99.0
SLYA8N_28210	Zinc-binding dehydrogenase, *smoD*	SCO1901	100/99.6
SLYA8N_28215	Membrane sugar transporter, *smoG*	SCO1900	100/99.8
SLYA8N_28220	Membrane sugar transport protein, *smoF*	SCO1899	100/100
SLYA8N_28225	Substrate binding protein, *smoE*	SCO1898	100/99.3
SLYA8N_28230	Transcriptional regulator deoR-type, *smoR*	SCO1897	100/99.7

Under the aromatic-consuming condition, the identified genes were significantly downregulated, exhibiting $\log_2$ fold changes lower than -4 (Table 12). Intriguingly, the mannitol uptake system included a zinc-binding dehydrogenase, suggesting that mannitol might be converted to fructose after uptake. Additionally, fructose phosphotransferase system-related genes were downregulated with $\log_2$ fold changes lower than -3. The phosphocarrier protein HPr, which is a phosphate donor for the phosphotransferase system, was also downregulated. The activation of both sugar ABC transporter and fructose phosphotransferase system in *S. lividans* may suggest

mannitol was possibly taken up by the cells through an ABC transporter and subsequently converted into fructose within the cytoplasm. This uptaken fructose was either converted into fructose 6-phosphate by fructokinase or released outside the cells and re-uptaken by fructose phosphotransferase system. This metabolic mechanism closely resembles that observed in the related actinobacterium *Corynebacterium glutamicum*, as elucidated in earlier studies (Hoffmann et al., 2018; Peng et al., 2011).

On the other hand, the supplementation of protocatechuate and 4-hydroxybenzoate triggered the shared catabolic pathways. In protocatechuate-amended culture, aromatic acid:H^+ symporter family MFS transporter was 5.6-fold upregulated. Genes involved in 4-hydroxybenzoate and protocatechuate degradation such as 4-hydroxybenzoate hydrolase, protocatechuate 3,4-dioxygenase and subsequent ring-cleavage enzymes were highly upregulated (Table 14).

Table 14. The influence of substrates on genes related to aromatic uptake and degradation pathways in *S. lividans* ΔYA8-DG2. The strain was cultivated on minimal medium containing either 10 mM mannitol, protocatechuate (PCA), or 4-hydroxybenzoate (4HB) as the sole carbon source. Samples were collected from the cultures after 12 hours. (Fig. 19). The expression levels are normalized to the mannitol-amended culture and are given as $\log_2$ fold change. The significance level (Benjamini-Hochberg, FDR) was set to < 0.05, n=3. The table was obtained from a previously published paper (Seo et al., 2023).

Gene	Annotation	PCA	4HB
SLYA8N_02125	Benzoylformate decarboxylase	5.35	6.61
SLYA8N_02130	Benzaldehyde dehydrogenase [NAD(+)]	6.69	8.36
SLYA8N_02135	Transmembrane transporter, Aromatic acid:H^+ symporter	5.66	7.30
SLYA8N_04990	Succinyl-CoA:3-ketoacid coenzyme A transferase subunit A	6.02	6.29
SLYA8N_04995	Succinyl-CoA:3-ketoacid coenzyme A transferase subunit B	5.89	6.22
SLYA8N_05000	β-Ketoadipyl-CoA thiolase	6.13	6.17
SLYA8N_05005	Protocatechuate 3,4-dioxygenase beta chain	5.78	5.04
SLYA8N_05010	Protocatechuate 3,4-dioxygenase alpha subunit	5.65	5.28
SLYA8N_05015	3-Carboxy-*cis, cis*-muconate cycloisomerase	5.94	5.81
SLYA8N_05020	4-Carboxymuconolactone decarboxylase	6.42	6.19
SLYA8N_22275	4-Hydroxybenzoate hydroxylase	3.23	9.01

The catabolism of 4-hydroxybenzoate and protocatechuate is achieved by protocatechuate 3,4-cleavage pathway, resulting in the production of 3-oxoadipyl-CoA, ultimately yields succinyl-CoA and acetyl-CoA. While glyoxylate shunt is a well-known mechanism for assimilation of C_2 compounds such as acetate (Renilla et al., 2012), *S. lividans* lacks isocitrate lyase, one of the enzymes required for glyoxylate shunt, suggesting the utilization of an alternative pathway (Lewis et al., 2010), such as ethylmalonyl-CoA pathway. This assumption was supported by the upregulation of key enzymes in ethylmalonyl-CoA pathways, such as crotonyl-CoA reductase (Ccr) and ethylmalonyl-CoA mutase, with $\log_2$ fold changes of 6.3 and 4.3, respectively (Fig. 19 and Table 15). This indicate that potential alterations in the ethylmalonyl-CoA pathway in aromatic-amended culture.

The production of succinyl-CoA acetyl-CoA also led to the upregulation of genes involved in both succinate dehydrogenase and gluconeogenesis pathway, including fructose 1,6-bisphosphatase, PEP carboxylase, and pyruvate carboxylase (Table 15). In addition to the reprogramming of gluconeogenesis, genes associated with the PEP-pyruvate-oxaloacetate node were also reprogrammed. The expression of pyruvate kinase and PEP carboxylase genes was downregulated, whereas genes involved in pyruvate formation, including malic enzyme and pyruvate phosphate dikinase, were upregulated.

Aside from carbon central metabolism, gene related to amino acid biosynthesis (Supplementary data: Table S6) were remained largely unchanged, indicating adapted production of amino acids. Despite notable changes in gene expression levels within central carbon metabolism, no significant alterations were observed in the genes associated with the bottromycin biosynthesis (Fig. 19), indicating that substrate choice had minor impact on bottromycin production. This suggests that the utilization of distinct substrates can be achieved by adjusting the high-flux central carbon pathways. Conclusively, the strain is capable of adapting varied environments, coupled

with the utilization of the synthetic promoter for stable cluster expression (Fig. 19), is crucial for its production performance.

Table 15. Gene expression levels related to gluconeogenesis, the phosphoenolpyruvate-pyruvate-oxaloacetate node, and ethylmalonyl-CoA pathway (log_2 fold change). The strain was cultivated on minimal medium containing 10 mM mannitol, protocatechuate (PCA), or 4-hydroxybenzoate (4HB) as the sole carbon source. Samples were harvested from the cultures after 12 hours (Fig. 19). The expression levels are normalized to the mannitol-amended culture and are given as log_2 fold change. The significance level (Benjamini-Hochberg, FDR) was set to < 0.05, n=3. The table was obtained from a previously published paper (Seo et al., 2023).

Gene	Annotation	PCA	4HB
Gluconeogenesis			
SLYA8N_13150	Fructose-1,6-bisphosphatase	2.06	2.98
SLYA8N_13500	Phosphoenolpyruvate carboxykinase [GTP]	3.34	3.28
SLYA8N_35210	Pyruvate carboxylase	1.12	0.46
Phosphoenolpyruvate-pyruvate-oxaloacetate node			
SLYA8N_11390	Pyruvate kinase	-1.28	-1.05
SLYA8N_12060	Putative NAD-dependent malic enzyme	1.14	2.06
SLYA8N_22045	Phosphoenolpyruvate carboxylase	-0.90	-3.63
SLYA8N_22940	NAD-dependent malic enzyme	0.16*	0.82
SLYA8N_25215	Pyruvate phosphate dikinase	5.70	6.14
SLYA8N_27640	Pyruvate kinase	-1.03	-1.57
Ethylmalonyl-CoA pathway			
SLYA8N_04575	Fatty oxidation protein	0.21*	-0.31*
SLYA8N_04850	Fatty acid oxidative multifunctional enzyme	-0.52	-1.04
SLYA8N_04855	Putative acyltransferase	-0.33*	-1.27
SLYA8N_06050	Oxidoreductase	3.87	3.31
SLYA8N_06055	Transcriptional regulator	0.41*	-0.41*
SLYA8N_06060	Crotonyl-CoA reductase	6.28	3.55
SLYA8N_06065	Protein MeaA	4.29	3.42
SLYA8N_06070	Citrate lyase	2.89	2.24
SLYA8N_06075	Hypothetical protein	2.98	2.68
SLYA8N_06080	Acyl-CoA dehydrogenase	1.58	1.15
SLYA8N_06790	Acetyl-/propionyl-coenzyme A carboxylase alpha chain	0.74	-0.61
SLYA8N_11430	Isobutyryl-CoA mutase A	0.30*	1.42
SLYA8N_11500	Putative acetyl-CoA acetyltransferase	0.65	1.47
SLYA8N_11505	Hypothetical protein	1.03	0.57
SLYA8N_11570	3-Hydroxybutyryl-CoA dehydrogenase	0.58	1.29
SLYA8N_13745	Propionyl-CoA carboxylase beta chain	0.80	-0.56
SLYA8N_13770	Acetyl-/propionyl-coenzyme A carboxylase alpha chain	0.58	-0.60
SLYA8N_14030	Methylmalonyl-CoA mutase	0.51	1.30
SLYA8N_14360	Isobutyryl-CoA mutase small subunit	0.42	0.34
SLYA8N_23780	Putative acyl-CoA dehydrogenase	1.24	1.57
SLYA8N_23785	Hydroxymethylglutaryl-CoA lyase	1.09	1.61
SLYA8N_23790	Acetyl-/propionyl-coenzyme A carboxylase alpha chain	0.99	1.26
SLYA8N_23795	Methylcrotonoyl-CoA carboxylase beta chain	1.35	1.51

* Genes not significant (Benjamini-Hochberg FDR > 0.05) but included for completeness.

4.2.4 Analysis of intracellular amino acids

Bottromycin production on both aromatics and mannitol, combined with the stability of amino acid biosynthesis genes, suggests that availability of amino acid synthesis might minimally influenced by substrates. To confirm the hypothesis, intracellular amino acids analysis in exponential phase was conducted and compared to transcriptomic data.

In general, high concentration of 2-oxoglutarate derived amino acids were observed (Fig. 20). L-glutamate was approximately in the aromatic supplemented culture was 1.5 -times higher than mannitol-supplied culture (118 µM $gCDW^{-1}$). In addition, concentration of L-glutamine was 4.1-times and 1.4-times higher in protocatechuate- and 4-hydroxybenzoate-amended culture, respectively. L-proline exhibited 2.1-times and 3.6-times higher increase, correspondingly. Transcriptomic data showed that succinyl-CoA from aromatics entered into TCA cycle resulting in downregulation of 2-oxoglutarate oxidoreductase genes (Fig. 19) and using bypass pathway, ultimately increasing abundance of 2-oxoglutarate-derived amino acids.

Surprisingly, L-cysteine exhibited an increase of more than 4-times in the aromatic amended culture. Specifically, more changes in intracellular amino acids observed in 4-hydroxybenzoate amended culture. A relatively high abundance of L-methionine, L-tryptophane, and L-phenylalanine was observed. In contrast, L-histidine, L-threonine, L-glycine, and L-serine present in relatively low amounts. Despite deviations on amino acid concentrations, the biosynthesis of bottromycin necessitates the utilization of 14 out of the 20 standard amino acids, indicating that *S. lividans* ΔYA8-DG2 possesses the ability to synthesize these amino acids in minimal media supplemented with either mannitol or aromatics. The analysis of intracellular amino acids further supported the hypothesis above as the majority of intracellular amino acids were detected and concentrations remained constant.

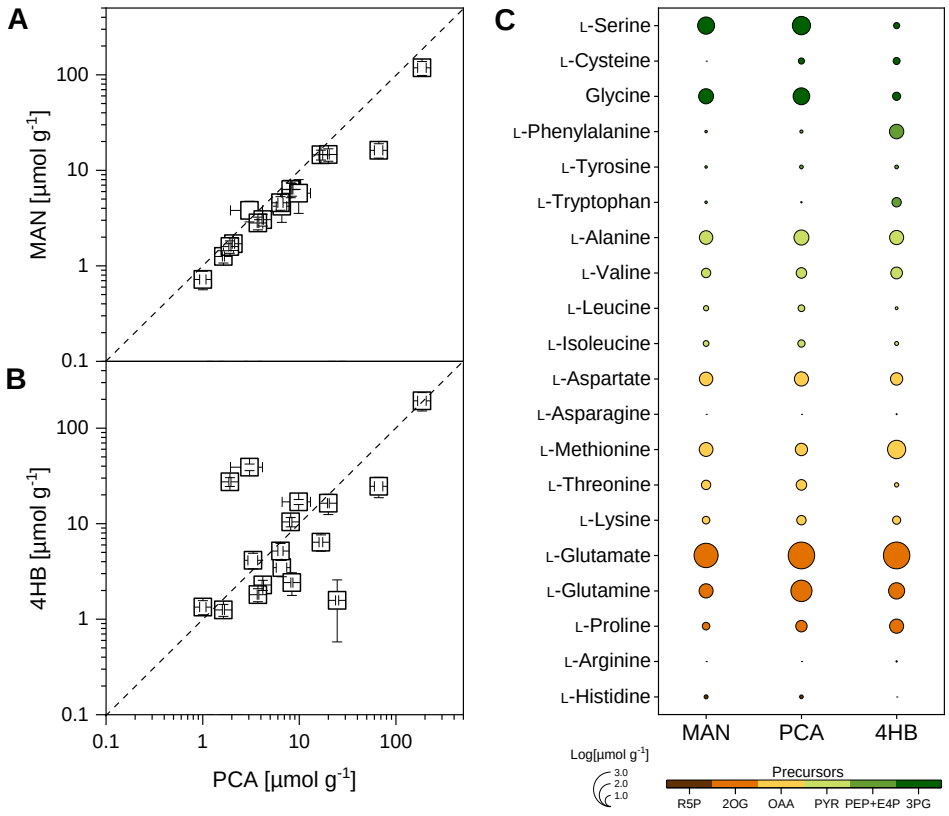

Figure. 20. The concentration of intracellular amino acids in *S. lividans* ΔYA8-DG2 on different substrates. The minimal medium contained either 10 mM of mannitol, protocatechuate, or 4-hydroxybenzoate. The samples were taken after 12 hours from inoculation. The data represent absolute amino acid concentrations, comparing overall concentrations between substrates (A, B) and substrate-specific differences linked to the biosynthetic origin of amino acids (C). Circle diameters on the log-scaled concentration axis depict the concentration, with mean values and standard deviations derived from three biological replicates (n=3) and technical duplicates. The figure was obtained from a previously published paper (Seo et al., 2023).

This indicates that modifying the high-flux carbon core pathways alone was sufficient to efficiently utilize these different substrates. For comparison, *Bacillus subtilis* mainly altered its central metabolism to maintain metabolic balance under salt stress (Kohlstedt et al., 2014). In summary, the inherent stability across diverse conditions, combined with the use of a synthetic promoter for steady cluster expression (Fig. 19), appears to be crucial for the exceptional production performance observed.

4.2.5 Analysis of intracellular CoA thioesters

As mentioned above, supplement of aromatics induce a significant upregulation of the ethylmalonyl-CoA pathway (Fig. 19 and Table 15), producing a wide range of CoA intermediates. To investigate the potential changes in CoA thioester pool levels between aromatic-amended and mannitol-amended cultures, metabolomic analyses were performed using *S. lividans* ΔYA8-DG2, a strain in which the impact of CoA utilization was minimized. The strain was cultivated in 10 mM either mannitol, protocatechuate or 4-hydroxybenzoate, and harvested in mid-exponential phase (12 h). The genes involved in ethylmalonyl-CoA pathway was highly upregulated in aromatic-amended culture (Fig. 19 and Table 15) together with overall concentration of CoA thioesters (Fig. 21). The total concentration of CoA thioesters in the mannitol-amended culture was found to be 105 nmol $gDCW^{-1}$, whereas the concentration increased to 1173 nmol $gDCW^{-1}$ in the protocatechuate-amended culture and increased to 866 nmol $gDCW^{-1}$ in the 4-hydroxybenzoate culture, indicating an approximately 11-fold and 8-fold increase, respectively.

Specifically, the concentrations of CoA thioesters involved in the aromatic degradation pathway, including 3-oxoadipyl-CoA, succinyl-CoA, and acetyl-CoA, showed significant increases. In protocatechuate-amended culture, the concentrations of 3-oxoadipyl-CoA, succinyl-CoA, and acetyl-CoA were increased by 703-fold, 41-fold, and 4-fold, respectively. Similarly, in 4-hydroxybenzoate-amended culture, the concentrations of these CoA thioesters were increased by 119-fold, 18-fold, and 4-fold, respectively, indicating that the degradation of aromatics led to an abundance of succinyl-CoA and acetyl-CoA.

Increased levels of ethylmalonyl-CoA intermediates and 3-oxoadipyl-CoA were observed in both aromatics. However, cells harvested from 4-hydroxybenzoate displayed lower quantities of CoA thioesters, likely due to lower uptake rates of 4-hydroxybenzoate. Protocatechuate (10 mM) (Fig. 16D) was depleted faster than 4-hydroxybenzoate (Fig. 16G).

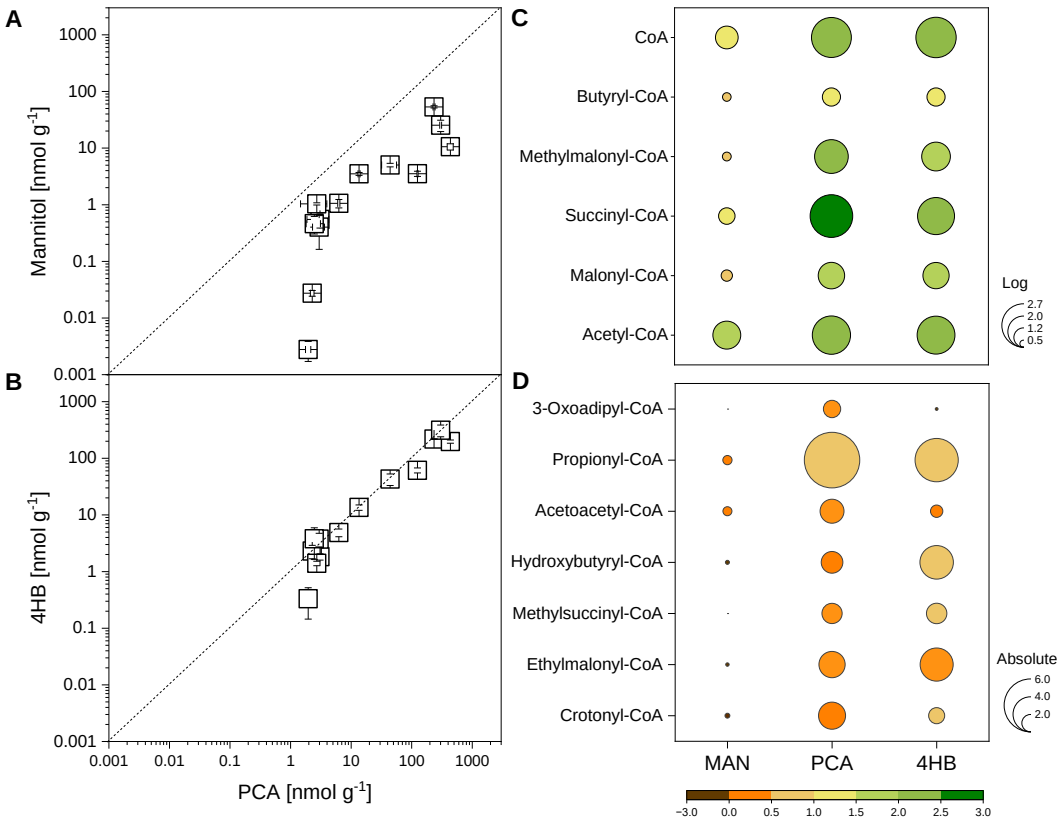

Figure. 21. The concentration of intracellular CoA thioester in *S. lividans* ΔYA8-DG2. The cells were cultivated in minimal medium containing 10 mM mannitol, protocatechuate, or 4-hydroxybenzoate, respectively. The data represent absolute concentrations of CoA thioesters collected 12 hours after inoculation on mannitol (A) and 4-hydroxybenzoate (B) compared to mannitol. The size and circles reflects the concentration. High abundance CoA thioesters (C) are displayed in log-scale, while low abundance CoA thioesters (D) are displayed in absolute concentrations. The data represent mean values and standard deviations from three biological replicates (n=3) and technical duplicates. The figure was obtained from a previously published paper (Seo et al., 2023).

4.2.6 Impact of substrates on production of pamamycin derivates

As the levels of CoA thioesters, which are precursors of polyketides -a commercially important class of natural products (Alber, 2011), increased in cultures amended with aromatic substrates. The production of polyketides was subsequently investigated. Pamamycin derivatives are

produced based on the availability of precursors, including malonyl-CoA, methylmalonyl-CoA, and ethylmalonyl-CoA (Gummerlich et al. 2021; Kuhl et al. 2020).

In order to produce pamamycin, the R2 cosmid containing the pamamycin biosynthetic gene cluster controlled by its native promoter (Rebets et al., 2015), was integrated into chromosomal DNA of *S. lividans* ΔYA8 at the attB site (locus tag, SLIV_ SLIV_19310), yielding the engineered strain named as *S. lividans* ΔYA8-R2. The integration of the pamamycin biosynthetic gene cluster was verified through PCR and sequencing.

The engineered mutant successfully produced pamamycin when cultivated on mannitol (30 mM) (Fig. 22A) and 4-hydroxybenzoate (30 mM) (Fig. 22B), respectively. Interestingly, the choice of carbon source significantly influenced production performance. Utilizing mannitol resulted in rapid growth during the early stage, whereas a nearly one-day lag phase was observed with 4-hydroxybenzoate, likely due to its toxicity. After adaptation, cells accumulated pamamycin in both conditions. Cells grown on mannitol continued to produce pamamycin during the stationary phase, ultimately achieving a final titre of 3.3 mg L^{-1} after 216 hours. In contrast, cells grown on 4-hydroxybenzoate did not produce further in the stationary phase, yielding a final concentration of 0.9 mg L^{-1}.

Interestingly, the type of substrate significantly affected the pamamycin spectrum. Pamamycin produced from mannitol-supplemented cultures had a high fraction of heavy pamamycins, including Pam 649 and Pam 663 (Fig. 22C). Conversely, cultures amended with 4-hydroxybenzoate predominantly produced light derivatives, such as Pam 621 and Pam 635, which constituted 80% of the total pamamycin (Fig. 22D). Additionally, a shift in the pamamycin spectrum was observed when transitioning from the exponential phase to the stationary phase.

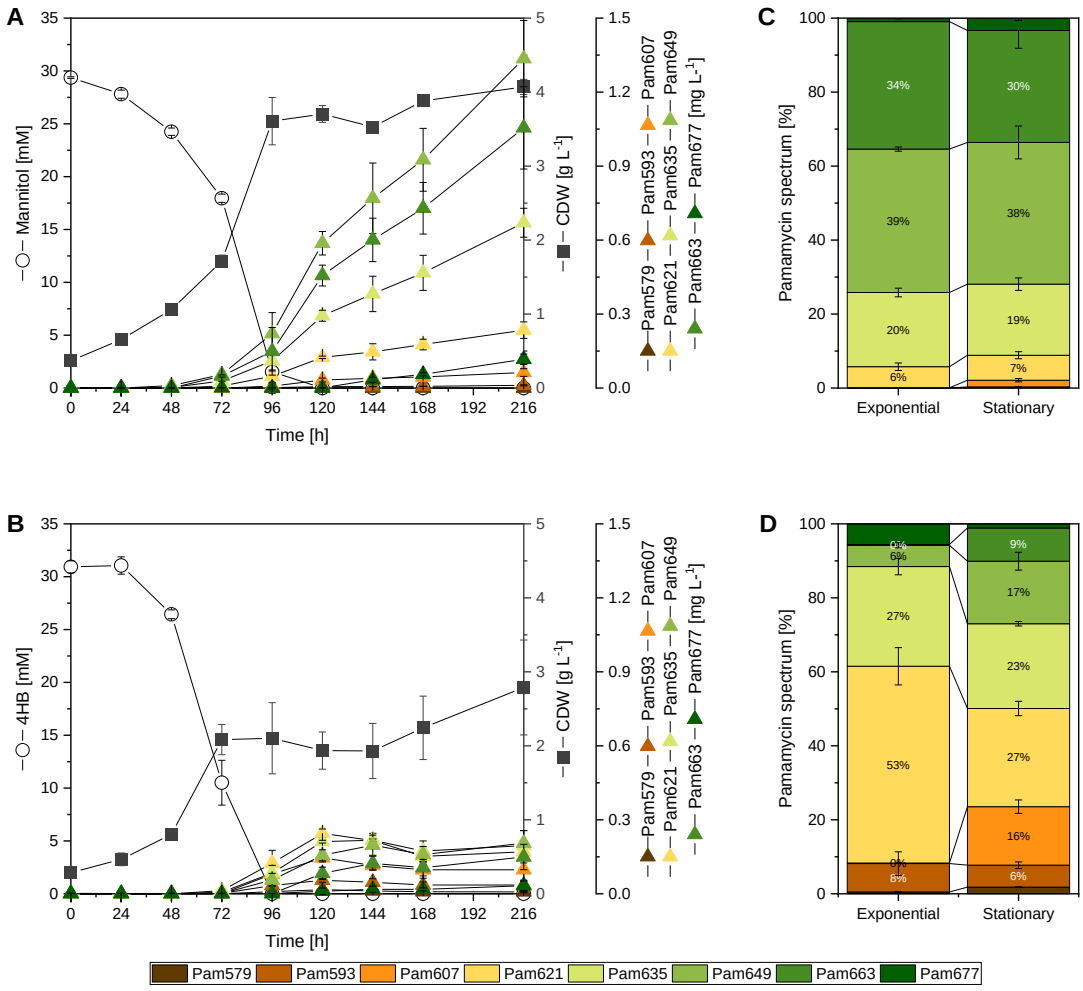

Figure 22. The impact of carbon source on biomass formation and pamamycin production in *S. lividans* ΔYA8-R2. The engineered strain was cultivated in minimal medium amended with either mannitol (30 mM) (A) or 4-hydroxybenzoate (30 mM) (B), respectively. The spectrum of pamamycin derivatives produced on mannitol (C) or 4-hydroxybenzoate (D) is displayed for both from mid-exponential phase (72 h) and stationary phase (216 h). The data represent mean values and standard deviations from three biological replicates (n=3). The figure was obtained from a previously published paper (Seo et al., 2023).

The biosynthesis of pamamycin utilizes succinyl-CoA as a starter unit, and is extended with three distinct CoA thioesters: malonyl-CoA, methylmalonyl-CoA, and ethylmalonyl-CoA (Rebets et al., 2015). In cells cultivated on aromatics, 3-oxoadipyl-CoA played a dual role. It was produced both during the catabolic breakdown of 4-hydroxybenzoate and as an intermediate in the biosynthesis

of pamamycin, originating from the combination of malonyl-CoA and succinyl-CoA. This specific interaction was crucial for the production of lighter pamamycin derivatives (Rebets et al., 2015). Given that the concentration of 3-oxoadipyl-CoA was significantly higher in aromatic-amended cultures (Fig. 21), this favoured the predominant formation of lighter pamamycin variants in 4HB-amended cultures. To gain a more thorough understanding, future research should investigate the enzymatic synthesis of methyl-3-oxoadipyl-CoA, using a method similar to the one employed for 3-oxoadipyl-CoA in our study. This would enable its LC-MS analysis in cell extracts. Methyl-3-oxoadipyl-CoA plays a crucial role in pamamycin biosynthesis, influencing the formation of heavier product variants.

The previous studies on production of pamamycin using *S. albus*, was focused on manipulation of the intracellular concentration of building blocks, achieved by genetic modification (Gummerlich et al., 2021), feeding the branched-chain amino acids (Gläser et al., 2021). In this study, the selection of substrates significantly alters the intracellular CoA ester profile (Fig. 21), thereby enabling diverse combinations of pamamycin derivatives (Fig. 22). The utilization of aromatics promotes the production of light pamamycins, while mannitol enhances the production of heavy pamamycins. This suggests that the choice of substrates could be a strategic option to increase selectivity towards the desired molecule.

4.2.7 Demonstration of pamamycin production from brown seaweed (*Himanthalia elongate*) hydrolysate

Pamamycin production using a seaweed hydrolysate, employing the metabolically engineered strain *S. lividans* ΔYA8-R2, was showcased. The brown seaweed *Himanthalia elongate*, known for its commercial potential due to high contents of mannitol, was chosen as a primary raw material. The dried seaweed was processed grinding, enzymatic treatment at a mildly acidic pH of 5.5, and autoclaving. The resulting extract was an aqueous hydrolysates containing 20 mM of mannitol and

14 mM of glucose, byproducts of the digestion process. After mixing with a buffer, hydrolysate was directly used for pamamycin production without any further nutritional additions or treatments.

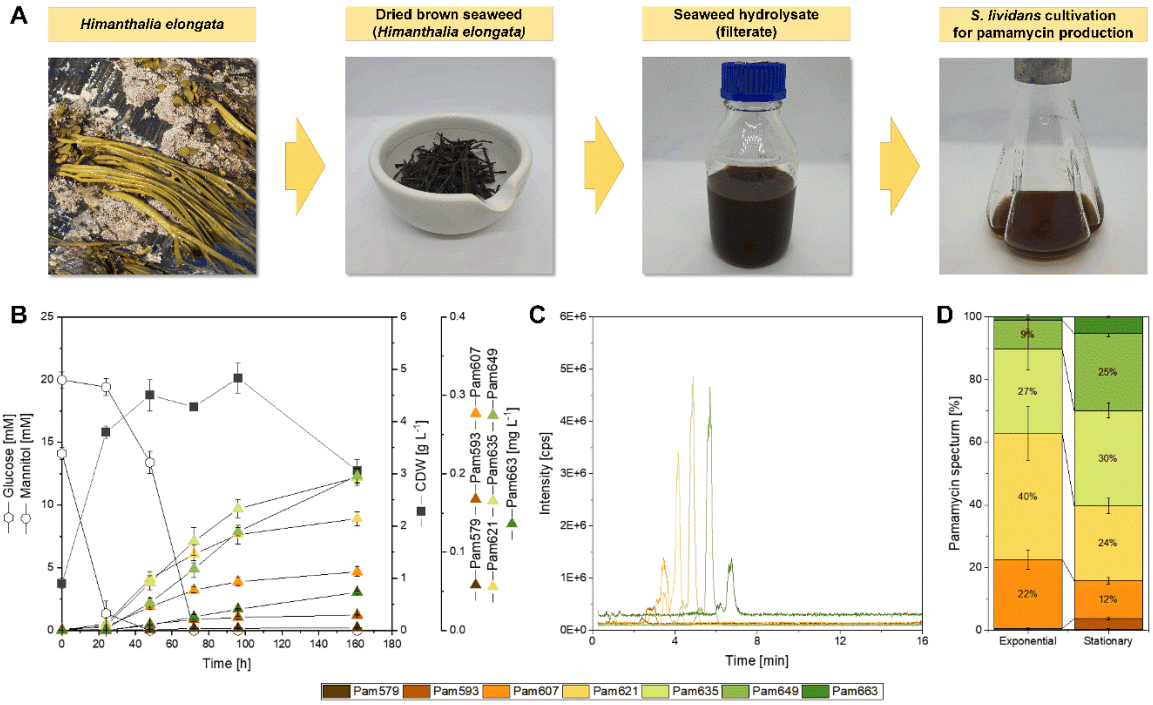

Figure 23. Production of pamamycin from a brown seaweed hydrolysate using metabolically engineered *S. lividans* ΔYA8-R2. The hydrolysate utilized in this study was prepared from *Himanthalia elongata* (Willem & Saxifraga) (credit for the photo of *H. elongate*: Willem VK, Saxifraga) (A). The engineered strain was cultivated on seaweed hydrolysate after mixing with MOPS buffer (pH 7.0) (B). The culture broth was analysed by LC-MS to verify pamamycin production (C). The pamamaycin derivatives were compared between the mid-exponential phase (24 h) and stationary phase (96 h). The data represent mean values and standard deviations from three biological replicates (n=3). The figure was obtained from a previously published paper (Seo et al., 2023).

While cultivating ΔYA8-R2 strain, the sugars in hydrolysate were consumed sequentially. Glucose was consumed first, resulting in biomass formation up to 4 g L^{-1} and a total pamamycin production of 0.02 mg L^{-1} (Fig. 23B). Following glucose consumption, mannitol is consumed, accelerating pamamycin biosynthesis and ultimately yielding a titre of 0.7 mg L^{-1}. Moreover, the shift between these two distinct phases induced variation in the pamamycin spectrum.

Beyond the fermentative production of natural products on food-based carbon sources such as glucose, starch, yeast extract, peptone, and soybean, this study demonstrated the production of natural product from alternative substrates such as protocatechuate, 4-hydroxybenzoate, and mannitol. Considering that the these substrates can be sourced from waste and by-products such as pulp and paper sector (Becker & Wittmann, 2019), seaweed-based food production and high-value ingredient extraction (Poblete-Castro et al., 2020). This study demonstrates potential transitioning microbial natural product formation from conventional materials to eco-friendlier raw materials.

5 Conclusion and Outlook

The applications of biotechnological tools on renewable feedstocks have shown promise for replacing traditional fossil-based feedstocks. However, given that the petroleum feedstock system has been already optimized and utilized for decades (Katakojwala & Mohan, 2021), sophisticated approaches, such as the production of high-value complex molecules from renewable feedstock, are necessary to replace the current systems with developing biotechnological methods (H. P. Meyer, 2011).

A promising approach involves the use of microbial cell factories, which are powerful tools for producing complex molecules from lignocellulosic biomass and algae biomass. They offer eco-friendly conversion compared to chemical catalysts, with selective and broad spectra of products. However, the native pathways of substrate uptake and metabolism in microbial cell factories is a major consideration for renewable feedstock utilization due to the significant heterogeneity of renewable feedstocks (Buschke et al., 2013).

In the first part of the study, the degradation pathway for lignin-derived aromatics in *C. glutamicum* was investigated by developing a targeted measurement for known and potential aromatic CoA thioester using LC-MS/MS. This LC-MS/MS method provided metabolomic evidence for the CoA-dependent β-oxidative pathway in *C. glutamicum* and enabled a comparison of the degradation capabilities between the wild type *C. glutamicum* and the engineered strain. Strikingly, the degradation of phenylpropanoids in *C. glutamicum* is more complex than previously understood. For example, the substrate preference of the enzymes dictates the substrate preference of the strain, as well as affecting the degradation capacities. Additionally, the release of acetyl-CoA from phenylpropanoids degradation influences central metabolism, indicating that sophisticated considerations are required for genetic engineering.

Considering the heterogeneity of lignin's nature, the utilization of various aromatic compounds is key to expanding the substrate spectrum. In general, the degradation of phenylpropanoids, including ferulate, *p*-coumarate, and caffeate, is controlled by single enzymes in bacteria, such as PhdA in *C. glutamicum* (Kallscheuer et al., 2016), Fcs in *P. putida* (Parales & Harwood, 1992), and FerA in *N. aromaticivorans* (Cecil et al., 2018). This study shows that strain improvements should not only consider degradation pathways, such as the deletion of catabolic genes and their regulators, but also the substrate preference of these enzymes. Given that the majority of the strains used for lignin valorisation, including *P. putida*, *C. glutamicum*, *Amycolatopsis* sp., and *Rhodococcus*, utilize CoA-dependent pathways, this molecular-specific LC-MS/MS method has the potential to be used for other bacteria. This enables a comparison of enzyme capabilities across different strains, facilitating more targeted and effective strain engineering.

Secondly, the valorisation of advanced renewable feedstocks using *S. lividans* was approached in an applied manner with a systemic understanding of catabolism in the strain. The cultivation on renewable feedstock-derived monomers , mannitol and protocatechuate, on defined media allows deciphering the substrate utilization system in *S. lividans*. The utilization of different substrates significantly affects the central metabolism of *S. lividans*. The catabolism of aromatic acid yielded activation of ethylmalonyl-CoA pathway for C_2 assimilation, as shown in transcriptomic and metabolomic data, differentiating the pamamycin spectrum in both substrates. From both mannitol and aromatic monomers, the production of bottromycin, an amino-acid-derived natural product, and pamamycins, CoA-derived natural products, was demonstrated. This provides proof of concept for the production of complex molecules from renewable feedstocks, underscoring the potential of utilizing *S. lividans* for the efficient conversion of diverse renewable substrates into valuable pharmaceuticals. Moreover, the utilization of seaweed hydrolysate, which underwent minimal pre-treatment, demonstrated the practical application of advanced renewable feedstocks.

Specific to the strain, *S. lividans* (Rückert et al., 2015) is recognized as a reliable heterologous host for the production of both natural products and proteins. In this context, evaluating *S. lividans* for synthesizing additional compounds from sustainable monomers appears promising. For instance, the stable availability of amino acids across different substrates (Fig. 20) allows this strain suitable for producing heterologous proteins like cellulase (Daniels et al., 2018) and human proteins (Bender et al., 1990).

In the context of renewable feedstock utilization, bioproduction from lignin has predominantly focused on the production of low-value high-volume chemicals, such as *cis, cis*-muconate (Kohlstedt et al., 2022; Weiland et al., 2023) and β-ketoadipic acid (Okamura-Abe et al., 2016; Suzuki et al., 2021). Given the high market value of pharmaceuticals, demonstrating the production of high-value low-volume natural products could enhance overall renewable feedstock valorisation strategies. Similarly, in seaweed biorefineries, natural product synthesis from algal residuals could be integrated into cascading value chains, where leftover hydrolysates are converted into value-added chemicals after extracting valuable bioactive molecules (Poblete-Castro et al., 2020). While current efforts primarily target biofuels and bulk chemicals like ethanol (Chades et al., 2018; Sasaki et al., 2018; I. Y. Sunwoo et al., 2018) and lactate (Mazumdar et al., 2014), they also present significant potential for natural product synthesis and higher-value outputs.

In conclusion, this study contributes to advancing the utilization of renewable feedstocks by elucidating the catabolic capabilities of key microbial cell factories, *C. glutamicum* and *S. lividans*, while also demonstrating the production of high-value, complex-structured natural products.

6 Appendix

6.1 Abbreviations and Units

2OG: 2-Oxoglutarate

3PG: 3-Phosphoglycerate

4HB: 4-Hydroxybenzoate

ABC: ATP-binding cassette

ACP: Acyl carrier protein

At4CL4: 4-Coumarate:CoA ligase in *Arabidopsis thaliana*

APIs: Active pharmaceutical ingredients

BGC: Biosynthetic gene cluster

CCR: Carbon catabolite repression

Ccr: Crotonyl-CoA reductase

CDW: Cell dry weight

COMT: Caffeate *O*-methyltransferase

CL: *p*-Coumarate:CoA ligase

DSMZ: German Collection of Microorganisms and Cell Cultures

E4P: Erythrose 4-phosphate

FadA: 3-Ketoacyl-CoA thiolase (fatty acid β-oxidation) in *C. glutamicum*

FadB: 3-Hydroxyacyl-CoA dehydrogenase (fatty acid β-oxidation) in *C. glutamicum*

FadE: Acyl-CoA dehydrogenase (fatty acid β-oxidation) in *C. glutamicum*

FDR: False discovery rate

FerA: Acetate-CoA ligase

HVLV: High-value Low-volume

LVHV: Low-value High-volume

MFS: Major facilitator superfamily

MRM: Multiple reaction monitoring

MWh: Megawatt-hour

NGS: Next-Generation Sequencing

NP: Natural product

NRP: non-ribosomal peptide

OAA: Oxaloacetate

OD: Optical density

PC: Pyruvate carboxylase

PCA: Protocatechuate

PCA: Principal component analysis

PcaI: 3-Oxoadipate:succinyl-CoA transferase subunits A

PcaJ: 3-Oxoadipate:succinyl-CoA transferase subunits B

PEP: Phosphoenolpyruvate

PEPCk: Phosphoenolpyruvate carboxykinase

PHA: Polyhydroxyalkanoate

PhdA: Acyl:CoA ligase (phenylpropanoid degradation) in *C. glutamicum*

PhdB: 3-Hydroxyacyl-CoA dehydrogenase (phenylpropanoid degradation) in *C. glutamicum*

PhdC: 3-Oxoacyl-CoA ketohydrolase (acetyl-CoA forming) (phenylpropanoid degradation) in *C. glutamicum*

PhdD: Acyl-CoA dehydrogenase (phenylpropanoid degradation) in *C. glutamicum*

PhdE: Enoyl-CoA hydratase (phenylpropanoid degradation) in *C. glutamicum*

PhdR: MarR-type repressor (phenylpropanoid degradation)

PhdT: Phenylpropanoid transporter

PK: Polyketide

PKS: Polyketide synthases

PTS: Phosphotransferase system

PYR: Pyruvate

RiPP: Ribosomally synthesized and post-translationally modified peptide

TB: Terrific broth

VanA: Vanillate *O*-demethylase subunit A

VanB: Vanillate *O*-demethylase subunit B

6.2 Supplementary data: Tables

Table S1. Primers for genetic engineering and sequencing. For plasmid-based expression, vector overhangs were underscored.

Primers	Sequence (5'→3')	Purpose
At4CL4_fwd	CTTTAAGAAGGAGATATACATATGGTTCTGCAGCAGCAA	Amplification of *At4CL4* sequence
At4CL4_rev	CTTTGTTAGCAGCCGGATCTCAGTGGTGGTGGTGGTGGT	Amplification of *At4CL4* sequence
phdA_fwd	CTTTAAGAAGGAGATATACATGAAAGTGAACCTCGGA	Amplification of *phdA* sequence
phdA_rev	GGTGGTGGTGGTGGTGCTTTGAAACGGGGATGGTGAA	Amplification of *phdA* sequence
phdE_fwd	AACTTTAAGAAGGAGATATACATGACTACTTCCACCACCC	Amplification of *phdE* sequence
phdE_rev	AGTGGTGGTGGTGGTGGTGCTTAGCGTAGAAGCGGGTGA	Amplification of *phdE* sequence
ferA_fwd	CTTTAAGAAGGAGATATACATGACCGGAACGAGTCTTTCC	Amplification of *ferA* sequence
ferA_rev	AGTGGTGGTGGTGGTGGTGCTTATCCACGAGCATCAAC	Amplification of *ferA* sequence
pcaI_fwd	CTTTAAGAAGGAGATATACATATGGCCGGACTGGACAAG	Amplification of *pcaI* sequence
pcaI_rev	GCTCGAGTGCGGCCGCAAGCTTGGCCTTGACGGTGCG	Amplification of *pcaI* sequence
pcaJ_fwd	CTTTAAGAAGGAGATATACATATGGCACTGACCCGCGAAC	Amplification of *pcaJ* sequence
pcaJ_rev	GCTCGAGTGCGGCCGCAAGCTTGAAGGTCATTTCCTTC	Amplification of *pcaJ* sequence
BotAC_fwd	ATGGGACCCGTAGTCGTATTCG	Verification for bottromycin cluster
BotAC_rev	TCAGGCGGAACGTCGTCCTT	Verification for bottromycin cluster
PamN_fwd	CGAGCACACCCTTCGAGGAA	Verification for pamamycin cluster
PamN_rev	GACGGCGTACACGCGGTC	Verification for pamamycin cluster

Table S2. LC-MS/MS settings for aromatic CoA thioester. All aromatic CoA thioesters were separately tuned to obtain declustering potential (DP), collision energy (CE), and cell exit potential (CXP).The parent ion indicates the proton adduct $[M+H]^+$ and the daughter ions were obtained by neural loss of 507 Da from the parent ion $[M+H-507]^+$. Masses of $^{12}C+^{13}C$ molecules were calculated based on Fig. 9, assuming CoA thioester backbone originates from non-labelled carbon. The parameters for $^{12}C+^{13}C$ molecules were derived from those of the non-labelled molecules.

Analyte	Parent ion (m/z)	Daughter ion (m/z)	DP [V]	CE [V]	CXP [V]
Feruloyl-CoA	944.2	437.2	111.6	39.9	22.8
$^{12}C+^{13}C$ Feruloyl-CoA	965.2	448.2	111.6	39.9	22.8
3-Hydroxyferuloyl-CoA	962.2	455	20.09	41.96	47.82
Vanillyl-CoA	918.1	411.1	100	30	15
p-Coumaroyl-CoA	914.1	407.2	4.85	37.97	18
$^{12}C+^{13}C$ *p*-Coumaroyl-CoA	935.1	418.1	4.85	37.97	18
3-Hydroxy-*p*-coumaroyl-CoA	932.3	425.3	39.43	53.1	20.27
Caffeoyl-CoA	930.1	423.2	199.9	44.9	29.1
$^{12}C+^{13}C$ Caffeoyl-CoA	951.1	434.1	199.9	44.9	29.1
Sinapoyl-CoA	974	467.2	14	41.01	25.12
$^{12}C+^{13}C$ Sinapoyl-CoA	995	478	14	41.01	25.12
Cinnamoyl-CoA	898.1	391.2	6.76	45.09	22.15
$^{12}C+^{13}C$ Cinnamoyl-CoA	919.1	402.1	6.76	45.09	22.15
Benzoyl-CoA	872.1	365.2	1.3	34.92	26.04
3-Oxoadipyl-CoA	910.3	403.1	172.97	43.2	24.3

Table S3. BLAST analysis of amino acid sequences of genes responsible of ethylmalonyl-CoA pathway in *S. lividans* ΔYA8-DG2 against *S. venezuelae* ATCC 15439.

Gene	Annotation	Reference	Coverage (%) / Identity (%)
SLYA8N_06050	Oxidoreductase	Hydroxybutyryl-CoA dehydrogenase	99 / 84.71
SLYA8N_06060	Crotonyl-CoA reductase	Crotonyl-CoA carboxylase	99 / 91.01
SLYA8N_06065	Protein MeaA	Ethylmalonyl-CoA mutase	100 / 87.91
SLYA8N_06070	Citrate lyase	L-Malyl-CoA lyase	93 / 92.74
SLYA8N_06075	MaoC hydratase		
SLYA8N_06080	Acyl-CoA dehydrogenase	Methylsuccinyl-CoA dehydrogenase	100 / 95.01

Table S4. 2. Gene expression data of *S. lividans* ΔYA8-DG2 reflecting genes linked to oxidative stress response on protocatechuate and 4-hydroxybenzoate compared to mannitol. The gene list was obtained from previous study on *S. coelicolor* A3(2) (J. S. Kim et al., 2012; Y. J. Kim et al., 2008).

Strains			Annotation	PCA		4HB	
***S. coelicolor* A3(2)**	***S. lividans* TK24**	***S. lividans* ΔYA8-DG2**		**Log_2 fold change**	**adjP**	**Log_2 fold change**	**adjP**
SCO7590	SLIV_01360	SLYA8N_01360	Catalase, KatA1	-0.86	1.55E-02	1.07	4.75E-06
SCO7298	SLIV_02805	SLYA8N_02805	Thioredoxin reductase	0.27	6.53E-01	-0.23	5.34E-01
SCO5438	SLIV_11315	SLYA8N_11315	Thioredoxin	-0.83	1.84E-01	0.41	3.70E-01
SCO5419	SLIV_11410	SLYA8N_11410	Thioredoxin	0.05	8.76E-01	0.99	3.22E-15
SCO5254	SLIV_12095	SLYA8N_12095	Superoxide dismutase [Ni], sodN	1.31	3.73E-09	-2.16	5.09E-24
SCO4444	SLIV_16210	SLYA8N_16210	Glutathione peroxidase	0.14	7.71E-01	0.81	5.37E-05
SCO3890	SLIV_18815	SLYA8N_18815	Thioredoxin reductase, trxB	-0.03	9.29E-01	1.18	2.88E-35
SCO3889	SLIV_18820	SLYA8N_18820	Thioredoxin, trxA	-0.06	8.08E-01	0.82	1.12E-18
SCO0999	SLIV_24510	SLYA8N_24510	Superoxide dismutase, sodF1	-1.79	4.42E-21	0.72	8.74E-04
SCO2633	SLIV_24510	SLYA8N_24510	Superoxide dismutase, sodF1	-1.79	4.42E-21	0.72	8.74E-04
SCO2554	SLIV_24915	SLYA8N_24915	Chaperone protein DnaJ, dnaJ2	0.07	7.84E-01	0.59	1.09E-08
SCO0885	SLIV_33510	SLYA8N_33510	Thioredoxin	0.17	6.62E-01	1.68	1.28E-18
SCO0666	SLIV_34610	SLYA8N_34610	Catalase, katE	-0.18	7.71E-01	1.76	5.70E-15
SCO0560	SLIV_35140	SLYA8N_35140	Catalase-peroxidase, katG	-0.40	7.89E-03	-0.81	6.32E-11
SCO0465	SLIV_35615	SLYA8N_35615	Non-heme chloroperoxidase, cpo	-0.21	7.67E-01	-0.44	2.07E-01
SCO0379	SLIV_36045	SLYA8N_36045	Catalase, katA3	1.21	3.31E-18	1.56	5.00E-35

Table S5. Gene expression data of *S. lividans* ΔYA8-DG2 reflecting genes linked to energy metabolism on protocatechuate and 4-hydroxybenzoate compared to mannitol. The gene list was obtained from previous study on *S. coelicolor* A3(2) (Lejeune et al., 2022).

S. lividans TK24	*S. lividans* ΔYA8-DG2	Annotation	**Log_2 fold change**	**adjP**	**Log_2 fold change**	**adjP**
SLIV_02810	SLYA8N_02810	NADH-quinone oxidoreductase subunit D 1	0.40	1.78E-01	0.27	2.31E-01
SLIV_03985	SLYA8N_03985	NADH:flavin oxidoreductase/NADH oxidase	1.40	1.19E-01	1.76	5.58E-03

Continuation of table S5.

SLIV_06600	SLYA8N_06600	cytochrome P450	-0.38	2.40E-02	-2.20	5.22E-48
SLIV_07935	SLYA8N_07935	protoporphyrinogen oxidase	0.17	8.77E-01	0.32	4.82E-01
SLIV_11620	SLYA8N_11620	ATP synthase epsilon chain	0.14	5.10E-01	0.66	1.61E-07
SLIV_11625	SLYA8N_11625	ATP synthase subunit beta	-0.06	7.89E-01	0.50	5.75E-07
SLIV_11630	SLYA8N_11630	ATP synthase gamma chain	0.04	8.69E-01	0.98	3.54E-19
SLIV_11635	SLYA8N_11635	ATP synthase subunit alpha	-0.01	9.73E-01	0.93	1.12E-18
SLIV_11640	SLYA8N_11640	ATP synthase subunit delta	0.05	8.70E-01	1.14	9.20E-19
SLIV_11645	SLYA8N_11645	ATP synthase subunit b	0.02	9.54E-01	0.58	1.55E-06
SLIV_11650	SLYA8N_11650	putative membrane protein	-0.04	9.16E-01	-0.41	1.77E-03
SLIV_11655	SLYA8N_11655	ATP synthase subunit a	-0.08	8.74E-01	-1.37	1.43E-15
SLIV_11660	SLYA8N_11660	ATP synthase I	-0.09	8.14E-01	-1.71	1.52E-28
SLIV_15230	SLYA8N_15230	NADH-quinone oxidoreductase subunit N 2	-0.47	1.42E-01	-4.66	1.20E-37
SLIV_15235	SLYA8N_15235	NADH dehydrogenase subunit NuoM2	-0.48	5.40E-02	-3.80	1.03E-52
SLIV_15240	SLYA8N_15240	NADH dehydrogenase subunit NuoL2	-0.62	1.88E-02	-2.86	4.80E-32
SLIV_15245	SLYA8N_15245	NADH dehydrogenase subunit NuoK2	-0.27	5.83E-01	-4.30	2.56E-25
SLIV_15250	SLYA8N_15250	NADH dehydrogenase subunit NuoJ2	-0.13	8.80E-01	-4.23	2.53E-19
SLIV_15255	SLYA8N_15255	NADH-quinone oxidoreductase subunit I 2	-0.24	4.44E-01	-2.85	2.79E-40
SLIV_15260	SLYA8N_15260	NADH dehydrogenase subunit NuoH2	-0.33	3.41E-01	-2.56	5.31E-26
SLIV_15390	SLYA8N_15390	NADH-quinone oxidoreductase subunit N 3	-0.96	8.42E-08	-0.82	2.23E-05
SLIV_15395	SLYA8N_15395	NADH-quinone oxidoreductase subunit M	-0.86	1.80E-06	-0.52	1.50E-02
SLIV_15400	SLYA8N_15400	NADH-quinone oxidoreductase subunit L	-1.00	1.33E-07	-0.67	7.32E-03
SLIV_15405	SLYA8N_15405	NADH dehydrogenase subunit K	-0.77	7.04E-04	-0.65	9.52E-03
SLIV_15410	SLYA8N_15410	NuoJ	-0.74	8.57E-04	-0.39	1.49E-01
SLIV_15415	SLYA8N_15415	NADH-quinone oxidoreductase subunit I 1	-0.96	3.79E-07	-0.16	5.76E-01
SLIV_15420	SLYA8N_15420	NADH-quinone oxidoreductase subunit H	-0.94	2.53E-08	-0.36	1.53E-01
SLIV_15425	SLYA8N_15425	NADH-quinone oxidoreductase subunit G	-0.75	1.30E-04	0.07	8.14E-01
SLIV_15430	SLYA8N_15430	NADH-quinone oxidoreductase subunit F	-0.82	8.30E-06	-0.08	7.80E-01
SLIV_15435	SLYA8N_15435	NADH-quinone oxidoreductase subunit E	-0.92	4.29E-06	-0.26	2.88E-01
SLIV_15440	SLYA8N_15440	NADH-quinone oxidoreductase subunit D 2	-0.89	3.88E-08	-0.84	5.35E-06
SLIV_15445	SLYA8N_15445	NADH-quinone oxidoreductase subunit C	-0.73	1.37E-04	-0.66	1.18E-03
SLIV_15450	SLYA8N_15450	NADH-quinone oxidoreductase subunit B 1	-0.90	1.25E-07	-0.69	2.87E-04

Continuation of table S5.

SLIV_15455	SLYA8N_15455	NADH dehydrogenase subunit A	-0.85	1.45E-07	-0.90	3.34E-07
SLIV_15470	SLYA8N_15470	electron transfer oxidoreductase	-0.20	3.42E-01	0.89	2.63E-12
SLIV_17655	SLYA8N_17655	Polyphosphate kinase, PPK	-0.26	5.49E-01	-1.90	1.80E-15
SLIV_17805	SLYA8N_17805	NADH dehydrogenase	-0.22	7.39E-01	-2.83	3.56E-17
SLIV_18595	SLYA8N_18595	cytochrome oxidase subunit I	0.01	9.92E-01	-0.06	8.09E-01
SLIV_21195	SLYA8N_21195	Redox-sensing transcriptional repressor rex	0.18	4.69E-01	-0.55	4.16E-04
SLIV_23265	SLYA8N_23265	cytochrome P450	-1.00	6.37E-14	-0.11	4.88E-01
SLIV_23270	SLYA8N_23270	cytochrome P450	-1.12	2.46E-12	-1.42	8.42E-23
SLIV_26945	SLYA8N_26945	response regulator	-0.35	2.04E-01	-1.76	4.44E-22
SLIV_26950	SLYA8N_26950	putative cytochrome c oxidase subunit 3	-0.39	6.35E-02	-0.80	9.64E-07
SLIV_26955	SLYA8N_26955	cytochrome C heme-binding subunit	-0.39	1.83E-02	-0.74	2.32E-07
SLIV_26960	SLYA8N_26960	Ubiquinol-cytochrome c reductase iron-sulfur subunit	-0.38	4.55E-02	-1.19	1.83E-16
SLIV_26965	SLYA8N_26965	Ubiquinol-cytochrome c reductase cytochrome b subunit	-0.37	1.55E-01	-1.60	2.15E-18
SLIV_26970	SLYA8N_26970	Anthranilate phosphoribosyltransferase 1	-0.35	1.70E-02	-1.16	1.40E-19
SLIV_29610	SLYA8N_29610	cytochrome P450	-0.52	1.21E-02	-2.66	1.09E-45
SLIV_32385	SLYA8N_32385	Electron transfer flavoprotein subunit beta	0.28	9.86E-03	0.94	8.68E-26
SLIV_32385	SLYA8N_32385	Electron transfer flavoprotein subunit beta	0.28	9.86E-03	0.94	8.68E-26
SLIV_32390	SLYA8N_32390	Electron transfer flavoprotein subunit alpha	0.30	4.07E-02	0.82	2.18E-13
SLIV_32390	SLYA8N_32390	Electron transfer flavoprotein subunit alpha	0.30	4.07E-02	0.82	2.18E-13
SLIV_34535	SLYA8N_34535	NADPH-ferredoxin reductase FprA	-0.01	9.79E-01	-0.67	2.18E-07
SLIV_35020	SLYA8N_35020	ATP/GTP binding protein	-1.13	1.36E-07	-3.92	7.96E-49
SLIV_35025	SLYA8N_35025	cytochrome P450	-0.99	2.16E-06	-3.78	8.36E-52
SLIV_35030	SLYA8N_35030	cytochrome P450	-0.07	9.36E-01	-0.07	0.862138732

Table S6. Gene expression data of *S. lividans* ΔYA8-DG2 reflecting genes linked to amino acid biosynthesis on protocatechuate and 4-hydroxybenzoate compared to mannitol. The gene list was obtained from KEGG (Kyoto Encyclopedia of Genes and Genomes). The gene expression data is available as open access (Seo et al., 2023) in the supplementary information: https://doi.org/10.1186/s12934-023-02266-0

6.3 Supplementary data: Figures

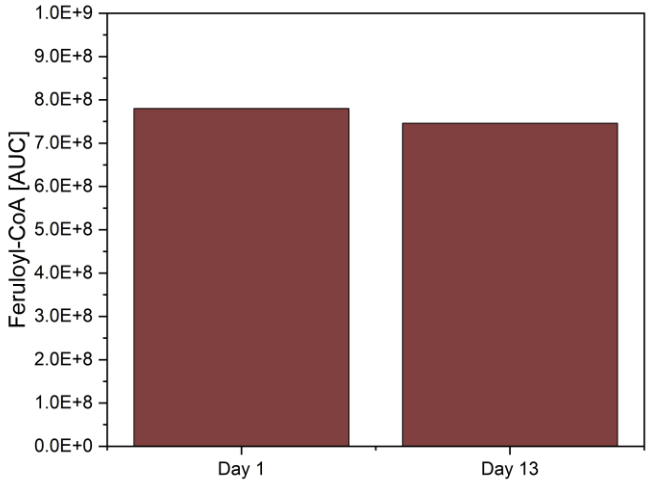

Figure S1. The stability of feruloyl-CoA in quenching solution. The aromatic CoA thioester extract was obtained from *C. glutamicum* WT culture (Fig. 6A). The extract was dissolved in quenching solution (pH 5.7) and analysed. Subsequently, the sample was stored at 4 °C for 13 days and re-analysed to observe the stability of feruloyl-CoA from biological samples.

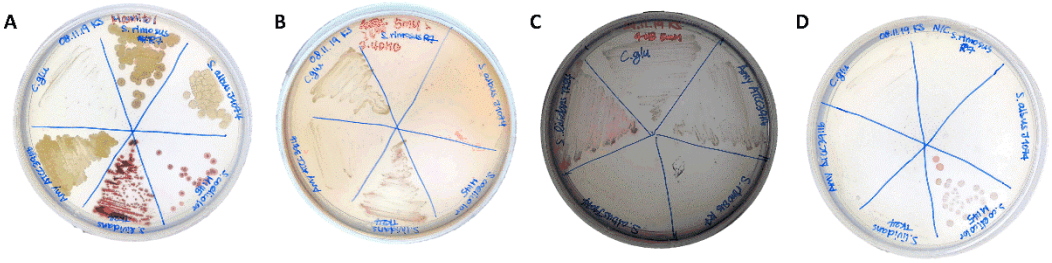

Figure S2: Substrate screening of *S. lividans* TK24. Minimal plate medium was used, containing either 10 g L^{-1} of mannitol (A), 5 mM of protocatechuic acid (B), or 5 mM of 4-hydroxybenzoic acid (C) as the sole carbon source, or no carbon source (D). The plates were incubated for 5 days at 28 °C. The different concentrations were selected based on the anticipated toxicity of the aromatic compounds (Cho et al., 1998).

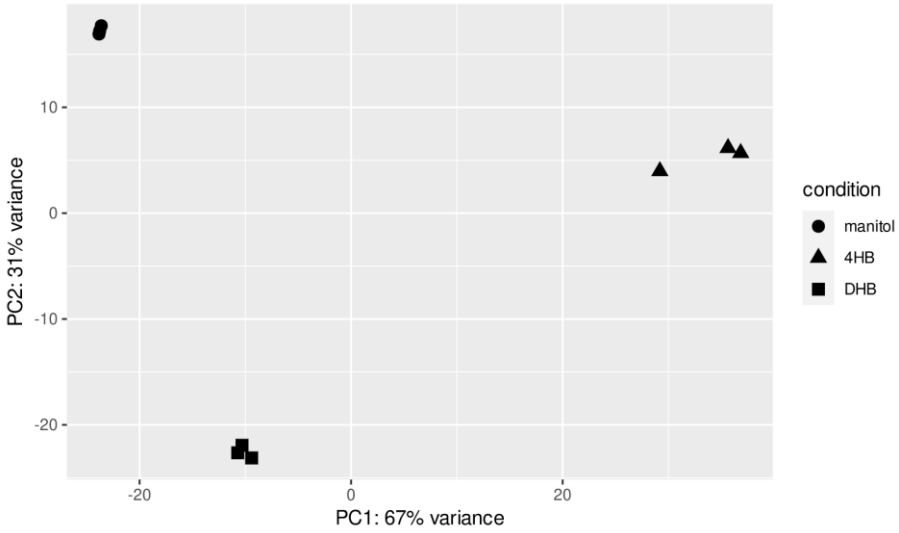

Figure S3. Quality assessment of RNA sequencing using principal component analysis (PCA). The data encompass the global transcriptomes of *S. lividans* ΔYA8-DG2 grown on 10 mM mannitol, 10 mM protocatechuate, or 10 mM 4-hydroxybenzoate, respectively. Samples were collected after 12 hours of growth, with three biological replicates (n=3) for each condition. PCA was used to assess the quality of the RNA sequencing data.

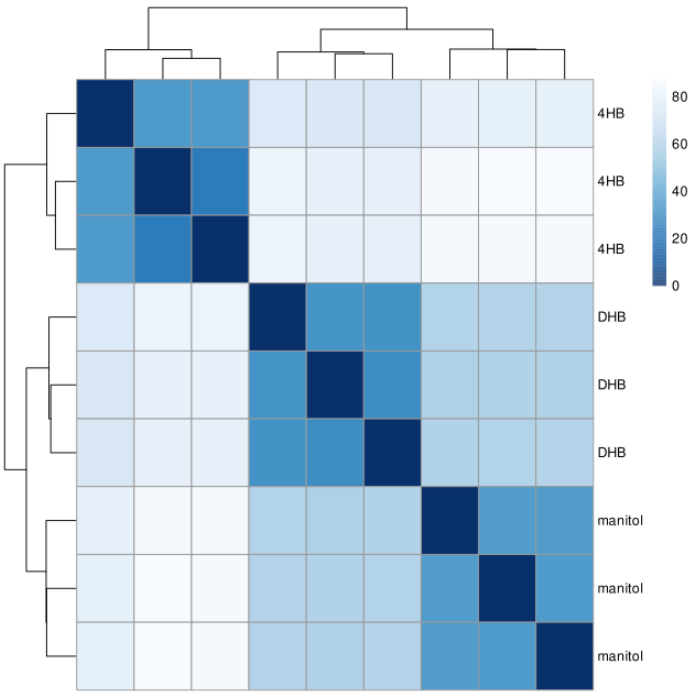

Figure S4. Sample distance plot. The data are derived from RNA sequencing of *S. lividans* ΔYA8-DG2, grown on 10 mM mannitol, 10 mM protocatechuate, or 10 mM 4-hydroxybenzoate. Samples were collected after 12 hours of growth, with three biological replicates (n=3) for each condition.

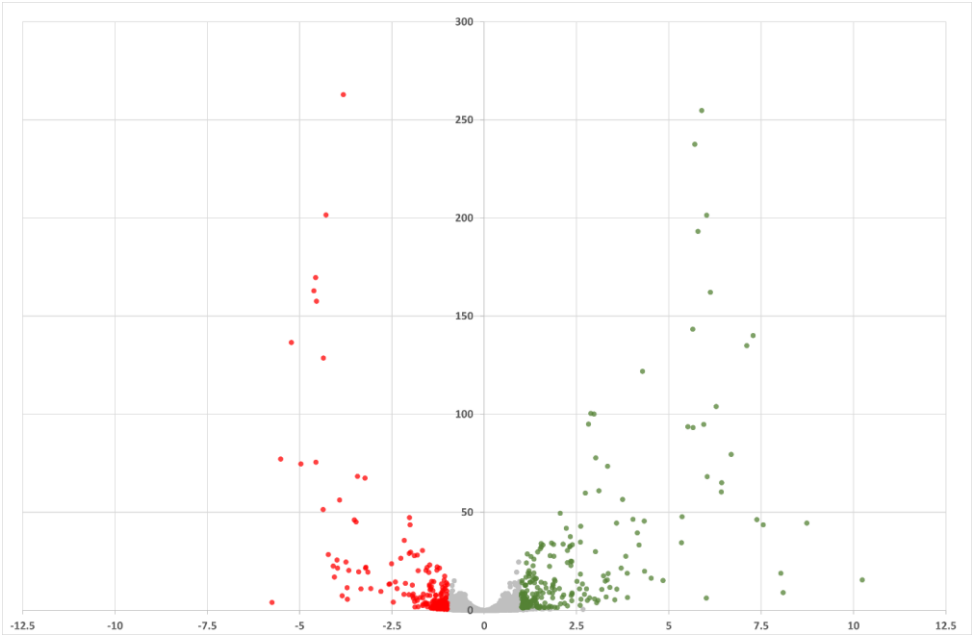

Figure S5. Volcano plot between mannitol and PCA. The data reflect the differences in gene expression between *S. lividans* ΔYA8-DG2 grown on mannitol and those grown on protocatechuate, with samples collected after 12 hours. Each condition includes three biological replicates (n=3).

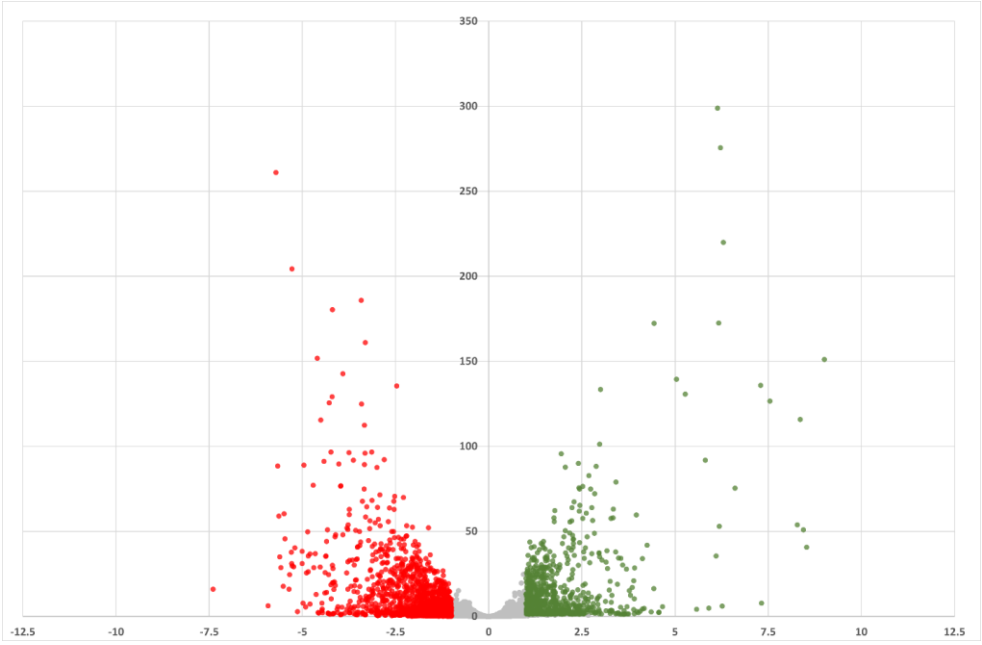

Figure S6. Volcano plot between mannitol and 4HB. The data reflect the differences in gene expression between *S. lividans* ΔYA8-DG2 grown on mannitol and those grown on protocatechuate, with samples collected after 12 hours. Each condition includes three biological replicates (n=3).

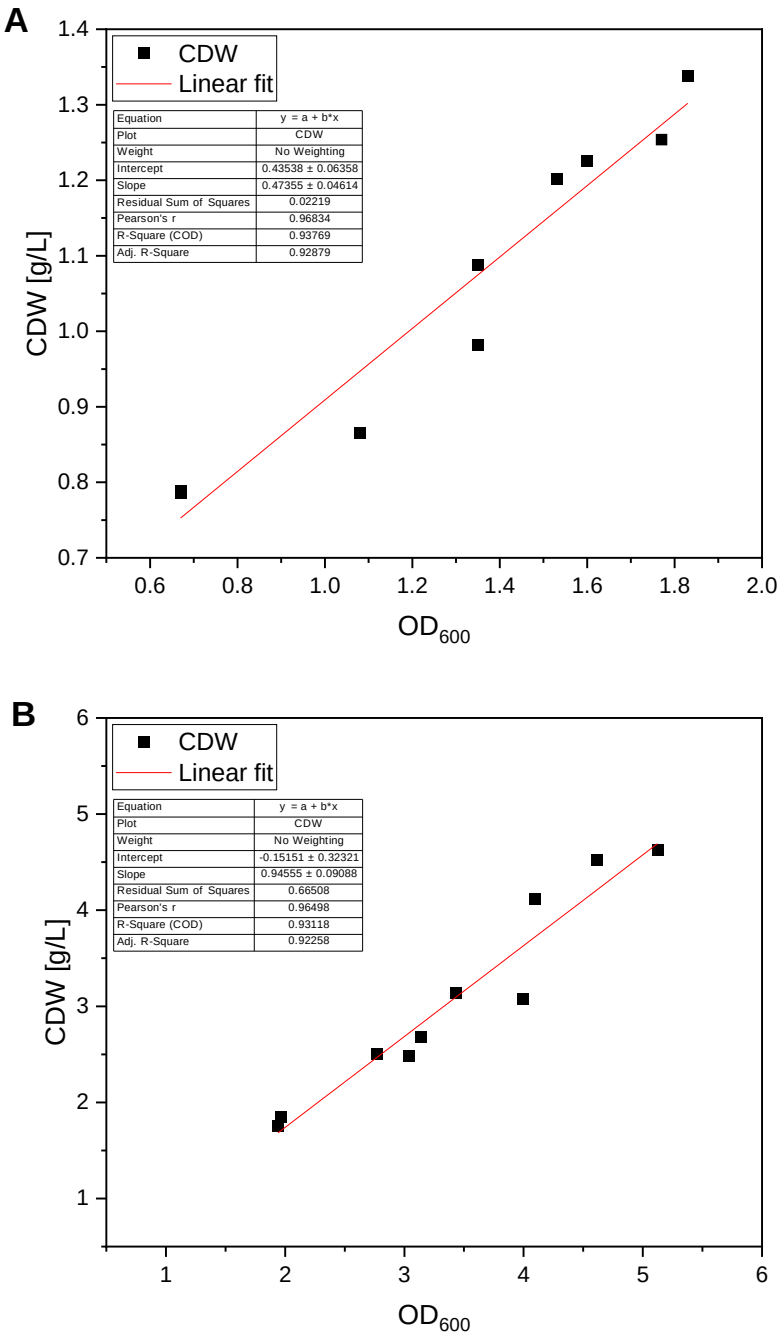

Figure S7. Correlation between OD and CDW for *S. lividans* ΔYA8-DG2. The strain was cultured with 10 mM protocatechuate (A) and 30 mM mannitol (B), and measurements were taken at various time points. Data represents biological triplicate experiments (n=3).

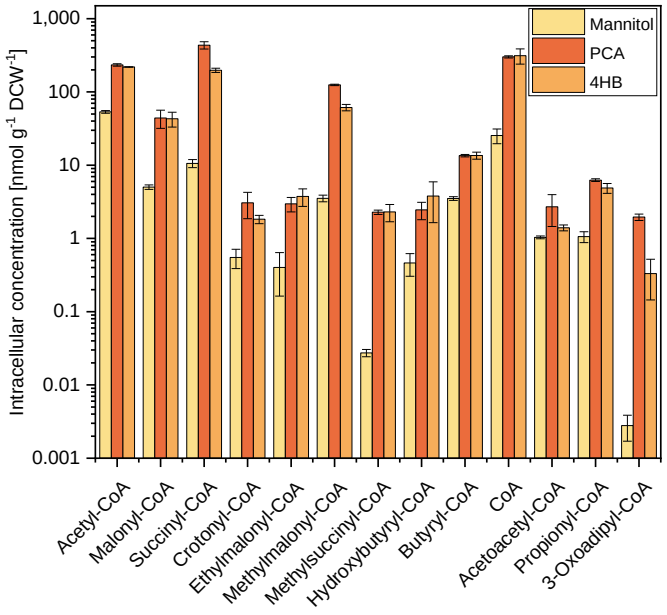

Figure S8. Absolute levels of intracellular CoA thioesters in for *S. lividans* ΔYA8-DG2. The data represent absolute concentrations during mid-exponential growth (12 h) in minimal medium containing 10 mM of either mannitol, protocatechuate, or 4-hydroxybenzoate, respectively. n=3.

7 Reference

Abdelaziz, O. Y., Brink, D. P., Prothmann, J., Ravi, K., Sun, M., García-Hidalgo, J., Sandahl, M., Hulteberg, C. P., Turner, C., Lidén, G., & Gorwa-Grauslund, M. F. (2016). Biological valorization of low molecular weight lignin. *Biotechnology advances, 34*(8), 1318-1346. doi: 10.1016/j.biotechadv.2016.10.001

Abe, S., Takayama, K. I., & Kinoshita, S. (1967). Taxonomical studies on glutamic acid-producing bacteria. *Journal of General and Applied Microbiology, 13*(3), 279-300. doi: 10.2323/Jgam.13.279

Abraham, A., Mathew, A. K., Park, H., Choi, O., Sindhu, R., Parameswaran, B., Pandey, A., Park, J. H., & Sang, B. I. (2020). Pretreatment strategies for enhanced biogas production from lignocellulosic biomass. *Bioresource technology, 301*, 122725. doi: 10.1016/j.biortech.2019.122725

Achterholt, S., Priefert, H., & Steinbüchel, A. (2000). Identification of *Amycolatopsis* sp. strain HR167 genes, involved in the bioconversion of ferulic acid to vanillin. *Applied microbiology and biotechnology, 54*(6), 799-807. doi: 10.1007/s002530000431

Aghapour, A. A., Moussavi, G., & Yaghmaeian, K. (2013). Biological degradation of catechol in wastewater using the sequencing continuous-inflow reactor (SCR). *Journal of environmental health science & engineering, 11*(1), 3. doi: 10.1186/2052-336X-11-3

Aguilera-Morales, M., Casas-Valdez, M., Carrillo-Domínguez, B., González-Acosta, B., & Pérez-Gil, F. (2005). Chemical composition and microbiological assays of marine algae *Enteromorpha* spp. as a potential food source. *Journal of Food Composition and Analysis, 18*(1), 79-88. doi: 10.1016/j.jfca.2003.12.012

Ahmed, Y., Rebets, Y., Estévez, M. R., Zapp, J., Myronovskyi, M., & Luzhetskyy, A. (2020). Engineering of *Streptomyces lividans* for heterologous expression of secondary metabolite gene clusters. *Microbial cell factories, 19*(1), 5. doi: 10.1186/s12934-020-1277-8

Ahsan, T., Chen, J. G., Wu, Y. H., & Irfan, M. (2017). Application of response surface methodology for optimization of medium components for the production of secondary metabolites by *Streptomyces diastatochromogenes* KX852460. *Amb Express, 7*. doi: 10.1186/s13568-017-0388-z

Akagawa, E., Kurita, K., Sugawara, T., Nakamura, K., Kasahara, Y., Ogasawara, N., & Yamane, K. (1995). Determination of a 17,484 bp nucleotide sequence around the 39 degrees region of the *Bacillus subtilis* chromosome and similarity analysis of the products of putative ORFs. *Microbiology, 141*(12), 3241-3245. doi: 10.1099/13500872-141-12-3241

Alber, B. E. (2011). Biotechnological potential of the ethylmalonyl-CoA pathway. *Applied microbiology and biotechnology, 89*(1), 17-25. doi: 10.1007/s00253-010-2873-z

Aliste, A. J., Vieira, F. F., & Del Mastro, N. L. (2000). Radiation effects on agar, alginates and carrageenan to be used as food additives. *Radiation Physics and Chemistry, 57*(3-6), 305-308. doi: 10.1016/S0969-806x(99)00471-5

Andreoni, V., Galli, E., & Galliani, G. (1984). Metabolism of ferulic ccid by a facultatively anaerobic strain of *Pseudomonas cepacia*. *Systematic and Applied Microbiology, 5*(3), 299-304. doi: 10.1016/S0723-2020(84)80032-6

Armando, J. W., Boghigian, B. A., & Pfeifer, B. A. (2012). LC-MS/MS quantification of short-chain acyl-CoA's in *Escherichia coli* demonstrates versatile propionyl-CoA synthetase substrate specificity. *Letters in applied microbiology, 54*(2), 140-148. doi: 10.1111/j.1472-765X.2011.03184.x

Arnison, P. G., Bibb, M. J., Bierbaum, G., Bowers, A. A., Bugni, T. S., Bulaj, G., Camarero, J. A., Campopiano, D. J., Challis, G. L., Clardy, J., Cotter, P. D., Craik, D. J., Dawson, M., Dittmann, E., Donadio, S., Dorrestein, P. C., Entian, K. D., Fischbach, M. A., Garavelli, J.

S., Göransson, U., Gruber, C. W., Haft, D. H., Hemscheidt, T. K., Hertweck, C., Hill, C., Horswill, A. R., Jaspars, M., Kelly, W. L., Klinman, J. P., Kuipers, O. P., Link, A. J., Liu, W., Marahiel, M. A., Mitchell, D. A., Moll, G. N., Moore, B. S., Müller, R., Nair, S. K., Nes, I. F., Norris, G. E., Olivera, B. M., Onaka, H., Patchett, M. L., Piel, J., Reaney, M. J., Rebuffat, S., Ross, R. P., Sahl, H. G., Schmidt, E. W., Selsted, M. E., Severinov, K., Shen, B., Sivonen, K., Smith, L., Stein, T., Süssmuth, R. D., Tagg, J. R., Tang, G. L., Truman, A. W., Vederas, J. C., Walsh, C. T., Walton, J. D., Wenzel, S. C., Willey, J. M., & van der Donk, W. A. (2013). Ribosomally synthesized and post-translationally modified peptide natural products: overview and recommendations for a universal nomenclature. *Natural product reports, 30*(1), 108-160. doi: 10.1039/c2np20085f

Baghel, R. S., Reddy, C. R. K., & Singh, R. P. (2021). Seaweed-based cellulose: Applications, and future perspectives. *Carbohydrate polymers, 267*, 118241. doi: 10.1016/j.carbpol.2021.118241

Bajwa, D. S., Pourhashem, G., Ullah, A. H., & Bajwa, S. G. (2019). A concise review of current lignin production, applications, products and their environmental impact. *Industrial Crops and Products, 139*. doi: 10.1016/j.indcrop.2019.111526

Barton, N., Horbal, L., Starck, S., Kohlstedt, M., Luzhetskyy, A., & Wittmann, C. (2018). Enabling the valorization of guaiacol-based lignin: Integrated chemical and biochemical production of *cis*,*cis*-muconic acid using metabolically engineered *Amycolatopsis* sp ATCC 39116. *Metabolic engineering, 45*, 200-210. doi: 10.1016/j.ymben.2017.12.001

Becker, J., Kuhl, M., Kohlstedt, M., Starck, S., & Wittmann, C. (2018a). Metabolic engineering of *Corynebacterium glutamicum* for the production of *cis, cis*-muconic acid from lignin. *Microbial Cell Factories, 17*. doi: 10.1186/s12934-018-0963-2

Becker, J., Rohles, C. M., & Wittmann, C. (2018b). Metabolically engineered *Corynebacterium glutamicum* for bio-based production of chemicals, fuels, materials, and healthcare products. *Metabolic engineering, 50*, 122-141. doi: 10.1016/j.ymben.2018.07.008

Becker, J., & Wittmann, C. (2012). Systems and synthetic metabolic engineering for amino acid production - the heartbeat of industrial strain development. *Current opinion in biotechnology, 23*(5), 718-726. doi: 10.1016/j.copbio.2011.12.025

Becker, J., & Wittmann, C. (2019). A field of dreams: Lignin valorization into chemicals, materials, fuels, and health-care products. *Biotechnology advances, 37*(6), 107360. doi: 10.1016/j.biotechadv.2019.02.016

Becker, J., Zelder, O., Häfner, S., Schröder, H., & Wittmann, C. (2011). From zero to hero-Design-based systems metabolic engineering of *Corynebacterium glutamicum* for L-lysine production. *Metabolic engineering, 13*(2), 159-168. doi: 10.1016/j.ymben.2011.01.003

Behrens, S., Mitchell, W., & Bahl, H. (2001). Molecular analysis of the mannitol operon of *Clostridium acetobutylicum* encoding a phosphotransferase system and a putative PTS-modulated regulator. *Microbiology, 147*(1), 75-86. doi: 10.1099/00221287-147-1-75

Bender, E., Koller, K. P., & Engels, J. W. (1990). Secretory synthesis of human interleukin-2 by *Streptomyces lividans*. *Gene, 86*(2), 227-232. doi: 10.1016/0378-1119(90)90283-w

Bérdy, J. (2012). Thoughts and facts about antibiotics: Where we are now and where we are heading. *Journal of Antibiotics, 65*(8), 385-395. doi: 10.1038/ja.2012.27

Bertram, R., Schlicht, M., Mahr, K., Nothaft, H., Saier, M. H., Jr., & Titgemeyer, F. (2004). In silico and transcriptional analysis of carbohydrate uptake systems of *Streptomyces coelicolor* A3(2). *Journal of bacteriology, 186*(5), 1362-1373. doi: 10.1128/JB.186.5.1362-1373.2004

Beuerle, T., & Pichersky, E. (2002). Enzymatic synthesis and purification of aromatic coenzyme A esters. *Analytical biochemistry, 302*(2), 305-312. doi: 10.1006/abio.2001.5574

Bleakley, S., & Hayes, M. (2017). Algal Proteins: Extraction, Application, and Challenges Concerning Production. *Foods, 6*(5). doi: 10.3390/foods6050033

Bolten, C. J., Kiefer, P., Letisse, F., Portais, J. C., & Wittmann, C. (2007). Sampling for metabolome analysis of microorganisms. *Analytical chemistry, 79*(10), 3843-3849. doi: 10.1021/ac0623888

Boudet, A. M. (1998). A new view of lignification. *Trends in Plant Science, 3*(2), 67-71. doi: 10.1016/S1360-1385(97)01176-X

Brinkrolf, K., Brune, I., & Tauch, A. (2006). Transcriptional regulation of catabolic pathways for aromatic compounds in *Corynebacterium glutamicum*. *Genetics and molecular research : GMR, 5*(4), 773-789.

Brünker, P., Altenbuchner, J., & Mattes, R. (1998). Structure and function of the genes involved in mannitol, arabitol and glucitol utilization from *Pseudomonas fluorescens* DSM50106. *Gene, 206*(1), 117-126. doi: 10.1016/s0378-1119(97)00574-x

Brunow, G. (2005). Methods to Reveal the Structure of Lignin. In A. Steinbüchel (Ed.), *Biopolymers Online*.

Buschke, N., Schäfer, R., Becker, J., & Wittmann, C. (2013). Metabolic engineering of industrial platform microorganisms for biorefinery applications-optimization of substrate spectrum and process robustness by rational and evolutive strategies. *Bioresource technology, 135*, 544-554. doi: 10.1016/j.biortech.2012.11.047

Cabruja, M., Lyonnet, B. B., Millán, G., Gramajo, H., & Gago, G. (2016). Analysis of coenzyme A activated compounds in actinomycetes. *Applied microbiology and biotechnology, 100*(16), 7239-7248. doi: 10.1007/s00253-016-7635-0

Cai, C. G., Xu, Z. X., Xu, M. L., Cai, M. F., & Jin, M. J. (2020). Development of a *Rhodococcus opacus* cell factory for valorizing lignin to muconate. *Acs Sustainable Chemistry & Engineering, 8*(4), 2016-2031. doi: 10.1021/acssuschemeng.9b06571

Cakić, N., Kopke, B., Rabus, R., & Wilkes, H. (2021). Suspect screening and targeted analysis of acyl coenzyme A thioesters in bacterial cultures using a high-resolution tribrid mass spectrometer. *Analytical and bioanalytical chemistry, 413*(14), 3599-3610. doi: 10.1007/s00216-021-03318-3

Calvo-Flores, F. G., & Martin-Martinez, F. J. (2022). Biorefineries: Achievements and challenges for a bio-based economy. *Frontiers in chemistry, 10*, 973417. doi: 10.3389/fchem.2022.973417

Campillo, T., Renoud, S., Kerzaon, I., Vial, L., Baude, J., Gaillard, V., Bellvert, F., Chamignon, C., Comte, G., Nesme, X., Lavire, C., & Hommais, F. (2014). Analysis of hydroxycinnamic acid degradation in *Agrobacterium fabrum* reveals a coenzyme A-dependent, beta-oxidative deacetylation pathway. *Applied and environmental microbiology, 80*(11), 3341-3349. doi: 10.1128/AEM.00475-14

Capron, M. E., Stewart, J. R., N'Yeurt, A. D., Chambers, M. D., Kim, J. K., Yarish, C., Jones, A. T., Blaylock, R. B., James, S. C., Fuhrman, R., Sherman, M. T., Piper, D., Harris, G., & Hasan, M. A. (2020). Restoring pre-industrial CO_2 levels while achieving sustainable development goals. *Energies, 13*(18). doi: 10.3390/En13184972

Cecchini, G., Schröder, I., Gunsalus, R. P., & Maklashina, E. (2002). Succinate dehydrogenase and fumarate reductase from *Escherichia coli*. *Biochimica et biophysica acta, 1553*(1-2), 140-157. doi: 10.1016/s0005-2728(01)00238-9

Cecil, J. H., Garcia, D. C., Giannone, R. J., & Michener, J. K. (2018). Rapid, parallel identification of catabolism pathways of lignin-derived aromatic compounds in *Novosphingobium aromaticivorans*. *Applied and environmental microbiology, 84*(22). doi: 10.1128/AEM.01185-18

Chades, T., Scully, S. M., Ingvadottir, E. M., & Orlygsson, J. (2018). Fermentation of mannitol extracts from brown macro algae by *Thermophilic Clostridia*. *Frontiers in microbiology, 9*, 1931. doi: 10.3389/fmicb.2018.01931

Chaudhury, D., Torkelson, E. R., Meyers, K. A., Acheson, J. F., Landucci, L., Pu, Y., Sun, Z., Tonelli, M., Bingman, C. A., Smith, R. A., Karlen, S. D., Mansfield, S. D., Ralph, J., & Fox,

B. G. (2023). Rapid biocatalytic synthesis of aromatic acid CoA thioesters by using microbial aromatic acid CoA ligases. *Chembiochem : a European journal of chemical biology, 24*(9), e202300001. doi: 10.1002/cbic.202300001

Chen, K., Ríos, J. J., Pérez-Gálvez, A., & Roca, M. (2017). Comprehensive chlorophyll composition in the main edible seaweeds. *Food chemistry, 228*, 625-633. doi: 10.1016/j.foodchem.2017.02.036

Chio, C. L., Sain, M., & Qin, W. S. (2019). Lignin utilization: A review of lignin depolymerization from various aspects. *Renewable & Sustainable Energy Reviews, 107*, 232-249. doi: 10.1016/j.rser.2019.03.008

Cho, J. Y., Moon, J. H., Seong, K. Y., & Park, K. H. (1998). Antimicrobial activity of 4-hydroxybenzoic acid and 4-hydroxycinnamic acid isolated and identified from rice hull. *Bioscience Biotechnology and Biochemistry, 62*(11), 2273-2276. doi: 10.1271/Bbb.62.2273

Chou, W. G., & Pogell, B. M. (1981). Mode of action of pamamycin in *Staphylococcus aureus*. *Antimicrobial agents and chemotherapy, 20*(4), 443-454. doi: 10.1128/AAC.20.4.443

Choudhary, B., Chauhan, O. P., & Mishra, A. (2021). Edible seaweeds: A potential novel source of bioactive metabolites and nutraceuticals with human health benefits. *Frontiers in Marine Science, 8*. doi: 10.3389/Fmars.2021.740054

Costanza, R., d'Arge, R., de Groot, R., Farber, S., Grasso, M., Hannon, B., Limburg, K., Naeem, S., O'Neill, R. V., Paruelo, J., Raskin, R. G., Sutton, P., & van den Belt, M. (1998). The value of the world's ecosystem services and natural capital (Reprinted from Nature, vol 387, pg 253, 1997). *Ecological Economics, 25*(1), 3-15. doi: 10.1016/S0921-8009(98)00020-2

Crone, W. J. K., Leeper, F. J., & Truman, A. W. (2012). Identification and characterisation of the gene cluster for the anti-MRSA antibiotic bottromycin: expanding the biosynthetic diversity of ribosomal peptides. *Chemical Science, 3*(12), 3516-3521. doi: 10.1039/c2sc21190d

Cummings, M., Breitling, R., & Takano, E. (2014). Steps towards the synthetic biology of polyketide biosynthesis. *FEMS microbiology letters, 351*(2), 116-125. doi: 10.1111/1574-6968.12365

Daniels, W., Bouvin, J., Busche, T., Rückert, C., Simoens, K., Karamanou, S., Van Mellaert, L., Friðjónsson, Ó. H., Nicolai, B., Economou, A., Kalinowski, J., Anné, J., & Bernaerts, K. (2018). Transcriptomic and fluxomic changes in *Streptomyces lividans* producing heterologous protein. *Microbial cell factories, 17*(1), 198. doi: 10.1186/s12934-018-1040-6

Dawson, R. M. C., Elliott, D. C., Elliott, W. H., & Jones, K. M. (2002). *Data for biochemical research* (3rd ed.). Oxford, UK: Clarendon press.

Dominguez, H., & Lindley, N. D. (1996). Complete sucrose metabolism requires fructose phosphotransferase activity in *Corynebacterium glutamicum* to ensure phosphorylation of liberated fructose. *Applied and environmental microbiology, 62*(10), 3878-3880. doi: 10.1128/aem.62.10.3878-3880.1996

Doty, M. S. (1946). Critical tide factors that are correlated with the vertical distribution of marine algae and other organisms along the pacific coast. *Ecology, 27*(4), 315-328. doi: 10.2307/1933542

Drescher, A., & Kienberger, M. (2022). A systematic review on waste as sustainable feedstock for bioactive molecules-extraction as isolation technology. *Processes, 10*(8). doi: 10.3390/Pr10081668

Dulaney, Eugene L. (1949). Observations on *Streptomyces Griseus*. III. Carbon sources for growth and streptomycin production. *Mycologia, 41*(1), 1-10. doi: 10.1080/00275514.1949.12017747

Dutot, M., Fagon, R., Hemon, M., & Rat, P. (2012). Antioxidant, anti-inflammatory, and anti-senescence activities of a phlorotannin-rich natural extract from brown seaweed

Ascophyllum nodosum. *Applied biochemistry and biotechnology, 167*(8), 2234-2240. doi: 10.1007/s12010-012-9761-1

El Gamal, A. A. (2010). Biological importance of marine algae. *Saudi pharmaceutical journal : SPJ : the official publication of the Saudi Pharmaceutical Society, 18*(1), 1-25. doi: 10.1016/j.jsps.2009.12.001

Elgersma, J. N. , Rusting, N., & van Berne, J. H. (1955). Werkwijze voor de bereiding van een antibiotische stof met behulp van actinomyceten van het geslacht *Streptomyces* 79749.

Elibol, M. (2004). Optimization of medium composition for actinorhodin production by *Streptomyces coelicolor* A3(2) with response surface methodology. *Process Biochemistry, 39*(9), 1057-1062. doi: 10.1016/S0032-9592(03)00232-2

Erickson, B., Nelson, J. E., & Winters, P. (2012). Perspective on opportunities in industrial biotechnology in renewable chemicals. *Biotechnology Journal, 7*(2), 176-185. doi: 10.1002/biot.201100069

FAO. (2021). FAO Global Fishery and Aquaculture Production Statistics. (March 2021).

Fleige, C., Meyer, F., & Steinbüchel, A. (2016). Metabolic engineering of the Actinomycete *Amycolatopsis* sp. strain ATCC 39116 towards enhanced production of natural vanillin. *Applied and environmental microbiology, 82*(11), 3410-3419. doi: 10.1128/AEM.00802-16

Franz, L., Kazmaier, U., Truman, A. W., & Koehnke, J. (2021). Bottromycins - biosynthesis, synthesis and activity. *Natural product reports, 38*(9), 1659-1683. doi: 10.1039/d0np00097c

Gaid, M. M., Sircar, D., Müller, A., Beuerle, T., Liu, B., Ernst, L., Hänsch, R., & Beerhues, L. (2012). Cinnamate:CoA ligase initiates the biosynthesis of a benzoate-derived xanthone phytoalexin in *Hypericum calycinum* cell cultures. *Plant physiology, 160*(3), 1267-1280. doi: 10.1104/pp.112.204180

Gallage, N. J., & Møller, B. L. (2015). Vanillin–bioconversion and bioengineering of the most popular plant flavor and its *De Novo* biosynthesis in the vanilla orchid. *Molecular Plant, 8*(1), 40-57. doi: 10.1016/j.molp.2014.11.008

Gläser, L., Kuhl, M., Jovanovic, S., Fritz, M., Vogeli, B., Erb, T. J., Becker, J., & Wittmann, C. (2020). A common approach for absolute quantification of short chain CoA thioesters in prokaryotic and eukaryotic microbes. *Microbial cell factories, 19*(1), 160. doi: 10.1186/s12934-020-01413-1

Gläser, L., Kuhl, M., Stegmüller, J., Rückert, C., Myronovskyi, M., Kalinowski, J., Luzhetskyy, A., & Wittmann, C. (2021). Superior production of heavy pamamycin derivatives using a *bkdR* deletion mutant of *Streptomyces albus* J1074/R2. *Microbial cell factories, 20*(1), 111. doi: 10.1186/s12934-021-01602-6

Gomez-Escribano, J. P., Song, L. J., Bibb, M. J., & Challis, G. L. (2012). Posttranslational β-methylation and macrolactamidination in the biosynthesis of the bottromycin complex of ribosomal peptide antibiotics. *Chemical Science, 3*(12), 3522-3525. doi: 10.1039/c2sc21183a

Gower, J., & King, S. (2019). Seaweed, seaweed everywhere. *Science, 365*(6448), 27. doi: 10.1126/science.aay0989

Graf, N., & Altenbuchner, J. (2014). Genetic engineering of *Pseudomonas putida* KT2440 for rapid and high-yield production of vanillin from ferulic acid. *Applied microbiology and biotechnology, 98*(1), 137-149. doi: 10.1007/s00253-013-5303-1

Groisillier, A., Labourel, A., Michel, G., & Tonon, T. (2015). The mannitol utilization system of the marine bacterium *Zobellia galactanivorans*. *Applied and environmental microbiology, 81*(5), 1799-1812. doi: 10.1128/AEM.02808-14

Gummerlich, N., Manderscheid, N., Rebets, Y., Myronovskyi, M., Gläser, L., Kuhl, M., Wittmann, C., & Luzhetskyy, A. (2021). Engineering the precursor pool to modulate the production of pamamycins in the heterologous host *S. albus* J1074. *Metabolic engineering, 67*, 11-18. doi: 10.1016/j.ymben.2021.05.004

Gurujeyalakshmi, G., & Mahadevan, A. (1987). Dissimilation of ferulic acid by *Bacillus subtilis*. *Current Microbiology, 16*(2), 69-73. doi: 10.1007/Bf01588174

Gust, B., Challis, G. L., Fowler, K., Kieser, T., & Chater, K. F. (2003). PCR-targeted *Streptomyces* gene replacement identifies a protein domain needed for biosynthesis of the sesquiterpene soil odor geosmin. *Proceedings of the National Academy of Sciences of the United States of America, 100*(4), 1541-1546. doi: 10.1073/pnas.0337542100

Hamberger, B., & Hahlbrock, K. (2004). The 4-coumarate:CoA ligase gene family in *Arabidopsis thaliana* comprises one rare, sinapate-activating and three commonly occurring isoenzymes. *Proceedings of the National Academy of Sciences of the United States of America, 101*(7), 2209-2214. doi: 10.1073/pnas.0307307101

Hanquet, G., Salom-Roig, X., & Lanners, S. (2016). New insights into the synthesis and biological activity of the pamamycin macrodiolides. *Chimia, 70*(1-2), 20-28. doi: 10.2533/chimia.2016.20

Harwood, C. S., & Parales, R. E. (1996). The beta-ketoadipate pathway and the biology of self-identity. *Annual review of microbiology, 50*, 553-590. doi: 10.1146/annurev.micro.50.1.553

Hashimoto, M., Katsura, H., Kato, R., Kawaide, H., & Natsume, M. (2011). Effect of pamamycin-607 on secondary metabolite production by *Streptomyces* spp. *Bioscience, biotechnology, and biochemistry, 75*(9), 1722-1726. doi: 10.1271/bbb.110251

He, Y, Li, X, Ben, H, Xue, X, & Yang, B. (2017). Lipid production from dilute alkali corn stover lignin by *Rhodococcus* strains. *ACS Sustainable Chemistry & Engineering, 5*(3), 2302-2311. doi: 10.1021/acssuschemeng.6b02627

Henstra, S. A., Duurkens, R. H., & Robillard, G. T. (2000). Multiple phosphorylation events regulate the activity of the mannitol transcriptional regulator *MtlR* of the *Bacillus stearothermophilus* phosphoenolpyruvate-dependent mannitol phosphotransferase system. *The Journal of biological chemistry, 275*(10), 7037-7044. doi: 10.1074/jbc.275.10.7037

Hilker, R., Stadermann, K. B., Doppmeier, D., Kalinowski, J., Stoye, J., Straube, J., Winnebald, J., & Goesmann, A. (2014). ReadXplorer--visualization and analysis of mapped sequences. *Bioinformatics, 30*(16), 2247-2254. doi: 10.1093/bioinformatics/btu205

Hoffmann, S. L., Jungmann, L., Schiefelbein, S., Peyriga, L., Cahoreau, E., Portais, J. C., Becker, J., & Wittmann, C. (2018). Lysine production from the sugar alcohol mannitol: Design of the cell factory *Corynebacterium glutamicum* SEA-3 through integrated analysis and engineering of metabolic pathway fluxes. *Metabolic engineering, 47*, 475-487. doi: 10.1016/j.ymben.2018.04.019

Hoffmann, S. L., Kohlstedt, M., Jungmann, L., Hutter, M., Poblete-Castro, I., Becker, J., & Wittmann, C. (2021). Cascaded valorization of brown seaweed to produce L-lysine and value-added products using *Corynebacterium glutamicum* streamlined by systems metabolic engineering. *Metabolic engineering, 67*, 293-307. doi: 10.1016/j.ymben.2021.07.010

Honeyman, A. L., & Curtiss, R., 3rd. (1992). Isolation, characterization, and nucleotide sequence of the *Streptococcus mutans* mannitol-phosphate dehydrogenase gene and the mannitol-specific factor III gene of the phosphoenolpyruvate phosphotransferase system. *Infection and immunity, 60*(8), 3369-3375. doi: 10.1128/iai.60.8.3369-3375.1992

Horbal, L., Marques, F., Nadmid, S., Mendes, M. V., & Luzhetskyy, A. (2018). Secondary metabolites overproduction through transcriptional gene cluster refactoring. *Metabolic engineering, 49*, 299-315. doi: 10.1016/j.ymben.2018.09.010

Hou, X., From, N., Angelidaki, I., Huijgen, W. J. J., & Bjerre, A. B. (2017). Butanol fermentation of the brown seaweed *Laminaria digitata* by *Clostridium beijerinckii* DSM-6422. *Bioresource technology, 238*, 16-21. doi: 10.1016/j.biortech.2017.04.035

Hou, Y., Tianero, M. D., Kwan, J. C., Wyche, T. P., Michel, C. R., Ellis, G. A., Vazquez-Rivera, E., Braun, D. R., Rose, W. E., Schmidt, E. W., & Bugni, T. S. (2012). Structure and

biosynthesis of the antibiotic bottromycin D. *Organic letters, 14*(19), 5050-5053. doi: 10.1021/ol3022758

Huang, Z., Dostal, L., & Rosazza, J. P. (1993). Microbial transformations of ferulic acid by *Saccharomyces cerevisiae* and *Pseudomonas fluorescens*. *Applied and environmental microbiology, 59*(7), 2244-2250. doi: 10.1128/aem.59.7.2244-2250.1993

Huo, L., Rachid, S., Stadler, M., Wenzel, S. C., & Müller, R. (2012). Synthetic biotechnology to study and engineer ribosomal bottromycin biosynthesis. *Chemistry & biology, 19*(10), 1278-1287. doi: 10.1016/j.chembiol.2012.08.013

Ithal, N., Recknor, J., Nettleton, D., Maier, T., Baum, T. J., & Mitchum, M. G. (2007). Developmental transcript profiling of cyst nematode feeding cells in soybean roots. *Molecular plant-microbe interactions : MPMI, 20*(5), 510-525. doi: 10.1094/MPMI-20-5-0510

Iwagami, S. G., Yang, K., & Davies, J. (2000). Characterization of the protocatechuic acid catabolic gene cluster from *Streptomyces* sp. strain 2065. *Applied and environmental microbiology, 66*(4), 1499-1508. doi: 10.1128/AEM.66.4.1499-1508.2000

Jong, E, Stichnothe, H, Bell, G, & Jørgensen, H. (2020). Bio-based chemicals : a 2020 update *IEA Bioenergy* (Vol. Task 42: 2020: 01). Wageningen: IEA.

Jurková, M., & Wurst, M. (1993). Biodegradation of aromatic carboxylic acids by *Pseudomonas mira*. *FEMS microbiology letters, 111*(2-3), 245-250.

Kalinowski, J., Bathe, B., Bartels, D., Bischoff, N., Bott, M., Burkovski, A., Dusch, N., Eggeling, L., Eikmanns, B. J., Gaigalat, L., Goesmann, A., Hartmann, M., Huthmacher, K., Krämer, R., Linke, B., McHardy, A. C., Meyer, F., Möckel, B., Pfefferle, W., Pühler, A., Rey, D. A., Rückert, C., Rupp, O., Sahm, H., Wendisch, V. F., Wiegräbe, I., & Tauch, A. (2003). The complete *Corynebacterium glutamicum* ATCC 13032 genome sequence and its impact on the production of L-aspartate-derived amino acids and vitamins. *Journal of biotechnology, 104*(1-3), 5-25. doi: 10.1016/s0168-1656(03)00154-8

Kallscheuer, N., Vogt, M., Bott, M., & Marienhagen, J. (2017). Functional expression of plant-derived *O*-methyltransferase, flavanone 3-hydroxylase, and flavonol synthase in *Corynebacterium glutamicum* for production of pterostilbene, kaempferol, and quercetin. *Journal of biotechnology, 258*, 190-196. doi: 10.1016/j.jbiotec.2017.01.006

Kallscheuer, N., Vogt, M., Kappelmann, J., Krumbach, K., Noack, S., Bott, M., & Marienhagen, J. (2016). Identification of the *phd* gene cluster responsible for phenylpropanoid utilization in *Corynebacterium glutamicum*. *Applied microbiology and biotechnology, 100*(4), 1871-1881. doi: 10.1007/s00253-015-7165-1

Kasai, D., Fujinami, T., Abe, T., Mase, K., Katayama, Y., Fukuda, M., & Masai, E. (2009). Uncovering the protocatechuate 2,3-cleavage pathway genes. *Journal of bacteriology, 191*(21), 6758-6768. doi: 10.1128/JB.00840-09

Katakojwala, R., & Mohan, S. V. (2021). A critical view on the environmental sustainability of biorefinery systems. *Current Opinion in Green and Sustainable Chemistry, 27*. doi: 10.1016/J.Cogsc.2020.100392

Kieser, T., Bibb, M. J., Buttner, M. J., Chater, K. F., & Hopwood, D. A. (2000). *Practical Streptomyces Genetics*. Norwich, UK: The John Innes Foundation.

Kim, J. S., Lee, H. N., Kim, P., Lee, H. S., & Kim, E. S. (2012). Negative role of *wblA* in response to oxidative stress in *Streptomyces coelicolor*. *Journal of Microbiology and Biotechnology, 22*(6), 736-741. doi: 10.4014/jmb.1112.12032

Kim, S., Chen, J., Cheng, T., Gindulyte, A., He, J., He, S., Li, Q., Shoemaker, B. A., Thiessen, P. A., Yu, B., Zaslavsky, L., Zhang, J., & Bolton, E. E. (2023). PubChem 2023 update. *Nucleic acids research, 51*(D1), D1373-D1380. doi: 10.1093/nar/gkac956

Kim, Y. J., Moon, M. H., Song, J. Y., Smith, C. P., Hong, S. K., & Chang, Y. K. (2008). Acidic pH shock induces the expressions of a wide range of stress-response genes. *BMC genomics, 9*, 604. doi: 10.1186/1471-2164-9-604

Kobayashi, Y., Ichioka, M., Hirose, T., Nagai, K., Matsumoto, A., Matsui, H., Hanaki, H., Masuma, R., Takahashi, Y., Ōmura, S., & Sunazuka, T. (2010). Bottromycin derivatives: efficient chemical modifications of the ester moiety and evaluation of anti-MRSA and anti-VRE activities. *Bioorganic & medicinal chemistry letters, 20*(20), 6116-6120. doi: 10.1016/j.bmcl.2010.08.037

Kohlstedt, M., Sappa, P. K., Meyer, H., Maaß, S., Zaprasis, A., Hoffmann, T., Becker, J., Steil, L., Hecker, M., van Dijl, J. M., Lalk, M., Mäder, U., Stülke, J., Bremer, E., Völker, U., & Wittmann, C. (2014). Adaptation of *Bacillus subtilis* carbon core metabolism to simultaneous nutrient limitation and osmotic challenge: a multi-omics perspective. *Environmental microbiology, 16*(6), 1898-1917. doi: 10.1111/1462-2920.12438

Kohlstedt, M., Weimer, A., Weiland, F., Stolzenberger, J., Selzer, M., Sanz, M., Kramps, L., & Wittmann, C. (2022). Biobased PET from lignin using an engineered *cis*, *cis*-muconate-producing *Pseudomonas putida* strain with superior robustness, energy and redox properties. *Metabolic engineering, 72*, 337-352. doi: 10.1016/j.ymben.2022.05.001

Kondo, S., Yasui, K., Natsume, M., Katayama, M., & Marumo, S. (1988). Isolation, physico-chemical properties and biological activity of pamamycin-607, an aerial mycelium-inducing substance from *Streptomyces alboniger*. *The Journal of antibiotics, 41*(9), 1196-1204. doi: 10.7164/antibiotics.41.1196

Kosa, M., & Ragauskas, A. J. (2012). Bioconversion of lignin model compounds with oleaginous *Rhodococci*. *Applied microbiology and biotechnology, 93*(2), 891-900. doi: 10.1007/s00253-011-3743-z

Krivoruchko, A., Zhang, Y., Siewers, V., Chen, Y., & Nielsen, J. (2015). Microbial acetyl-CoA metabolism and metabolic engineering. *Metabolic engineering, 28*, 28-42. doi: 10.1016/j.ymben.2014.11.009

Kuhl, M., Gläser, L., Rebets, Y., Rückert, C., Sarkar, N., Hartsch, T., Kalinowski, J., Luzhetskyy, A., & Wittmann, C. (2020). Microparticles globally reprogram *Streptomyces albus* toward accelerated morphogenesis, streamlined carbon core metabolism, and enhanced production of the antituberculosis polyketide pamamycin. *Biotechnology and bioengineering, 117*(12), 3858-3875. doi: 10.1002/bit.27537

Kuhl, M., Rückert, C., Gläser, L., Beganovic, S., Luzhetskyy, A., Kalinowski, J., & Wittmann, C. (2021). Microparticles enhance the formation of seven major classes of natural products in native and metabolically engineered actinobacteria through accelerated morphological development. *Biotechnology and bioengineering, 118*(8), 3076-3093. doi: 10.1002/bit.27818

Kumar, B., & Verma, P. (2021). Biomass-based biorefineries: An important architype towards a circular economy. *Fuel, 288*. doi: 10.1016/J.Fuel.2020.119622

Lancefield, C. S., Rashid, G. M. M., Bouxin, F., Wasak, A., Tu, W. C., Hallett, J., Zein, S., Rodríguez, J., Jackson, S. D., Westwood, N. J., & Bugg, T. D. H. (2016). Investigation of the chemocatalytic and biocatalytic valorization of a range of different lignin preparations: The importance of β-O-4 content. *Acs Sustainable Chemistry & Engineering, 4*(12), 6921-6930. doi: 10.1021/acssuschemeng.6b01855

Langmead, B., & Salzberg, S. L. (2012). Fast gapped-read alignment with Bowtie 2. *Nature methods, 9*(4), 357-359. doi: 10.1038/nmeth.1923

Leandro, A., Pereira, L., & Gonçalves, A. M. M. (2019). Diverse applications of marine macroalgae. *Marine drugs, 18*(1). doi: 10.3390/md18010017

Lee, R. A., & Lavoie, J. (2013). From first- to third-generation biofuels: Challenges of producing a commodity from a biomass of increasing complexity. *Animal Frontiers, 3*(2), 6-11. doi: 10.2527/af.2013-0010

Lejeune, C., Sago, L., Cornu, D., Redeker, V., & Virolle, M. (2022). A Proteomic Analysis Indicates That Oxidative Stress Is the Common Feature Triggering Antibiotic Production in

Streptomyces coelicolor and in the *pptA* Mutant of *Streptomyces lividans*. *Frontiers in microbiology, 12*. doi: 10.3389/fmicb.2021.813993

Lewis, R. A., Laing, E., Allenby, N., Bucca, G., Brenner, V., Harrison, M., Kierzek, A. M., & Smith, C. P. (2010). Metabolic and evolutionary insights into the closely-related species *Streptomyces coelicolor* and *Streptomyces lividans* deduced from high-resolution comparative genomic hybridization. *BMC genomics, 11*, 682. doi: 10.1186/1471-2164-11-682

Li, Q., Zhang, S., Berthiaume, J. M., Simons, B., & Zhang, G. F. (2014). Novel approach in LC-MS/MS using MRM to generate a full profile of acyl-CoAs: discovery of acyl-dephospho-CoAs. *Journal of lipid research, 55*(3), 592-602. doi: 10.1194/jlr.D045112

Lichtenthaler, F. W., & Peters, S. (2004). Carbohydrates as green raw materials for the chemical industry. *Comptes Rendus Chimie, 7*(2), 65-90. doi: 10.1016/j.crci.2004.02.002

Linger, J. G., Vardon, D. R., Guarnieri, M. T., Karp, E. M., Hunsinger, G. B., Franden, M. A., Johnson, C. W., Chupka, G., Strathmann, T. J., Pienkos, P. T., & Beckham, G. T. (2014). Lignin valorization through integrated biological funneling and chemical catalysis. *Proceedings of the National Academy of Sciences of the United States of America, 111*(33), 12013-12018. doi: 10.1073/pnas.1410657111

Liu, H., Marsafari, M., Wang, F., Deng, L., & Xu, P. (2019). Engineering acetyl-CoA metabolic shortcut for eco-friendly production of polyketides triacetic acid lactone in *Yarrowia lipolytica*. *Metabolic engineering, 56*, 60-68. doi: 10.1016/j.ymben.2019.08.017

Liu, Q., Luo, L., & Zheng, L. (2018). Lignins: Biosynthesis and biological functions in plants. *International journal of molecular sciences, 19*(2). doi: 10.3390/ijms19020335

Liu, Z. H., Xie, S., Lin, F., Jin, M., & Yuan, J. S. (2018). Combinatorial pretreatment and fermentation optimization enabled a record yield on lignin bioconversion. *Biotechnology for biofuels, 11*, 21. doi: 10.1186/s13068-018-1021-3

Llamas-Ramírez, R., Takahashi-Iñiguez, T., & Flores, M. E. (2020). The phosphoenolpyruvate-pyruvate-oxaloacetate node genes and enzymes in *Streptomyces coelicolor* M145. *International microbiology : the official journal of the Spanish Society for Microbiology, 23*(3), 429-439. doi: 10.1007/s10123-019-00116-x

Lomartire, S., & Gonçalves, A. M. M. (2023). Algal phycocolloids: Bioactivities and pharmaceutical applications. *Marine drugs, 21*(7). doi: 10.3390/Md21070384

Love, M. I., Huber, W., & Anders, S. (2014). Moderated estimation of fold change and dispersion for RNA-seq data with DESeq2. *Genome biology, 15*(12), 550. doi: 10.1186/s13059-014-0550-8

Lubbers, R. J. M., Dilokpimol, A., Visser, J., & de Vries, R. P. (2021). *Aspergillus niger* uses the peroxisomal CoA-dependent beta-oxidative genes to degrade the hydroxycinnamic acids caffeic acid, ferulic acid, and *p*-coumaric acid. *Applied microbiology and biotechnology, 105*(10), 4199-4211. doi: 10.1007/s00253-021-11311-0

Luo, H, & Abu-Omar, M. M. (2017). Chemicals from lignin. In Martin A. Abraham (Ed.), *Encyclopedia of Sustainable Technologies* (pp. 573-585). Oxford: Elsevier.

Ma, Q. H., & Xu, Y. (2008). Characterization of a caffeic acid 3-*O*-methyltransferase from wheat and its function in lignin biosynthesis. *Biochimie, 90*(3), 515-524. doi: 10.1016/j.biochi.2007.09.016

Marella, E. R., Holkenbrink, C., Siewers, V., & Borodina, I. (2018). Engineering microbial fatty acid metabolism for biofuels and biochemicals. *Current opinion in biotechnology, 50*, 39-46. doi: 10.1016/j.copbio.2017.10.002

Masai, E., Harada, K., Peng, X., Kitayama, H., Katayama, Y., & Fukuda, M. (2002). Cloning and characterization of the ferulic acid catabolic genes of *Sphingomonas paucimobilis* SYK-6. *Applied and environmental microbiology, 68*(9), 4416-4424. doi: 10.1128/AEM.68.9.4416-4424.2002

Masai, E., Katayama, Y., & Fukuda, M. (2007). Genetic and biochemical investigations on bacterial catabolic pathways for lignin-derived aromatic compounds. *Bioscience, biotechnology, and biochemistry, 71*(1), 1-15. doi: 10.1271/bbb.60437

Mateos, L. M., Villadangos, A. F., de la Rubia, A. G., Mourenza, A., Marcos-Pascual, L., Letek, M., Pedre, B., Messens, J., & Gil, J. A. (2017). The arsenic detoxification system in *Corynebacteria*: Basis and application for bioremediation and redox control. *Advances in applied microbiology, 99*, 103-137. doi: 10.1016/bs.aambs.2017.01.001

Mathews, S. L., Pawlak, J., & Grunden, A. M. (2015). Bacterial biodegradation and bioconversion of industrial lignocellulosic streams. *Applied microbiology and biotechnology, 99*(7), 2939-2954. doi: 10.1007/s00253-015-6471-y

Mazumdar, S., Bang, J., & Oh, M. K. (2014). L-lactate production from seaweed hydrolysate of *Laminaria japonica* using metabolically engineered *Escherichia coli*. *Applied biochemistry and biotechnology, 172*(4), 1938-1952. doi: 10.1007/s12010-013-0653-9

McCann, P. A., & Pogell, B. M. (1979). Pamamycin: a new antibiotic and stimulator of aerial mycelia formation. *The Journal of antibiotics, 32*(7), 673-678. doi: 10.7164/antibiotics.32.673

Melero, J. A., Iglesias, J., & Garcia, A. (2012). Biomass as renewable feedstock in standard refinery units. Feasibility, opportunities and challenges. *Energy & Environmental Science, 5*(6), 7393-7420. doi: 10.1039/c2ee21231e

Merkens, H., Beckers, G., Wirtz, A., & Burkovski, A. (2005). Vanillate metabolism in *Corynebacterium glutamicum*. *Current Microbiology, 51*(1), 59-65. doi: 10.1007/s00284-005-4531-8

Meyer, F., Netzer, J., Meinert, C., Voigt, B., Riedel, K., & Steinbüchel, A. (2018). A proteomic analysis of ferulic acid metabolism in *Amycolatopsis* sp. ATCC 39116. *Applied microbiology and biotechnology, 102*(14), 6119-6142. doi: 10.1007/s00253-018-9061-y

Meyer, H. P. (2011). Sustainability and biotechnology. *Organic Process Research & Development, 15*(1), 180-188. doi: 10.1021/op100206p

Mishra, B., Varjani, S., Agrawal, D. C., Mandal, S. K., Ngo, H. H., Taherzadeh, M. J., Chang, J. S., You, S. M., & Guo, W. S. (2020). Engineering biocatalytic material for the remediation of pollutants: A comprehensive review. *Environmental Technology & Innovation, 20*. doi: 10.1016/j.eti.2020.101063

Mohammad, S. H., & Bhukya, B. (2022). Biotransformation of toxic lignin and aromatic compounds of lignocellulosic feedstock into eco-friendly biopolymers by *Pseudomonas putida* KT2440. *Bioresource technology, 363*, 128001. doi: 10.1016/j.biortech.2022.128001

Moura, J. C., Bonine, C. A., de Oliveira Fernandes Viana, J., Dornelas, M. C., & Mazzafera, P. (2010). Abiotic and biotic stresses and changes in the lignin content and composition in plants. *Journal of integrative plant biology, 52*(4), 360-376. doi: 10.1111/j.1744-7909.2010.00892.x

Myronovskyi, M., & Luzhetskyy, A. (2019). Heterologous production of small molecules in the optimized *Streptomyces* hosts. *Natural product reports, 36*(9), 1281-1294. doi: 10.1039/c9np00023b

Narbad, A., & Gasson, M. J. (1998). Metabolism of ferulic acid via vanillin using a novel CoA-dependent pathway in a newly-isolated strain of *Pseudomonas fluorescens*. *Microbiology, 144*(5), 1397-1405. doi: 10.1099/00221287-144-5-1397

Neubauer, S., Chu, D. B., Marx, H., Sauer, M., Hann, S., & Koellensperger, G. (2015). LC-MS/MS-based analysis of coenzyme A and short-chain acyl-coenzyme A thioesters. *Analytical and bioanalytical chemistry, 407*(22), 6681-6688. doi: 10.1007/s00216-015-8825-9

Novotny, M. J., Reizer, J., Esch, F., & Saier, M. H., Jr. (1984). Purification and properties of D-mannitol-1-phosphate dehydrogenase and D-glucitol-6-phosphate dehydrogenase from *Escherichia coli*. *Journal of bacteriology, 159*(3), 986-990. doi: 10.1128/jb.159.3.986-990.1984

OECD, Organisation for Economic Co-operation Development. (1994). *Biotechnology for a clean environment: prevention, detection, remediation*: Organisation for Economic Co-operation and Development.

Ögmundarson, Ó, Sukumara, S, Laurent, A, & Fantke, P. (2020). Environmental hotspots of lactic acid production systems. *GCB Bioenergy, 12*(1), 19-38. doi: 10.1111/gcbb.12652

Ohmiya, K., Takeuchi, M., Chen, W., Shimizu, S., & Kawakami, H. (1986). Anaerobic reduction of ferulic acid to dihydroferulic acid by *Wolinella succinogenes* from cow rumen. *Applied microbiology and biotechnology, 23*(3-4), 274-279.

Okamura-Abe, Y., Abe, T., Nishimura, K., Kawata, Y., Sato-Izawa, K., Otsuka, Y., Nakamura, M., Kajita, S., Masai, E., Sonoki, T., & Katayama, Y. (2016). Beta-ketoadipic acid and muconolactone production from a lignin-related aromatic compound through the protocatechuate 3,4-metabolic pathway. *Journal of bioscience and bioengineering, 121*(6), 652-658. doi: 10.1016/j.jbiosc.2015.11.007

Olsson, J, Toth, G. B., & Albers, E. (2020). Biochemical composition of red, green and brown seaweeds on the Swedish west coast. *Journal of applied phycology, 32*(5), 3305-3317. doi: 10.1007/s10811-020-02145-w

Otaka, T., & Kaji, A. (1976). Mode of action of bottromycin A_2: Release of aminoacyl- or peptidyl-tRNA from ribosomes. *The Journal of biological chemistry, 251*(8), 2299-2306.

Otaka, T., & Kaji, A. (1981). Mode of action of bottromycin A_2: effect on peptide bond formation. *FEBS letters, 123*(2), 173-176. doi: 10.1016/0014-5793(81)80280-3

Otaka, T., & Kaji, A. (1983). Mode of action of bottromycin A_2: effect of bottromycin A_2 on polysomes. *FEBS letters, 153*(1), 53-59. doi: 10.1016/0014-5793(83)80118-5

Palladino, A. A., Chen, J., Kallish, S., Stanley, C. A., & Bennett, M. J. (2012). Measurement of tissue acyl-CoAs using flow-injection tandem mass spectrometry: acyl-CoA profiles in short-chain fatty acid oxidation defects. *Molecular genetics and metabolism, 107*(4), 679-683. doi: 10.1016/j.ymgme.2012.10.007

Parales, R. E., & Harwood, C. S. (1992). Characterization of the genes encoding beta-ketoadipate: succinyl-coenzyme A transferase in *Pseudomonas putida*. *Journal of bacteriology, 174*(14), 4657-4666. doi: 10.1128/jb.174.14.4657-4666.1992

Park, D., Swayambhu, G., Lyga, T., & Pfeifer, B. A. (2021). Complex natural product production methods and options. *Synthetic and systems biotechnology, 6*(1), 1-11. doi: 10.1016/j.synbio.2020.12.001

Park, J., Kelly, M. A., Kang, J. S. X., Seemakurti, S. S., Ramirez, J. L., Hatzell, M. C., Sievers, C., & Bommarius, A. S. (2021). Production of active pharmaceutical ingredients (APIs) from lignin-derived phenol and catechol. *Green Chemistry, 23*(19), 7488-7498. doi: 10.1039/d1gc02158c

Peng, X., Okai, N., Vertès, A. A., Inatomi, K., Inui, M., & Yukawa, H. (2011). Characterization of the mannitol catabolic operon of *Corynebacterium glutamicum*. *Applied microbiology and biotechnology, 91*(5), 1375-1387. doi: 10.1007/s00253-011-3352-x

Pérez-García, F., Klein, V. J., Brito, L. F., & Brautaset, T. (2022). From brown seaweed to a sustainable microbial feedstock for the production of riboflavin. *Frontiers in bioengineering and biotechnology, 10*, 863690. doi: 10.3389/fbioe.2022.863690

Peter, D. M., Vögeli, B., Cortina, N. S., & Erb, T. J. (2016). A chemo-enzymatic road map to the synthesis of CoA esters. *Molecules, 21*(4), 517. doi: 10.3390/molecules21040517

Pham, J. V., Yilma, M. A., Feliz, A., Majid, M. T., Maffetone, N., Walker, J. R., Kim, E., Cho, H. J., Reynolds, J. M., Song, M. C., Park, S. R., & Yoon, Y. J. (2019). A review of the microbial production of bioactive natural products and biologics. *Frontiers in microbiology, 10*, 1404. doi: 10.3389/fmicb.2019.01404

Plaggenborg, R., Overhage, J., Loos, A., Archer, J. A., Lessard, P., Sinskey, A. J., Steinbüchel, A., & Priefert, H. (2006). Potential of *Rhodococcus* strains for biotechnological vanillin

production from ferulic acid and eugenol. *Applied microbiology and biotechnology, 72*(4), 745-755. doi: 10.1007/s00253-005-0302-5

Plaggenborg, R., Overhage, J., Steinbüchel, A., & Priefert, H. (2003). Functional analyses of genes involved in the metabolism of ferulic acid in *Pseudomonas putida* KT2440. *Applied microbiology and biotechnology, 61*(5-6), 528-535. doi: 10.1007/s00253-003-1260-4

Plaggenborg, R., Steinbüchel, A., & Priefert, H. (2001). The coenzyme A-dependent, non-beta-oxidation pathway and not direct deacetylation is the major route for ferulic acid degradation in *Delftia acidovorans*. *FEMS microbiology letters, 205*(1), 9-16. doi: 10.1111/j.1574-6968.2001.tb10918.x

Poblete-Castro, I., Hoffmann, S. L., Becker, J., & Wittmann, C. (2020). Cascaded valorization of seaweed using microbial cell factories. *Current opinion in biotechnology, 65*, 102-113. doi: 10.1016/j.copbio.2020.02.008

Ponnusamy, V. K., Nguyen, D. D., Dharmaraja, J., Shobana, S., Banu, J. R., Saratale, R. G., Chang, S. W., & Kumar, G. (2019). A review on lignin structure, pretreatments, fermentation reactions and biorefinery potential. *Bioresource technology, 271*, 462-472. doi: 10.1016/j.biortech.2018.09.070

Popp, J., Kovács, S., Oláh, J., Divéki, Z., & Balázs, E. (2021). Bioeconomy: Biomass and biomass-based energy supply and demand. *New Biotechnology, 60*, 76-84. doi: 10.1016/j.nbt.2020.10.004

Postma, P. W., Lengeler, J. W., & Jacobson, G. R. (1993). Phosphoenolpyruvate:carbohydrate phosphotransferase systems of bacteria. *Microbiological reviews, 57*(3), 543-594. doi: 10.1128/mr.57.3.543-594.1993

Potts, T., Du, J. J., Paul, M., May, P., Beitle, R., & Hestekin, J. (2012). The production of butanol from Jamaica bay macro algae. *Environmental Progress & Sustainable Energy, 31*(1), 29-36. doi: 10.1002/ep.10606

Priefert, H., Overhage, J., & Steinbüchel, A. (1999). Identification and molecular characterization of the eugenol hydroxylase genes (*ehyA*/*ehyB*) of *Pseudomonas* sp. strain HR199. *Archives of microbiology, 172*(6), 354-363. doi: 10.1007/s002030050772

Priefert, H., Rabenhorst, J., & Steinbüchel, A. (2001). Biotechnological production of vanillin. *Applied microbiology and biotechnology, 56*(3-4), 296-314. doi: 10.1007/s002530100687

Qualley, A. V., Cooper, B. R., & Dudareva, N. (2012a). Profiling hydroxycinnamoyl-coenzyme A thioesters: unlocking the back door of phenylpropanoid metabolism. *Analytical biochemistry, 420*(2), 182-184. doi: 10.1016/j.ab.2011.09.010

Qualley, A. V., Widhalm, J. R., Adebesin, F., Kish, C. M., & Dudareva, N. (2012b). Completion of the core beta-oxidative pathway of benzoic acid biosynthesis in plants. *Proceedings of the National Academy of Sciences of the United States of America, 109*(40), 16383-16388. doi: 10.1073/pnas.1211001109

Quinn, G. A., Banat, A. M., Abdelhameed, A. M., & Banat, I. M. (2020). *Streptomyces* from traditional medicine: sources of new innovations in antibiotic discovery. *Journal of medical microbiology, 69*(8), 1040-1048. doi: 10.1099/jmm.0.001232

Ralph, J, Lundquist, K, Brunow, G, Lu, F, Kim, H, Schatz, P. F., Marita, J. M., Hatfield, R. D., Ralph, S. A., Christensen, J, & Boerjan, W. (2004). Lignins: Natural polymers from oxidative coupling of 4-hydroxyphenyl- propanoids. *Phytochemistry Reviews, 3*(1), 29-60. doi: 10.1023/B:PHYT.0000047809.65444.a4

Rautengarten, C., Baidoo, E., Keasling, J. D., & Scheller, H. V. (2010). A Simple Method for Enzymatic Synthesis of Unlabeled and Radiolabeled Hydroxycinnamate-CoA. *Bioenergy Research, 3*(2), 115-122. doi: 10.1007/s12155-010-9085-3

Ray, D., Anand, U., Jha, N. K., Korzeniewska, E., Bontempi, E., Proćków, J., & Dey, A. (2022). The soil bacterium, *Corynebacterium glutamicum*, from biosynthesis of value-added products to bioremediation: A master of many trades. *Environmental research, 213*, 113622. doi: 10.1016/j.envres.2022.113622

Rebets, Y., Brotz, E., Manderscheid, N., Tokovenko, B., Myronovskyi, M., Metz, P., Petzke, L., & Luzhetskyy, A. (2015). Insights into the pamamycin biosynthesis. *Angewandte Chemie, 54*(7), 2280-2284. doi: 10.1002/anie.201408901

Reddy, N., & Yang, Y. (2005). Biofibers from agricultural byproducts for industrial applications. *Trends in biotechnology, 23*(1), 22-27. doi: 10.1016/j.tibtech.2004.11.002

Reed, R. H., Davison, I. R., Chudek, J. A., & Foster, R. (1985). The osmotic role of mannitol in the *Phaeophyta* - an appraisal. *Phycologia, 24*(1), 35-47. doi: 10.2216/i0031-8884-24-1-35.1

Renilla, S., Bernal, V., Fuhrer, T., Castaño-Cerezo, S., Pastor, J. M., Iborra, J. L., Sauer, U., & Cánovas, M. (2012). Acetate scavenging activity in *Escherichia coli*: interplay of acetyl-CoA synthetase and the PEP-glyoxylate cycle in chemostat cultures. *Applied microbiology and biotechnology, 93*(5), 2109-2124. doi: 10.1007/s00253-011-3536-4

Rivera, L. G., & Bartlett, M. G. (2018). Chromatographic methods for the determination of acyl-CoAs. *Analytical Methods, 10*(44), 5252-5264. doi: 10.1039/c8ay01472h

Rohles, C. M., Giesselmann, G., Kohlstedt, M., Wittmann, C., & Becker, J. (2016). Systems metabolic engineering of *Corynebacterium glutamicum* for the production of the carbon-5 platform chemicals 5-aminovalerate and glutarate. *Microbial cell factories, 15*(1), 154. doi: 10.1186/s12934-016-0553-0

Rosazza, J. P. N., Huang, Z., Dostal, L., Volm, T., & Rousseau, B. (1995). Review: Biocatalytic transformations of ferulic acid: An abundant aromatic natural product. *Journal of Industrial Microbiology, 15*(6), 457-471. doi: 10.1007/Bf01570016

Rückert, C., Albersmeier, A., Busche, T., Jaenicke, S., Winkler, A., Friðjónsson, O. H., Hreggviðsson, G. O., Lambert, C., Badcock, D., Bernaerts, K., Anne, J., Economou, A., & Kalinowski, J. (2015). Complete genome sequence of *Streptomyces lividans* TK24. *Journal of biotechnology, 199*, 21-22. doi: 10.1016/j.jbiotec.2015.02.004

Sadhukhan, J., Gadkari, S., Martinez-Hernandez, E., Ng, K. S., Shemfe, M., Torres-Garcia, E., & Lynch, J. (2019). Novel macroalgae (seaweed) biorefinery systems for integrated chemical, protein, salt, nutrient and mineral extractions and environmental protection by green synthesis and life cycle sustainability assessments. *Green Chemistry, 21*(10), 2635-2655. doi: 10.1039/c9gc00607a

Sagong, H. Y., Son, H. F., Choi, S. Y., Lee, S. Y., & Kim, K. J. (2018). Structural Insights into polyhydroxyalkanoates biosynthesis. *Trends in Biochemical Sciences, 43*(10), 790-805. doi: 10.1016/j.tibs.2018.08.005

Sainsbury, P. D., Hardiman, E. M., Ahmad, M., Otani, H., Seghezzi, N., Eltis, L. D., & Bugg, T. D. (2013). Breaking down lignin to high-value chemicals: the conversion of lignocellulose to vanillin in a gene deletion mutant of *Rhodococcus jostii* RHA1. *ACS chemical biology, 8*(10), 2151-2156. doi: 10.1021/cb400505a

Salehi, B., Sharifi-Rad, J., Seca, A. M. L., Pinto, Dcga, Michalak, I., Trincone, A., Mishra, A. P., Nigam, M., Zam, W., & Martins, N. (2019). Current trends on seaweeds: Looking at chemical composition, phytopharmacology, and cosmetic applications. *Molecules, 24*(22). doi: 10.3390/molecules24224182

Salvachúa, D., Rydzak, T., Auwae, R., De Capite, A., Black, B. A., Bouvier, J. T., Cleveland, N. S., Elmore, J. R., Furches, A., Huenemann, J. D., Katahira, R., Michener, W. E., Peterson, D. J., Rohrer, H., Vardon, D. R., Beckham, G. T., & Guss, A. M. (2020). Metabolic engineering of *Pseudomonas putida* for increased polyhydroxyalkanoate production from lignin. *Microbial Biotechnology, 13*(3), 813-813. doi: 10.1111/1751-7915.13547

Sánchez, S., Chávez, A., Forero, A., García-Huante, Y., Romero, A., Sánchez, M., Rocha, D., Sánchez, B., Ávalos, M., Guzmán-Trampe, S., Rodríguez-Sanoja, R., Langley, E., & Ruiz, B. (2010). Carbon source regulation of antibiotic production. *Journal of Antibiotics, 63*(8), 442-459. doi: 10.1038/ja.2010.78

Sand, M., Mingote, A. I., Santos, H., Muller, V., & Averhoff, B. (2013). Mannitol, a compatible solute synthesized by *Acinetobacter baylyi* in a two-step pathway including a salt-induced

and salt-dependent mannitol-1-phosphate dehydrogenase. *Environmental microbiology, 15*(8), 2187-2197. doi: 10.1111/1462-2920.12090

Sasaki, Y., Takagi, T., Motone, K., Shibata, T., Kuroda, K., & Ueda, M. (2018). Direct bioethanol production from brown macroalgae by co-culture of two engineered *Saccharomyces cerevisiae* strains. *Bioscience, biotechnology, and biochemistry, 82*(8), 1459-1462. doi: 10.1080/09168451.2018.1467262

Sayre, R. (2010). Microalgae: The potential for carbon capture. *Bioscience, 60*(9), 722-727. doi: 10.1525/bio.2010.60.9.9

Schnell, S, & Schink, B. (1991). Anaerobic aniline degradation via reductive deamination of 4-aminobenzoyl-CoA in *Desulfobacterium anilini*. *Archives of microbiology, 155*(2), 183-190. doi: 10.1007/bf00248615

Schrader, K. K., & Blevins, W. T. (2001). Effects of carbon source, phosphorus concentration, and several micronutrients on biomass and geosmin production by *Streptomyces halstedii*. *Journal of industrial microbiology & biotechnology, 26*(4), 241-247. doi: 10.1038/sj.jim.7000121

Schuetz, M., Benske, A., Smith, R. A., Watanabe, Y., Tobimatsu, Y., Ralph, J., Demura, T., Ellis, B., & Samuels, A. L. (2014). Laccases direct lignification in the discrete secondary cell wall domains of protoxylem. *Plant physiology, 166*(2), 798-807. doi: 10.1104/pp.114.245597

Schutyser, W., Renders, T., Van den Bosch, S., Koelewijn, S. F., Beckham, G. T., & Sels, B. F. (2018). Chemicals from lignin: an interplay of lignocellulose fractionation, depolymerisation, and upgrading. *Chemical Society reviews, 47*(3), 852-908. doi: 10.1039/c7cs00566k

Schwechheimer, S. K., Becker, J., Peyriga, L., Portais, J. C., Sauer, D., Müller, R., Hoff, B., Haefner, S., Schröder, H., Zelder, O., & Wittmann, C. (2018). Improved riboflavin production with *Ashbya gossypii* from vegetable oil based on ^{13}C metabolic network analysis with combined labeling analysis by GC/MS, LC/MS, 1D, and 2D NMR. *Metabolic engineering, 47*, 357-373. doi: 10.1016/j.ymben.2018.04.005

Seo, K., Shu, W., Rückert-Reed, C., Gerlinger, P., Erb, T. J., Kalinowski, J., & Wittmann, C. (2023). From waste to health-supporting molecules: biosynthesis of natural products from lignin-, plastic- and seaweed-based monomers using metabolically engineered *Streptomyces lividans*. *Microbial Cell Factories, 22*(1), 262. doi: 10.1186/s12934-023-02266-0

Siegel, D., Permentier, H., Reijngoud, D. J., & Bischoff, R. (2014). Chemical and technical challenges in the analysis of central carbon metabolites by liquid-chromatography mass spectrometry. *Journal of Chromatography B-Analytical Technologies in the Biomedical and Life Sciences, 966*, 21-33. doi: 10.1016/j.jchromb.2013.11.022

Singh, A., Prajapati, P., Vyas, S., Gaur, V. K., Sindhu, R., Binod, P., Kumar, V., Singhania, R. R., Awasthi, M. K., Zhang, Z., & Varjani, S. (2023). A Comprehensive review of feedstocks as sustainable substrates for next-generation biofuels. *BioEnergy Research, 16*(1), 105-122. doi: 10.1007/s12155-022-10440-2

Skinnider, M. A., Johnston, C. W., Edgar, R. E., Dejong, C. A., Merwin, N. J., Rees, P. N., & Magarvey, N. A. (2016). Genomic charting of ribosomally synthesized natural product chemical space facilitates targeted mining. *Proceedings of the National Academy of Sciences of the United States of America, 113*(42), E6343-E6351. doi: 10.1073/pnas.1609014113

Smolarski, N. (2012). High-value opportunities for lignin: Unlocking its potential. *Frost & Sullivan*.

Song, S., Peng, H., Wang, Q., Liu, Z., Dong, X., Wen, C., Ai, C., Zhang, Y., Wang, Z., & Zhu, B. (2020). Inhibitory activities of marine sulfated polysaccharides against SARS-CoV-2. *Food & function, 11*(9), 7415-7420. doi: 10.1039/d0fo02017f

Sonoki, T., Takahashi, K., Sugita, H., Hatamura, M., Azuma, Y., Sato, T., Suzuki, S., Kamimura, N., & Masai, E. (2018). Glucose-free *cis*, *cis*-muconic acid production via new metabolic designs corresponding to the heterogeneity of lignin. *ACS Sustainable Chemistry & Engineering, 6*(1), 1256-1264. doi: 10.1021/acssuschemeng.7b03597

Stiger-Pouvreau, V., Jégou, C., Cérantola, S., Guérard, F., & Le Lann, K. (2014). Phlorotannins in *Sargassaceae* species from Brittany (France): Interesting molecules for ecophysiological and valorisation purposes. *Sea Plants, 71*, 379-411. doi: 10.1016/B978-0-12-408062-1.00013-5

Straathof, A. J. J., Wahl, S. A., Benjamin, K. R., Takors, R., Wierckx, N., & Noorman, H. J. (2019). Grand research challenges for sustainable industrial biotechnology. *Trends in biotechnology, 37*(10), 1042-1050. doi: 10.1016/j.tibtech.2019.04.002

Sunwoo, I., Kwon, J. E., Jeong, G. T., & Kim, S. K. (2019). Optimization of hyper-thermal acid hydrolysis and enzymatic saccharification of *Ascophyllum nodosum* for ethanol production with mannitol-adapted yeasts. *Bioprocess and biosystems engineering, 42*(8), 1255-1262. doi: 10.1007/s00449-019-02123-8

Sunwoo, I. Y., Hau, N. T., Ra, C. H., Jeong, G. T., & Kim, S. K. (2018). Acetone-butanol-ethanol production from waste seaweed collected from Gwangalli beach, Busan, Korea, based on pH-controlled and sequential fermentation using two strains. *Applied biochemistry and biotechnology, 185*(4), 1075-1087. doi: 10.1007/s12010-018-2711-9

Suzuki, Y, Otsuka, Y, Araki, T, Kamimura, N, Masai, E, Nakamura, M, & Katayama, Y. (2021). Lignin valorization through efficient microbial production of β-ketoadipate from industrial black liquor. *Bioresource technology, 337*, 125489. doi: https://doi.org/10.1016/j.biortech.2021.125489

Świzdor, A., Panek, A., Milecka-Tronina, N., & Kołek, T. (2012). Biotransformations utilizing β-oxidation cycle reactions in the synthesis of natural compounds and medicines. *International journal of molecular sciences, 13*(12), 16514-16543. doi: 10.3390/ijms131216514

Tabassum, M. R., Xia, A., & Murphy, J. D. (2017). Potential of seaweed as a feedstock for renewable gaseous fuel production in Ireland. *Renewable & Sustainable Energy Reviews, 68*, 136-146. doi: 10.1016/j.rser.2016.09.111

Takeno, S., Takasaki, M., Urabayashi, A., Mimura, A., Muramatsu, T., Mitsuhashi, S., & Ikeda, M. (2013). Development of fatty acid-producing *Corynebacterium glutamicum* strains. *Applied and environmental microbiology, 79*(21), 6776-6783. doi: 10.1128/AEM.02003-13

Tan, B. L., & Norhaizan, M. E. (2019). Carotenoids: How effective are they to prevent age-related diseases? *Molecules, 24*(9). doi: 10.3390/molecules24091801

Team, R Core. (2014). R: A language and environment for statistical computing. R Foundation for Statistical Computing, Vienna, Austria.

Toms, A., & Wood, J. M. (1970). The degradation of trans-ferulic acid by *Pseudomonas acidovorans*. *Biochemistry, 9*(2), 337-343. doi: 10.1021/bi00804a021

Torres, M. D., Kraan, S, & Domínguez, H. (2019). Seaweed biorefinery. *Reviews in environmental science and bio/technology, 18*(2), 335-388. doi: 10.1007/s11157-019-09496-y

Vicente, R. L., Gullón, S., Marín, S., & Mellado, R. P. (2016). The three *Streptomyces lividans* HtrA-like proteases involved in the secretion stress response act in a cooperative manner. *PloS one, 11*(12), e0168112. doi: 10.1371/journal.pone.0168112

Vilg, J., Nylund, G., Werner, T., Qvirist, L., Mayers, J., Pavia, H., Undeland, I. , & Albers, E. (2015). Seasonal and spatial variation in biochemical composition of *Saccharina latissima* during a potential harvesting season for Western Sweden. *Botanica Marina, 58*(6), 435-447. doi: 10.1515/bot-2015-0034

Vior, N. M., Cea-Torrescassana, E., Eyles, T. H., Chandra, G., & Truman, A. W. (2020). Regulation of bottromycin biosynthesis involves an internal transcriptional start site and a cluster-situated modulator. *Frontiers in microbiology, 11*, 495. doi: 10.3389/fmicb.2020.00495

Waisvisz, J. M., van der Hoeven, M. G., & Nijenhuis, B. te. (1957a). The structure of the sulfur-containing moiety of bottromycin. *Journal of the American Chemical Society, 79*(16), 4524-4527. doi: 10.1021/ja01573a074

Waisvisz, J. M., van der Hoeven, M. G., van Peppen, J., & Zwennis, W. C. M. (1957b). Bottromycin .1. A new sulfur-containing antibiotic. *Journal of the American Chemical Society, 79*(16), 4520-4521. doi: 10.1021/Ja01573a072

Wang, Y., Fang, X., An, F., Wang, G., & Zhang, X. (2011). Improvement of antibiotic activity of *Xenorhabdus bovienii* by medium optimization using response surface methodology. *Microbial cell factories, 10*, 98. doi: 10.1186/1475-2859-10-98

Warnes, Maintainer Gregory R, Bolker, Ben, Bonebakker, Lodewijk, & Gentleman, Robert. (2016). Package 'gplots'. Various R Programming Tools for Plotting Data.

Watanabe, S., Hamano, M., Kakeshita, H., Bunai, K., Tojo, S., Yamaguchi, H., Fujita, Y., Wong, S. L., & Yamane, K. (2003). Mannitol-1-phosphate dehydrogenase (MtlD) is required for mannitol and glucitol assimilation in *Bacillus subtilis*: possible cooperation of *mtl* and *gut* operons. *Journal of bacteriology, 185*(16), 4816-4824. doi: 10.1128/JB.185.16.4816-4824.2003

Weiland, F., Barton, N., Kohlstedt, M., Becker, J., & Wittmann, C. (2023). Systems metabolic engineering upgrades *Corynebacterium glutamicum* to high-efficiency *cis*, *cis*-muconic acid production from lignin-based aromatics. *Metabolic engineering, 75*, 153-169. doi: 10.1016/j.ymben.2022.12.005

Weiland, F., Kohlstedt, M., & Wittmann, C. (2022). Guiding stars to the field of dreams: Metabolically engineered pathways and microbial platforms for a sustainable lignin-based industry. *Metabolic engineering, 71*, 13-41. doi: 10.1016/j.ymben.2021.11.011

Wendisch, V. F., Brito, L. F., Gil Lopez, M., Hennig, G., Pfeifenschneider, J., Sgobba, E., & Veldmann, K. H. (2016). The flexible feedstock concept in Industrial Biotechnology: Metabolic engineering of *Escherichia coli*, *Corynebacterium glutamicum*, *Pseudomonas*, *Bacillus* and yeast strains for access to alternative carbon sources. *Journal of biotechnology, 234*, 139-157. doi: 10.1016/j.jbiotec.2016.07.022

Wendisch, V. F., de Graaf, A. A., Sahm, H., & Eikmanns, B. J. (2000). Quantitative determination of metabolic fluxes during coutilization of two carbon sources: comparative analyses with *Corynebacterium glutamicum* during growth on acetate and/or glucose. *Journal of bacteriology, 182*(11), 3088-3096. doi: 10.1128/JB.182.11.3088-3096.2000

Wendisch, V. F., Spies, M., Reinscheid, D. J., Schnicke, S., Sahm, H., & Eikmanns, B. J. (1997). Regulation of acetate metabolism in *Corynebacterium glutamicum*: transcriptional control of the isocitrate lyase and malate synthase genes. *Archives of microbiology, 168*(4), 262-269. doi: 10.1007/s002030050497

Wiegmann, K., Hensler, M., Wöhlbrand, L., Ulbrich, M., Schomburg, D., & Rabus, R. (2014). Carbohydrate catabolism in *Phaeobacter inhibens* DSM 17395, a member of the marine roseobacter clade. *Applied and environmental microbiology, 80*(15), 4725-4737. doi: 10.1128/AEM.00719-14

Wilkins, M. R., Gasteiger, E., Bairoch, A., Sanchez, J. C., Williams, K. L., Appel, R. D., & Hochstrasser, D. F. (1999). Protein identification and analysis tools in the ExPASy server. *Methods in molecular biology, 112*, 531-552. doi: 10.1385/1-59259-584-7:531

Willem, V. K., & Saxifraga. (2018). Himanthalia elongata 5. *http://www.freenatureimages.eu/*.

Wittmann, C. (2010). Analysis and engineering of metabolic pathway fluxes in *Corynebacterium glutamicum*. *Advances in biochemical engineering/biotechnology, 120*, 21-49. doi: 10.1007/10_2009_58

Woo, M. N., Jeon, S. M., Shin, Y. C., Lee, M. K., Kang, M. A., & Choi, M. S. (2009). Anti-obese property of fucoxanthin is partly mediated by altering lipid-regulating enzymes and uncoupling proteins of visceral adipose tissue in mice. *Molecular nutrition & food research, 53*(12), 1603-1611. doi: 10.1002/mnfr.200900079

Xia, A., Jacob, A., Herrmann, C., Tabassum, M. R., & Murphy, J. D. (2015). Production of hydrogen, ethanol and volatile fatty acids from the seaweed carbohydrate mannitol. *Bioresource technology, 193*, 488-497. doi: 10.1016/j.biortech.2015.06.130

Xu, X., Kim, J. Y., Oh, Y. R., & Park, J. M. (2014). Production of biodiesel from carbon sources of macroalgae, *Laminaria japonica*. *Bioresource technology, 169*, 455-461. doi: 10.1016/j.biortech.2014.07.015

Xu, Z., Lei, P., Zhai, R., Wen, Z., & Jin, M. (2019). Recent advances in lignin valorization with bacterial cultures: microorganisms, metabolic pathways, and bio-products. *Biotechnology for biofuels, 12*, 32. doi: 10.1186/s13068-019-1376-0

Yang, W. W., Tang, H. Z., Ni, J., Wu, Q. L., Hua, D. L., Tao, F., & Xu, P. (2013). Characterization of two enzymes that convert ferulic acid to vanillin. *Plos One, 8*(6). doi: 10.1371/journal.pone.0067339

Yong, W. T. L., Thien, V. Y., Rupert, R., & Rodrigues, K. F. (2022). Seaweed: A potential climate change solution. *Renewable & Sustainable Energy Reviews, 159*. doi: 10.1016/J.Rser.2022.112222

Zhang, B., Jiang, Y., Li, Z., Wang, F., & Wu, X. Y. (2020). Recent progress on chemical production from non-food renewable feedstocks using *Corynebacterium glutamicum*. *Frontiers in bioengineering and biotechnology, 8*, 606047. doi: 10.3389/fbioe.2020.606047

Zhang, R., Zhao, C. H., Chang, H. C., Chai, M. Z., Li, B. Z., & Yuan, Y. J. (2019). Lignin valorization meets synthetic biology. *Engineering in life sciences, 19*(6), 463-470. doi: 10.1002/elsc.201800133

Zhao, Y. R., Bourgougnon, N., Lanoisellé, J. L., & Lendormi, T. (2022). Biofuel production from seaweeds: A comprehensive review. *Energies, 15*(24). doi: 10.3390/En15249395

Zhou, B., Xiao, J. F., Tuli, L., & Ressom, H. W. (2012). LC-MS-based metabolomics. *Molecular bioSystems, 8*(2), 470-481. doi: 10.1039/c1mb05350g

Zhou, N. N., Thilakarathna, W. P. D. W., He, Q. S., & Rupasinghe, H. P. V. (2022). A Review: depolymerization of lignin to generate high-value bio-products: Opportunities, challenges, and prospects. *Frontiers in Energy Research, 9*. doi: 10.3389/Fenrg.2021.758744